UNIVERSIDAD AUTÓNOMA DE MADRID

Departamento de Biología Molecular

Store-operated calcium entry in neural cells. A role in Charcot-Marie-Tooth disease.

Paloma González Sánchez

Madrid, 2017

Departamento de Biología Molecular

Facultad de Ciencias

Universidad Autónoma de Madrid

Store-operated calcium entry in neural cells.

A role in Charcot-Marie-Tooth disease.

Memoria presentada por la licenciada en Química Paloma González Sánchez para optar al título de Doctor en Ciencias en la modalidad de formato clásico bajo la supervisión de:

Directora de la tesis:

Dra. Jorgina Satrústegui Gil-Delgado

Codirectora de la tesis:

Dra. Araceli del Arco Martínez

Este trabajo ha sido realizado en el Departamento de Biología Molecular, Centro de Biología Molecular "Severo Ochoa" (C.S.I.C. – U.A.M.). La realización de esta Tesis ha sido posible gracias a una ayuda del Programa de Becas Lanzadera del Centro de Investigación Biomédica en Red de Enfermedades Raras (CIBERER), una ayuda predoctoral del programa propio de ayudas para la formación de personal investigador UAM y a Contratos Predoctorales de la Universidad Autónoma de Madrid y la Fundación Severo Ochoa.

Agradecimientos:

Aquí estoy, a punto de escribir las últimas líneas de mi tesis, y finalmente relajada, me doy cuenta que tengo que agradecer a muchísimas personas el haberme ayudado, profesional o emocionalmente, a hacer este trabajo posible.

En primer lugar no puedo poner a otra persona sino Ina, mi directora de tesis. Muchísimas gracias por tu esfuerzo, por haberme dado la oportunidad de aprender a tu lado, por estar disponible 24/7, por tu infinita paciencia para discutir los mismos resultados una y otra vez hasta que me quedaran claros, y sobre todo, por darnos la oportunidad de volar solos.

A Araceli, mi co-directora, no hay palabras para agradecerte todo el tiempo invertido en nosotros. Aunque tengas que poner una transfección, pasar mil P100 de células en cultivos, analizar infinitos videos de FRET, hacer un clonaje y tomar fotos en el microscopio siendo las 8 de la tarde de un viernes, siempre siempre siempre contestas con un sí a: - Ara, ¿tienes 5 minutos?. Incluso cuando nos gritas y nos dices que no te molestemos más que tienes mucho trabajo, acabas viniendo y preguntándonos tu cómo nos va con el problema. Gracias por ser un pozo sin fondo de sabiduría y enseñarme tanto, las conversaciones científicas con Inés siempre termina igual: Ara seguro que lo sabe.

A todo el laboratorio 321, a Laura, a Bea Pardo, por tus enseñanzas tanto científicas como de la vida, y por todas las risas en el lab, que han sido muchas. A Isabel Manso, por tener paciencia y sacar ratones de debajo de las piedras cuando me hacían falta.

A mis niñas, con las que he compartido la mayor parte de mi tiempo de vida desde que empecé en el lab, sin cada una de vosotras esto no sería lo mismo, yo no sería la misma (aunque seguiría teniendo un maravilloso acento andaluz y podría seguir diciendo *las una*…supongo que todo tiene pros y contras). A Inés, porque me encanta! Por las conversaciones sobre ciencia y preguntárnoslo todo, hasta el más ínfimo detalle (incluso si las pinzas con las que se cogen los cubres para cultivar células influye en el estado del cultivo…), por intentar ingenuamente hacer el cálculo de moléculas de ATP gastadas con diferentes estímulos, por involucrarte tanto en los tema estrellas de cada semana, por hacer que sea tan fácil hacerte feliz, y por supuesto por las cervezas y por haber sido uno de mis más grandes apoyos en la etapa final de la tesis, especialmente difícil para mí. A Paula, mi otro gran apoyo en esta etapa, mi compi de CMT, quería darte las gracias por hacer tan fácil trabajar contigo, por estar siempre dispuesta a sacrificarte, a hacer el cambio de medio a las 12 horas o llevar a cabo técnicas que sabes que no me dejan dormir, por haberte leído todo lo que he escrito, incluso esta tesis, y darme consejos sobre cómo mejorarlo, por las discusiones sobre los resultados, por los cines y por Marvel! y porque me encanta cuando vas al aseo. No se me ocurre nadie mejor con la que pasar por este proceso que no seas tú. A Carmen, que aunque ahora se ha ido de "estancia" a otro lab, la echamos

mucho de menos, gracias por tu forma de ver la vida, siempre positiva, da igual lo que pase que nunca te derrumbas, por ser tan transparente y por las infinitas risas en las comidas. A Irene, por ayudarme en tantas cosas, por sacar neuronas suficiente para sembrar millones de placas en los malditos cultivos Aralar, por quedarte sin placas con tal de poner las mías, por hacer fácil hablar contigo. A todos los estudiantes nuevos que van llegando, Guillermo, David, Alba y muchos más.

A los que ya se fueron, obviamente el primero mi *Cahlo*, por tu acogida cuando llegué y no tenía ni idea de nada, por tu paciencia y por enseñármelo absolutamente todo; técnicas, cultivos, análisis y hasta a pensar, porque no tengo duda alguna que serás un gran científico. A Iren, una de las mejores personas que conozco, me siento superafortunada de haberme cruzado contigo, gracias por todas las cosas que me has enseñado, no sólo científicas, por estar disponible siempre que tengo un problema aun estando lejos. A Nacho, con el que coincidí poquito, pero suficiente para aprender sitios de Madrid donde escuchar buena música, y por supuesto para escuchar la suya.

No todo se queda dentro del 321. Primero tengo que darle las gracias a mi profesor de la Universidad de Málaga que me dio por primera vez la oportunidad de entrar en un laboratorio de Bioquímica, Javier Márquez. A Carolina, mi primera profe de laboratorio y de la que aprendí muchísimo, por tus risas y tu tiempo, gracias. Gracias a nuestros vecinos-hermanos científicos, los Cuezva, en especial a Maria, Javi, Fulvio, Pau, Cris y Yoli (Cristina para la familia), por hacer casi de su laboratorio una extensión del nuestro, si nos falta algo sólo tenemos que cruzar enfrente, y por las cervezas de los viernes recordando historias. A Enrique, por estar siempre dispuesto a echar una mano, por acordarte y preguntarme cada vez que nos cruzamos en el pasillo. A Jose Antonio Esteban y su laboratorio, por haber tenido tanto interés en el proyecto y la paciencia para enseñarme un poquito de electrofisiología. A Nathan, por la hora de terapia de todas las semanas, muchas gracias por tu apoyo durante todo este tiempo, y por preocuparte por mí. A los servicios de microscopia, genómica y citometría por hacer suyos mis problemas, y hacer todo lo posible por solucionarlos.

A Francesc Palau y su laboratorio de Valencia. A David, Manoli, Paula, Fátima, Arantxa, Edu y Azahara, por su gran acogida durante el tiempo que estuve con ellos. A Manoli y Paula en especial, por lo bien que trabajáis, por enseñarme tanto sobre CMT, por vuestra humildad y el cariño que me disteis y que todavía siento.

A mi máster, no pude tener más suerte cuando llegue a Madrid que encontraros a vosotros, a todos: Yasir, Eneko, Gabi, Ana, Isa Plasen, Isa Móstoles, Carlos, Ángela, Andrea, Isa, Arturo y Manu (porque sabes que eres del máster no?). Gracias por las conversaciones infinitas, por las divertidas discusiones, por las cervezas entre horas, y por la Fontana y las salidas un lunes hasta las 7 de la mañana. Mención especial se merecen Isa y Arturo, por muchísimas cosas, por

cuidarme tanto, por traerme tarta el día de mi cumpleaños, por estudiar hasta la madrugada antes de un examen, y porque ahora que estamos un poco más alejados los echo muchísimo de menos.

A Andrea y Amaya, porque sin ellas, literalmente, esta tesis no estaría escrita a día de hoy. Andrea, eres una de las mejores cosas que me ha dado el mudarme a Madrid y elegir ese máster, muchas gracias por salir en mi auxilio cuando más lo necesitaba, y por haberme traído a Amaya. Gracias por dejarme llenar el piso de papers y versiones de tesis, por leértela y corregírmela, por hacerme la comida cuando no hacía otra cosa en 24 horas que teclear en el ordenador, por las noches de Brooklyn 99 que me han mantenido cuerda, y por hacerme sentir en casa desde el segundo 0. Jamás podré agradeceros lo suficiente que me acogierais en vuestra casa sin tener espacio, que montarais una cama en mitad del salón y que me dijerais que si no salía bien nos íbamos las tres juntas a otro piso.

A mis químicos, a Laura, por tener la capacidad de hacer que yo misma me conteste a las preguntas nada más levantar el teléfono, por todas las noches en tu casa o en la mía estudiando prácticamente juntas todas las asignaturas de la carrera. A Jessy, porque de ti he aprendido muchas cosas, una de las que más admiro es tu entrega a los demás, y si todavía a día de hoy sigo teniendo algo de fe en la humanidad, es por ti. A las dos por ayudarme tanto en la carrera, y por quitarme los agobios antes de los exámenes con una sola frase. A Javi, porque aunque todavía estoy buscando algo más que tengamos en común que nuestro amor hacia la cerveza, siempre estás ahí cuando te escribo, porque haces que me ría a carcajadas y me haces hacer cosas locas, como meter pies en alcantarillas. Soy muy afortunada de teneros todavía en mi vida, sé que os tendré siempre y sabéis que juntos formamos un equipo perfecto.

A mis niñas, las primarias y auténticas, Noe, Mery, Sara y Vero, por estar ahí siempre, sea lo que sea y cuando sea, desde pequeñitas cuando nos pasamos la tarde en el murillo o cuando nos veíamos en el banquito todos los días después de cole, porque al teneros a vosotras es imposible sentirse nunca sola. Gracias porque aunque ahora vivimos un poco repartidas por el mundo, cuando nos vemos parece que el tiempo no ha pasado, gracias por las infinitas noches de Heineken, El Cosa y Pandillero juvenil.

A Chema, porque si esta tesis lleva sacrificio mucha parte es suya. Gracias por haberme acompañado durante todo este proceso haciendo de mi vida un lugar habitable y maravilloso, por haberme dado fuerzas para poder con todo, por haberme apoyado siempre. Gracias por hacerme ser quien soy, por enseñarme a no tenerle miedo a nada, y por: *si no luchas por tus sueños, ¿quién luchara por ellos? Si no luchas por tu vida, dala por perdida*.

Finalmente lo más importante, mi familia. A mis padres y mi hermana Albich, porque sois lo más maravilloso que podría haberme imaginado nunca. Infinitas gracias por haberme apoyado siempre. Por enseñarme que las cosas cuestan pero el esfuerzo siempre merece la pena, por

repetirme una y otra vez que las cosas pasan, porque la voluntad nunca hay que quitársela a las personas, por estar siempre disponibles para mí, por las conversaciones en las que no tenemos nada especial que contarnos, por los viajes exprés a Madrid sólo para conducir un coche a Málaga, porque sabéis cuando tengo un mal momento, y porque sin vuestros ánimos todo sería mucho más cuesta arriba. Os quiero.

INDEX

FIGURE INDEX

ABBREVIATIONS

2-APB: 2-Aminoethoxydiphenyl borate

Ach: Acetylcholine

AGC: Aspartate glutamate carrier

Ant: Antimycin A

ANT: Adenine nucleotide translocase

BAPTA-AM: 1,2-bis (2-aminophenoxy) ethane-N,N,N',N'-tetraacetic

BHQ: 2,5-di-tert-butylhydroquinone

CaMC: Calcium binding mitochondrial carrier

Ca_{mit}: Mitochondrial calcium

CCE: Capacitative Ca^{2+} entry

Cch: Carbachol

CICR: Calcium-induced calcium release

CMT: Charcot-Marie-Tooth disease

CNS: Central nervous system

CNQX: 6-cyano-7-nitroquinoxaline-2,3-dione

DAG: Diacylglycerol

DHPG: (S)-3,5-dihydroxyphenylglycine

DIV: Days *in vitro*

DL-TBOA: DL-Threo-β-Benzyloxyaspartic acid

DMEM: Dulbecco´s modified eagle´s medium Ham´s Nutrient Mixture F-12

DNP: 2,4-dinitrophenol

ER: Endoplasmic reticulum

ETC: Electron transport chain

GDAP1: Ganglioside-induced differentiation associated protein 1

GPCR: G-protein coupled receptor

HCSS: Hepes-buffered control solution

IMM: Inner mitochondrial membrane

I_{CRAC}: Ca^{2+}-release-activated Ca^{2+} current

IP_3: Inositol 1,4,5-triphosphate

IP_3R: Inositol triphosphate receptor

I_{SOC}:	Store-operated current
LTD:	Long-term depression
LTP:	Long-term potentiation
mAChR:	Muscarinic acetylcholine receptor
MAMs:	Mitochondrial-associated membranes
MAS:	NADH malate-aspartate shuttle
MCU:	Mitochondrial calcium uniporter
MCV:	Motor nerve conduction velocity
mEPSC:	Mini excitatory postsynaptic current
mGluR:	Metabotropic glutamate receptor
MK-801:	(5S,10R)-(+)-5-Methyl-10,11-dihydro-5H-dibenzo[a,d]cyclohepten-5,10-imine hydrogen maleate
nAChR:	Nicotine acetylcholine receptor
NCX:	Na^+/Ca^{2+} exchanger
NCLX:	Mitochondrial Na^+/Ca^{2+} exchanger
OCR:	Oxygen consumption rate
Olig:	Oligomycin
OMM:	Outer mitochondrial membrane
OXPHOS:	Oxidative phosphorylation
PIP_2:	Phosphatidylinositol 4,5-biphosphate
PLCβ:	Phospholipase C β
PMCA:	Plasma membrane Ca^{2+}-ATPase
PNS:	Peripheral nervous system
Pyr:	Pyruvate
rAAV:	Recombinant adeno-associated virus
Rot:	Rotenone
RyR:	Ryanodine receptor
SCaMC:	Short calcium binding carrier
SERCA:	Sarcoendoplasmic reticulum calcium ATPase
shRNA:	Small hairpin RNA
SOCE:	Store-operated calcium entry
STIM:	Stromal interaction molecule

TCA:	Tricarboxylic acid cycle
Tg:	Thapsigargin
TRPC:	Transient receptor potential channels
TTX:	Tetrodotoxin
VGCC:	Voltage gated calcium channels
$\Delta\mu H^+$:	Proton electrochemical gradient
$[Ca^{2+}]_i$:	Cytosolic calcium

PRESENTACIÓN

El calcio (Ca^{2+}) es un segundo mensajero que regula numerosos procesos en las células eucariotas (Brini et al., 2013). Por ello, la concentración de Ca^{2+} está altamente regulada en los diferentes compartimentos celulares. Este control es especialmente relevante en neuronas, en las que se llevan a cabo procesos como la transmisión sináptica y plasticidad sináptica, implicados en diversas funciones como la memoria o el aprendizaje y que están regulados por calcio (Cavazzini et al., 2005, Zucker, 1999). Además de canales iónicos, intercambiadores o bombas iónicas que controlan la concentración de Ca^{2+} en el interior celular (Grienberger and Konnerth, 2012), el retículo endoplasmático (RE) y la mitocondria ejercen un papel muy importante en la homeostasis del Ca^{2+} en la célula (Verkhratsky, 2005, De Stefani et al., 2016). Uno de los mecanismos moleculares implicado en la regulación de los niveles de Ca^{2+} celulares es el denominado *store-operated calcium entry* (SOCE), mecanismo que se activa cuando disminuyen los niveles de Ca^{2+} del RE y que conduce a la entrada de Ca^{2+} del exterior celular al citosol (Putney, 1986). Aunque inicialmente se relacionó al SOCE con el relleno de Ca^{2+} de los depósitos intracelulares, en la actualidad se considera que sus funciones fisiológicas son más amplias.

En esta tesis doctoral, uno de los objetivos que se propusieron fue investigar la desregulación de la homeostasis del Ca^{2+} en un modelo celular de la neuropatía de Charcot-Marie-Tooth (CMT) causada por mutaciones en el gen *GDAP1*. La proteína GDAP1 se localiza en la membrana externa de la mitocondria (Wagner et al., 2009) y se ha relacionado con procesos de fisión y fusión mitocondrial (Niemann et al., 2005, Pedrola et al., 2008, Niemann et al., 2009, Huber et al., 2013) o del control redox (Noack et al., 2012, Niemann et al., 2014). Resultados obtenidos en nuestro laboratorio y realizados en colaboración con el grupo de investigación del Dr. Francesc Palau utilizando un modelo de silenciamiento de la proteína GDAP1 en la línea de neuroblastoma humano SH-SY5Y, indicaron que la proteína GDAP1 interacciona con las proteínas de transporte vesicular RAB6B y caytaxina (Pla-Martin et al., 2013), involucrando a GDAP1 en el movimiento mitocondrial. Además, la interacción RE-mitocondria se encontraba alterada. Estudiando procesos de movilización de Ca^{2+} del RE, hemos encontramos una reducción de la entrada de Ca^{2+} a través del SOCE en las células silenciadas para GDAP1. Esta disminución se asoció a un fallo en la captura del Ca^{2+} por parte de la mitocondria, función que se ha descrito relevante para evitar la auto-inactivación del canal dependiente de Ca^{2+} ((Valero et al., 2008, Nunez et al., 2006, Malli et al., 2003) y resultados obtenidos en esta tesis). El impedimento para capturar Ca^{2+} en las mitocondrias deficientes en GDAP1 no se debe a un problema de la propia captura de Ca^{2+} sino a un problema en su localización subcelular (Pla-Martin et al., 2013). Tras la activación del SOCE, la ausencia de GDAP1 impide la correcta localización de las mitocondrias cerca del canal del SOCE en la membrana plasmática imposibilitando la correcta captura de Ca^{2+}.

Hemos investigado las consecuencias funcionales de la disminución del SOCE utilizando la línea celular de neuroblastoma humano SH-SY5Y, y hemos observado que el Ca^{2+} que entra por

los canales SOCE tiene la capacidad de estimular la respiración mitocondrial, siendo la señalización del Ca^{2+} (independientemente del incremento en el gasto de ATP) necesaria para la correcta estimulación, como se ha descrito en neuronas corticales (Llorente-Folch et al., 2013, Rueda et al., 2014). Sin embargo, en las células deficientes en GDAP1 hemos encontrado un fallo en la estimulación de la respiración dependiente de SOCE. Ampliando el estudio a variantes mutadas de GDAP1 descritas en pacientes de CMT, hemos observado que mutaciones recesivas de GDAP1 localizadas en el α-loop (dominio de interacción proteína-proteína) presentan las mismas alteraciones que la deficiencia de GDAP1, lo que sugiere que el mecanismo patológico de la enfermedad de CMT causada por mutaciones recesivas de GDAP1 localizadas en el α-loop podría deberse a alteraciones/deficiencias bioenergéticas de las neuronas implicadas.

El otro objetivo de esta tesis doctoral es el estudio del SOCE en neuronas. Este mecanismo ha sido ampliamente estudiado en células no excitables, pero su papel en neuronas es controvertido (Lu and Fivaz, 2016). En este trabajo, hemos encontramos que el SOCE tiene lugar en neuronas corticales primarias de ratón, pero, al contrario de lo que observamos en la línea celular de neuroblastoma, el SOCE en neuronas no está regulado por la captura de Ca^{2+} por parte de la mitocondria. Hemos investigado además la participación del SOCE en estímulos fisiológicos capaces de movilizar el Ca^{2+} del RE, como son la estimulación de los receptores muscarínicos de acetilcolina (mAChRs) y los receptores metabotrópicos de glutamato (mGluRs), observando en ambos casos la participación del SOCE. Encontramos que la actividad SOCE es necesaria para que la estimulación de los receptores muscarínicos incremente las señales oscilatorias espontáneas de Ca^{2+}. Dado que la señalización de Ca^{2+} estimula la respiración mitocondrial y la producción de ATP (Llorente-Folch et al., 2013), nos propusimos estudiar la posible implicación de este mecanismo en el metabolismo energético, y observamos que el aumento de las señales de Ca^{2+} mediado por un agonista muscarínico tiene la capacidad de estimular la respiración mitocondrial, siendo la actividad de la lanzadera de NADH ARALAR-MAS indispensable para el correcto acoplamiento de la señal de Ca^{2+} y la estimulación de la fosforilación oxidativa. En relación a los mGluRs, investigamos la función del SOCE tanto en la propia señal de Ca^{2+} citosólica inducida por agonistas de mGluR como en una de las funciones más estudiadas de estos receptores en el SNC, la depresión a largo plazo (LTD), y observamos que la activación del SOCE era necesaria tanto para el correcto mantenimiento de Ca^{2+} citosólico tras la estimulación de los mGluRs como para la generación de LTD mediada por los mGluRs usando estimulación química. Todos estos resultados sugieren no solo la existencia del SOCE en neuronas sino un papel relevante en varios procesos, como se ha postulado recientemente (Majewski and Kuznicki, 2015).

ABSTRACT

Calcium (Ca^{2+}) is a universal second messenger in eukaryotic cells that regulates numerous cellular processes. Cells have developed highly specific mechanisms to control the concentration of Ca^{2+} in each cellular location. The store-operated calcium entry (SOCE) is a mechanism that allows Ca^{2+} influx from the external medium into the cytosol when the ER-Ca^{2+} levels decrease, being one of its functions the replenishment of intracellular Ca^{2+} stores. We have addressed the role of SOCE in different neural cells, neuroblastoma cells and primary mouse cortical neurons. In neuroblastoma cells, we have found that SOCE activity is facilitated by mitochondrial Ca^{2+} uptake, preventing its Ca^{2+}-dependent inactivation and Ca^{2+} entry through SOC channels impacts on cell metabolism, stimulating mitochondrial respiration. SOCE-driven Ca^{2+} entry and SOCE-stimulated respiration were impaired in a cellular model of Charcot-Marie-Tooth disease caused by *GDAP1* gene, suggesting that a failure in bioenergetics may be a pathological mechanism involved in the disease. In neurons, the existence of SOCE pathway is under debate, but we have found that SOCE takes place in cortical neurons, although contrary to findings in neuroblastoma cell lines, it is not modulated by Ca^{2+} uptake into mitochondria. Moreover, we have investigated the role of neuronal SOCE in the response to physiological stimuli which have the ability to mobilize Ca^{2+} from intracellular stores, and we found that SOCE is involved in both mAChRs and mGluRs function: a) SOCE plays a role in muscarinic-enhanced spontaneous Ca^{2+} oscillations and the subsequent stimulation of mitochondrial respiration; and b) SOCE is required for the response to the mGluRs I agonist DHPG, to maintain cytosolic Ca^{2+} and develop DHPG-LTD.

INTRODUCTION

1. Charcot-Marie-Tooth disease caused by mutations in *GDAP1* gene

Charcot-Marie-Tooth (CMT) disease is a peripheral motor and sensory neuropathy. It is one of the most common inherited neuromuscular diseases with a population prevalence of 1 in 2500 (Reilly et al., 2011). CMT is characterized by distal wasting, weakness and sensory loss that starts in the lower limbs and progresses slowly in a length-dependent manner. This neuropathy is divided into demyelinating and axonal forms on the basis of motor nerve conduction velocities (MCVs) (Juarez and Palau, 2012). More than 60 genes have been linked to CMT disease (Rossor et al., 2013), which encode proteins with different locations, Schwann cells and axons, and that are involved in very different functions, including compaction and maintenance of myelin, transport through myelin, transcription regulation associated with myelination, cell signaling, cytoskeleton formation, axonal transport, mitochondrial dynamics and metabolism, vesicle and endosomal trafficking, and chaperones. Whatever the metabolic or structural defect that primarily affects the myelin or the axon, the final common pathway in peripheral neuropathies is represented by an axonal degenerative process (Krajewski et al., 2000, Scherer and Wrabetz, 2008, Juarez and Palau, 2012).

Mutations in the *GDAP1(ganglioside-induced-differentiation-associated protein 1)* gene show phenotypic and Mendelian heterogeneity in CMT patients and lead to several forms of CMT including recessive demyelinating (CMT4A) (Baxter et al., 2002), recessive axonal (AR-CMT2K) (Cuesta et al., 2002), recessive with intermediate clinical features (CMTRIA) (Senderek et al., 2003) and a dominant inheritance pattern and axonal features (CMT2K) (Claramunt et al., 2005, Sivera et al., 2010).

GDAP1 is highly expressed in neurons and it is localized to the mitochondrial outer membrane (Niemann et al., 2005; Pedrola et al., 2005). GDAP1 has a single transmembrane domain and its targeting to the outer mitochondrial membrane and function are dependent on its tail anchor (Wagner et al., 2009). This protein has two glutathione-S-transferase (GST) type domains (Marco et al., 2004) separated by a region called α-loop, and a C-terminal transmembrane domain. It has been related to mitochondrial fission/fusion (Niemann et al., 2005, Pedrola et al., 2008, Niemann et al., 2009, Huber et al., 2013) or redox processes (Noack et al., 2012, Niemann et al., 2014). Previous findings obtained in our laboratory carried out in collaboration with Francesc Palau´s research group using a *GDAP1*-silenced stable cell line, reported an interaction between GDAP1 and RAB6B, a protein involved in retrograde vesicle trafficking (Matanis et al., 2002), and caytaxin, a protein participating in the anterograde movement of mitochondria (Aoyama et al., 2009), which suggested a role of GDAP1 in mitochondrial transport within the cell. Both GDAP1 and RAB6B were located at the mitochondrial-associated membranes (MAMs), suggesting a possible role in the movement of

mitochondria toward the endoplasmic reticulum (ER). Therefore, the interaction between mitochondria and ER was investigated, and a marked reduction in contacts between these two organelles was found in *GDAP1*-silenced cells. However, transfer of ER-Ca^{2+} signals to mitochondria was not affected by GDAP1 deficiency (Pla-Martin et al., 2013). In the present Doctoral Thesis we decided to study in greater detail how GDAP1 depletion and different mutations of GDAP1 could disturb Ca^{2+} homeostasis and the mechanisms involved in this highly controlled equilibrium, together with a possible affectation in energy production by mitochondria as it has been previously hypothesized (Cassereau et al., 2011).

It is worth mentioning that due to the strategic localization of GDAP1 in the outer mitochondrial membrane, and the number of interacting partners of the protein, it is expected that mutations in the protein can give rise to numerous nonexclusive effects on cell function.

2. Physiological calcium signaling in neurons

Calcium (Ca^{2+}) is a universal second messenger that regulates numerous cellular processes of all eukaryotic cells, including the control of metabolism, muscle contraction, exocytosis, transcription of numerous genes or programmed cell death (Brini et al., 2013). It is of critical importance to neurons as it participates in the transmission of synaptic information and many forms of activity-dependent synaptic plasticity acting both in the presynaptic and/or postsynaptic neuron (Cavazzini et al., 2005, Zucker, 1999).

The resting total calcium concentration in neurons is about 1 mM, however, baseline free Ca^{2+} in the cytosol is kept around 100 nM (Pivovarova and Andrews, 2010), it means that the vast majority of intracellular calcium is bound to cytosolic proteins or sequestered in intracellular stores, especially in the ER (Glancy and Balaban, 2012). One of the most important parts of Ca^{2+} signaling is the cell´s ability to regulate this signal, since cells use the concentration of Ca^{2+} as a mechanism to drive many cellular processes. In order for a cell to elicit a cellular response due to a Ca^{2+} signaling, it must be able to regulate the concentration of Ca^{2+} in different cellular locations. Thus, neurons have developed a sophisticated mechanism that balances Ca^{2+} levels.

2.1 The neuronal Ca^{2+} signaling toolkit

Ion channels, exchangers, and pumps both in the plasma membrane and the membranes of mitochondria, endoplasmic reticulum, Golgi apparatus and nucleus contribute to the Ca^{2+} toolkit. All of them together with the action of G-couple receptor proteins (GPCRs) and Ca^{2+} binding proteins are involved in shaping neuronal Ca^{2+} signaling (Clapham, 2007). Figure 1 summarized some of the most important sources of neuronal Ca^{2+} signaling.

Ca^{2+} enters from extracellular medium by the plasma membrane channels, which can be classified in three groups according to their mechanism of opening: the voltage-gated Ca^{2+} channels (VGCCs), the receptor-operated Ca^{2+} channels (ROCs) and the store-operated Ca^{2+} channels (SOCs) (Brini et al., 2014). The VGCCs use the electrochemical gradient of the plasma membrane to control the Ca^{2+} inflow. They are able to create a huge increase in intracellular Ca^{2+} concentration in a matter of milliseconds, having a critical role in the generation and propagation of the action potential (Benarroch, 2010). The ROCs are activated by the binding of specific ligands to the extracellular domain. In this group are the ionotropic glutamate receptors: the N-methyl-D-aspartate receptors (NMDARs), which mediate the major part of the postsynaptic Ca^{2+} influx in the dendritic spines, being particularly important in long-term modifications of synaptic strength (Zucker, 1999), and the Ca^{2+}-permeable α-amino-3-hydroxil-5-methyl-4-isoxazolepropionic acid receptors (AMPARs), which mediate fast excitatory synaptic transmission in central nervous system (CNS); and the ionotropic nicotine acetylcholine receptors (nAChRs) (Grienberger and Konnerth, 2012). The G-protein coupled receptors, as metabotropic glutamate receptors (mGluRs) or metabotropic acetylcholine receptors (mAChRs) are also included in this group. They are widely distributed in the CNS and generate Ca^{2+} signals through the activation of distinct downstream signaling cascades (Niswender and Conn, 2010, Ishii and Kurachi, 2006). Other ROCs are the purinergic receptors, the ARC channels and the transient receptor potential (TRP) channels (Brini et al., 2014). Finally, the SOCs channels are activated by the emptying of the Ca^{2+} stores, in a process named store-operated Ca^{2+} entry (SOCE). SOCE function is not limited to refilling the intracellular Ca^{2+} stores, as was originally proposed (Putney, 1986), but can elicit a Ca^{2+} response itself (Majewski and Kuznicki, 2015).

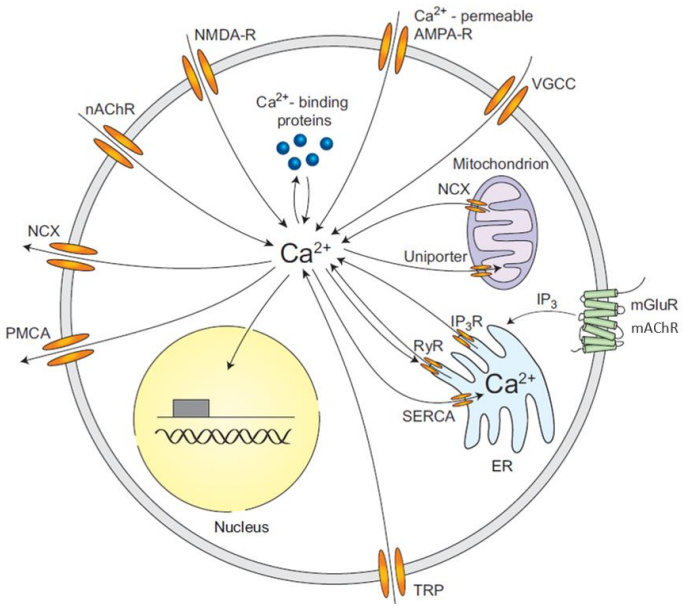

Figure 1. Neuronal Ca^{2+} signaling toolkit. Calcium enters through N-methyl-D-aspartate receptors (NMDARs), calcium-permeable a-amino-3-hydroxy-5-methyl-4-isoxazolepropionic acid receptors (AMPARs), voltage-gated calcium channels (VGCCs), nicotinic acetylcholine receptors (nAChR), and transient receptor potential (TRP) channels. Metabotropic glutamate and acetylcholine receptors mobilize Ca^{2+} from intracellular stores by IP_3 receptors. Calcium efflux is mediated by the plasma membrane calcium ATPase (PMCA), the sodium-calcium exchanger (NCX), and the sarco-/endoplasmic reticulum calcium ATPase (SERCA). Also, mitochondria are important for neuronal calcium homeostasis by Ca^{2+} uptake through MCU. Modified from (Grienberger and Konnerth, 2012).

Ca^{2+} extrusion from the cytoplasm is carried out by ion pumps in the plasma membrane, which are NCX, the Na^{+}/Ca^{2+} exchanger, Na^{+}/K^{+} ATPase pump and PMCA, the Ca^{2+}/H^{+} ATPase exchanger, their function is totally necessary especially when dealing with large increases in the intracellular Ca^{2+} concentration, as actions potentials (Karlstad et al., 2012).

Finally, organelles also have a relevant role in the control of Ca^{2+} homeostasis. In particular, Ca^{2+} uptake, sequestration and release by the endoplasmic reticulum and mitochondria, the two major Ca^{2+}-regulating organelles, play essential roles in modulating and interpreting Ca^{2+} signals.

2.2 The endoplasmic reticulum

Neurons have an elaborate endoplasmic reticulum that extends throughout the cell. It is a continuous dynamic network of tubular membranes that connect the soma to the neuron´s dendritic and axonal arbors and protrudes into large dendritic spines, where it finally terminates as the spine apparatus (Bourne and Harris, 2012, Spacek and Harris, 1997).

The ER represents the main Ca^{2+} store in neurons and contributes to the dynamics of Ca^{2+} signaling by acting either as a source or as a sink of Ca^{2+} (Berridge, 1998). ER calcium stores are activated by two types of receptors, the inositol 1, 4, 5-trisphosphate receptor (IP_3R), and the ryanodine receptor (RyR). The IP_3R family comprises three isoforms, 1-3, and the predominant neuronal one is IP_3R1. The RyR also has three isoform, RyR, 1-3, which are primarily found in muscle cells, and are responsible for contraction, but are also found throughout the brain (Verkhratsky, 2005). IP_3-mediated Ca^{2+} release is mostly triggered by neurotransmitters such as glutamate or acetylcholine, while RyR can be activated by elevation of the cytosolic Ca^{2+} levels (Figure 1). This process is named Ca^{2+}-induced Ca^{2+} release (CICR) and it has been involved in the amplification of the Ca^{2+} influx generated by action potential firing in neurons (Tsien and Tsien, 1990). Both IP_3 and RyR are regulated by different factors, but maybe the most important one is Ca^{2+} itself, being the most effective activation when Ca^{2+} and IP_3 are presented together (Berridge, 1993). ER-Ca^{2+} uptake plays a role in ensuring the maintenance of resting cytosolic Ca^{2+} levels, this function is carried out by the activity of sarco(endo)plasmic reticulum calcium ATPase (SERCA), which includes three isoforms, 1-3 (Verkhratsky, 2005).

The characteristic structure, which allows ER to integrate information over long distances, and the capability to uptake/release Ca^{2+} upon a synaptic stimulus, make this organelle a key player in synaptic plasticity. Thus, the involvement of calcium stores in neuronal plasticity has been studied extensively (Bardo et al., 2006, Fitzjohn and Collingridge, 2002, Maggio and Vlachos, 2014). Earlier, the importance of Ca^{2+} stores was demonstrated by the blocking of LTD by drugs interfering the release of Ca^{2+} from stores (Harvey and Collingridge, 1992). ER-Ca^{2+} mobilization by the action of acetylcholine has been shown to be related with a subsequent change in AMPARs and NMDARs functions (Fernandez de Sevilla et al., 2008). And IP_3-dependent Ca^{2+}

release in dendritic spines plays a key role in long-term depression (LTD) in cerebellum (Miyata et al., 2000) and hippocampus (Holbro et al., 2009). In presynaptic terminals, it has been recently shown that ER-Ca^{2+} levels controls the neurotransmitter release (de Juan-Sanz et al., 2017).

2.3 The mitochondrion

Mitochondria are the other major players in the regulation of Ca^{2+} signals, but they also perform a wide range of essential cellular functions, several of them controlled by Ca^{2+} itself. The best known is the synthesis of ATP by oxidative phosphorylation (OXPHOS), but also these organelles contain several metabolic pathways such as the citric acid cycle and β-oxidation of fatty acids (Nunnari and Suomalainen, 2012). Mitochondria are the main site where reactive oxygen species are generated and they are fundamental for certain biological processes such as calcium cell signaling, heat production, cell proliferation and necrotic or apoptotic cell death.

The mitochondrion is a double-membrane organelle present in eukaryotic cells. Outer mitochondrial membrane (OMM) has a protein-to-phospholipid ratio similar to eukaryotic plasma membrane and contains a large number of integral proteins, porins, that allow molecules of 4-5 KDa or less molecular weight to freely diffuse from one side to the other (Benz et al., 1990). Contrary, the inner mitochondrial membrane (IMM) is highly impermeable to almost all ions and molecules requiring special membrane transporters to enter or exit the matrix. Inner membrane cisternal invaginations called cristae house assembled respiratory complexes and have highly curved edges that are stabilized by the dimerization or multimerization of ATP synthase complexes (Davies et al., 2012).

2.3.1 Mitochondrial Ca^{2+} handling

Mitochondrial Ca^{2+} uptake and release modulate the dynamic of cytosolic Ca^{2+} signals and may thus influence neuronal behavior. Mitochondrial Ca^{2+} buffering decreases the peak amplitude of stimulus-induced cytosolic Ca^{2+} transients and slows the recovery by slowly recycling Ca^{2+} into the cytosol (Brocard et al., 2001, Wang and Thayer, 2002, Wang and Thayer, 1996, White and Reynolds, 1995). It has been described that mitochondria may participate in certain forms of synaptic plasticity, due to the capacity of shaping the spatiotemporal pattern of cytosolic Ca^{2+} (Kann and Kovacs, 2007).

Ca^{2+} accumulation into the mitochondrial matrix requires the crossing of two membranes. OMM permeability is attributed to the abundant expression of porins, which are also involved in the transport of ATP, ADP, pyruvate, malate, and other metabolites (Blachly-Dyson and Forte, 2001). The mitochondrial calcium uniporter (MCU) is the channel that mediates Ca^{2+} entry into the mitochondrial matrix (De Stefani et al., 2011, Baughman et al., 2011). Different proteins have been shown to interact with MCU, forming the MCU complex and modulating its properties (Fig.

2) (Raffaello et al., 2016). Proteins forming the MCU complex include the essential MCU regulator (EMRE) (Sancak et al., 2013), the Ca^{2+} sensitivity modulators MICU1 and MICU2 (Perocchi et al., 2010, Mallilankaraman et al., 2012b, Patron et al., 2014), the dominant negative subunit MCUb (Raffaello et al., 2013), and the regulator (MCUR) (Mallilankaraman et al., 2012a). However, other routes of Ca^{2+} entry are under debate, which may be responsible for the residual mitochondrial Ca^{2+} uptake in MCU deficient cells (Pan et al., 2013).

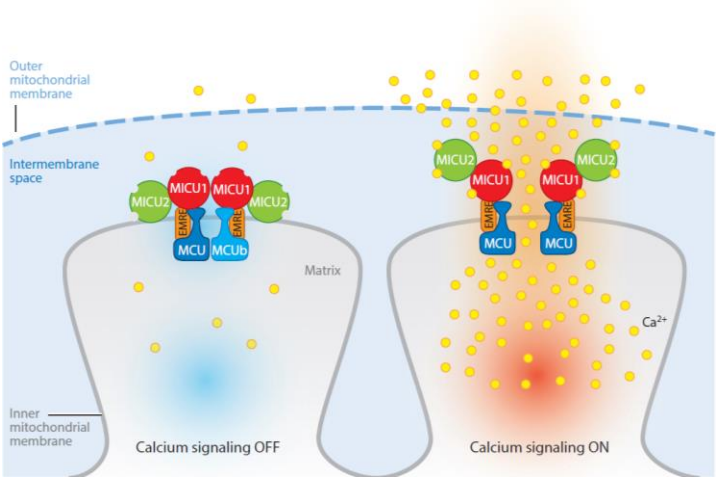

Figure 2. Schematic representation of the Mitochondrial Calcium Uniporter (MCU) complex. Left: In resting condition, mitochondrial Ca^{2+} uptake is controlled by a complex that can consist of MCU and MCUb (the channel-forming subunits) together with EMRE, MICU1, and MICU2. In particular, MICU1/MICU2 heterodimers act as MCU gatekeepers and prevent vicious calcium cycles. Right: Activation of cellular Ca^{2+} signaling results in an increase of cytosolic Ca^{2+} that induces a conformational change in MICU1/MICU2 heterodimers and triggers the MCU opening. From (De Stefani et al., 2016).

Efflux pathways are also essential for equilibrating mitochondrial and cytosolic Ca^{2+} (Takeuchi et al., 2015). The major pathway is the Na^+/Ca^{2+} exchanger (NCLX), which requires a Na^+ gradient for Ca^{2+} extrusion generated by the Na^+/H^+ exchanger (Palty et al., 2010). The role of the Ca^{2+}/H^+ exchanger remained elusive (Waldeck-Weiermair et al., 2011, Drago et al., 2011).

A relevant aspect of mitochondrial Ca^{2+} handling is related to the fact that mitochondria are highly motile organelles, showing anterograde and retrograde transport in dendrites and axons (Mironov, 2006). Mitochondria are transported along microtubules by the dynein-kinesin system, and along filaments by myosin motors (Hollenbeck and Saxton, 2005). It is known that mitochondrial transport is regulated by cytosolic Ca^{2+} concentration, being anchored in domains with high Ca^{2+} levels (Rintoul et al., 2003, Cai and Sheng, 2009). Recently, it has been shown that the matrix Ca^{2+} also acts as a signal regulating mitochondrial motility (Chang et al., 2011). This mechanism may enhance mitochondrial Ca^{2+} uptake and serve for energy supply in response to local demands (Yi et al., 2004).

2.3.2 Ca^{2+} regulation of mitochondrial functions: Mitochondrial respiration

One of the main mitochondrial functions is the ATP synthesis by oxidative phosphorylation. Glycolysis is able to produce ATP in the cytosol but, in aerobic cells, the majority of ATP is produced by the ATP synthase. ATP levels are strictly controlled and ATP expenditure is tightly linked to ATP production (Glancy and Balaban, 2012).

OXPHOS is the metabolic pathway in which cells use enzymes to oxidize nutrients, thereby releasing energy which is used to synthesize ATP. This process takes place into the mitochondrion, in the IMM, where the electron transport chain (ETC) and the ATP synthase are located. The ETC transfers electrons from NADH in the complex I or succinate-$FADH_2$ in complex II, through the ubiquinone pool, complex III and cytochrome C to complex IV, where they are transferred to O_2, generating H_2O. This electron movement is used to generate a proton electrochemical gradient ($\Delta\mu H^+$), which is mainly used to synthesize ATP from ADP in the ATP synthase (Complex V) (Mitchell and Moyle, 1967).

In excitable cells, Ca^{2+} regulates cell function both by activation of ATP consumption (contraction, movement, Ca^{2+} pumps) and by activating ATP production through stimulation of OXPHOS (Hayakawa et al., 2005, Glancy and Balaban, 2012, Rizzuto et al., 2012, Jouaville et al., 1999). This Ca^{2+}-activated increase in ATP production by OXPHOS may result in metabolic homeostasis, i.e. an increase in workload under conditions where the ATP/ADP and $NADH/NAD^+$ levels remain constant, as described by (Glancy and Balaban, 2012), or it may only result in metabolic changes in microdomains sensed by the appropriate targets. Recently, our group has demonstrated that Ca^{2+} signaling in mitochondria, independent of Ca^{2+}-increased ATP demand, is required to stimulate respiration under different workloads in intact cortical neurons (Llorente-Folch et al., 2013, Llorente-Folch et al., 2015, Rueda et al., 2014).

Ca^{2+} regulation of OXPHOS is thought to occur thanks to two different mechanisms: i) Ca^{2+} entry in mitochondria, or ii) the action of Ca^{2+} on the external side of the inner mitochondrial membrane (Fig. 3).

2.3.2.1 Intramitochondrial calcium

Ca^{2+} entry in mitochondria through MCU regulates different enzymes in the matrix, including the tricarboxylic acid cycle (TCA) dehydrogenases: pyruvate dehydrogenase (PDH), isocitrate dehydrogenase (ICDH) and α-ketoglutarate dehydrogenase (α-KDH) (Denton, 2009, Balaban, 2009). Matrix Ca^{2+} also modulates F_1-F_oATPase activity by reducing its resistance to form ATP at a given driving force, and the complex III, but the specific mechanisms remains elusive (Glancy and Balaban, 2012). Moreover, OXPHOS is also regulated by the activity of the

adenine nucleotide translocase (ANT). The mitochondrial ANT performs an electrogenic exchange of ADP^{3-} with ATP^{4-} between the cytosol and the mitochondrial matrix without modifying the net content of AdNs (Klingenberg, 2008). It has been described that intramitochondrial calcium diminishes the ANT activity, concomitantly lowering ADP content, which affects F_1-F_oATPase activity (Moreno-Sanchez, 1983) (Fig. 3).

2.3.2.2 Extramitochondrial calcium

Calcium, in the external side of the IMM, can regulate mitochondrial respiration by activating the calcium binding mitochondrial carriers (CaMCs). This group of mitochondrial carriers is characterized by the presence of EF-hand domains oriented towards the intermembrane space, where they bind cytosolic calcium, and it is formed by two carriers: the aspartate glutamate carriers (AGCs) and the ATP-Mg^{2+}/Pi carriers (SCaMCs) (Satrustegui et al., 2007, del Arco and Satrustegui, 2004, Fiermonte et al., 2004).

Aspartate glutamate carriers (AGCs): These carriers catalyze the exchange of mitochondrial aspartate against cytosolic glutamate and constitute an essential part of the malate-aspartate shuttle (MAS) (Satrustegui et al., 2007). AGCs are activated by modest increases of extramitochondrial Ca^{2+} at concentrations not far from the resting state. For example, Aralar/AGC1, the isoform prevailing in the brain, has an $S_{0.5}$ of 324 nM Ca^{2+} (Palmieri et al., 2001, Pardo et al., 2006, Contreras et al., 2007). Extramitochondrial Ca^{2+} activation of Aralar/AGC1-MAS activity results in the net transfer of reducing equivalents (NADH) from the cytosol to mitochondria matrix, increasing substrate supply to mitochondria (Fig. 3). This transfer of NADH into the matrix enhances pyruvate production from glucose and lactate, regenerating NAD^+ in cytosol (Gellerich et al., 2012, Gellerich et al., 2013). In cortical neurons, the activity of Aralar/AGC1-MAS is essential to maintain the basal respiration and to response to different workload (Llorente-Folch et al., 2013, Rueda et al., 2014).

ATP-Mg^{2+}/Pi carriers (SCaMCs): These carriers perform the electroneutral exchange of ATP-Mg^{2-} or $HADP^-$ with HPO_4^{2-} between the cytosol and the mitochondrial matrix (Joyal and Aprille, 1992, Fiermonte et al., 2004). The SCaMCs are activated by extramitochondrial Ca^{2+} with an $S_{0.5}$ of activation within the range of the MCU complex of approx. 3–4 μM for the brain and liver isoform SCaMC-3/Slc25a23 (Amigo et al., 2013). SCaMC activity regulates the total adenine nucleotide pool in the mitochondrial matrix; the sum of ATP+ADP+AMP (Fig. 3), playing an important role in the regulation of the mitochondrial metabolic pathways. It has been shown to play an essential role in high workloads in neurons (Llorente-Folch et al., 2013, Rueda et al., 2014).

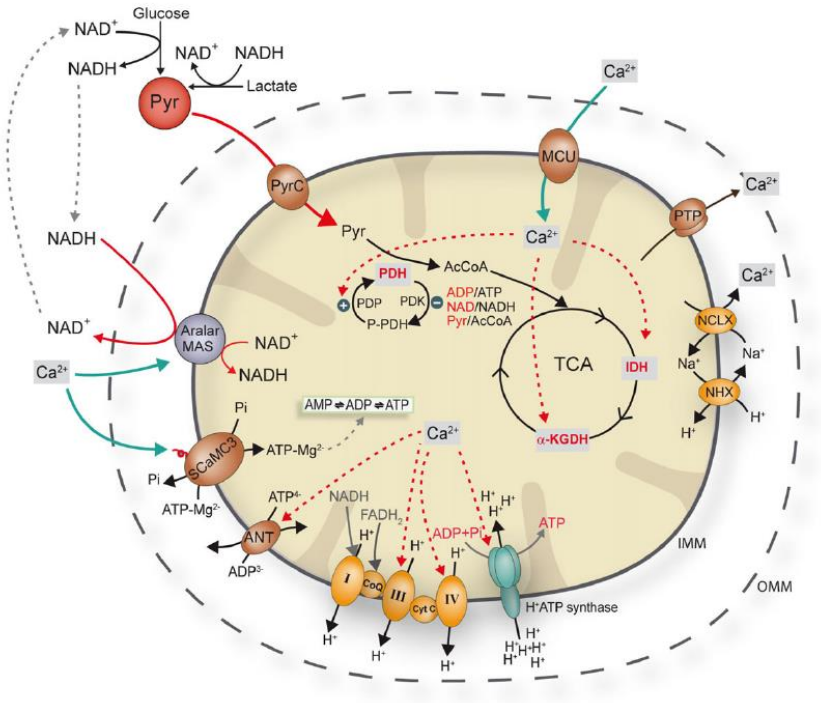

Figure 3. Schematic representation of Ca^{2+} regulation of mitochondrial respiration. Tricarboxylic acid cycle enzymes, the isocitrate dehydrogenase (IDH), the α-ketoglutarate dehydrogenase (α-KGDH), and the pyruvate dehydrogenase (PDH) are activated by matrix Ca^{2+}. Complex IV and complex III may also be regulated by intramitochondrial Ca^{2+}. Matrix Ca^{2+} may also regulate OXPHOS through an effect on the ANT and on the F_1F_o-ATP synthase. Extramitochondrial Ca^{2+} activates Aralar/AGC1-MAS activity and SCaMC-3. P-PDH, phosphorylated pyruvate dehydrogenase; PDK, pyruvate dehydrogenase kinase; PDP, pyruvate dehydrogenase phosphatase; Pyr, pyruvate; AcCoA, acetyl coenzyme A; TCA: tricarboxylic acid cycle; NHX, Na^+/H^+ exchanger. Taken from (Llorente-Folch et al., 2015).

3. The store-operated calcium entry

The concept of store-operated calcium entry was proposed in 1986 by Putney. This idea originated from a series of experiments in parotid acinar cells investigating the relationship between Ca^{2+} release from internal stores, Ca^{2+} entry, and store refilling. It was observed that the amount of Ca^{2+} in the ER controlled the extent of Ca^{2+} influx from the external medium. This process was initially called capacitative Ca^{2+} entry (CCE) (Putney, 1986). Later, it was renamed store-operated calcium entry (SOCE) to refer more explicitly to its mode of activation and to distinguish from receptor-, ligand- and voltage-operated Ca^{2+} channels. Electrophysiological studies provided evidences to support this Ca^{2+} entry mechanism. In mast cells, the process of emptying the stores activated a Ca^{2+} current called Ca^{2+}-release-activated Ca^{2+} current (I_{CRAC}) (Hoth and Penner, 1992), which is non-voltage activated and remarkably selective for Ca^{2+}, and it has been found in several cell types mainly of hemapoietic origin (Parekh and Penner, 1997). I_{CRAC} was the first store-operated current (I_{SOC}) described, but it is not the only one. It is now

apparent that store-operated influx includes a family of Ca^{2+}-permeable channels, with different properties in different cell types (Parekh and Putney, 2005).

Different molecular players have been shown to participate in SOCE (Albarran et al., 2016). Stromal interaction molecule (STIM) proteins are highly conserved sensors of Ca^{2+} concentration in the ER and ubiquitously expressed in different tissues (Williams et al., 2001). Both STIM1 and STIM2, a more Ca^{2+}-sensitive homologue, were described as essential proteins involved in SOCE (Brandman et al., 2007, Roos et al., 2005, Liou et al., 2005). Orai family proteins form the store-operated Ca^{2+} (SOC) channels in the plasma membrane (Feske et al., 2006, Yeromin et al., 2006, Rosado et al., 2015). Also the family of transient receptor potential cation (TRPC) channels has been proposed to act as SOC channels (Ambudkar et al., 2007, Worley et al., 2007, Dionisio et al., 2012), and an interaction between Orai, STIM1 and TRPC1 has been found (Cheng et al., 2008, Ambudkar et al., 2016). However, the role of TRPCs in SOCE is under debate (Choi et al., 2014, DeHaven et al., 2009).

Activation of SOCE by store depletion is a highly dynamic process. After a decrease in ER-Ca^{2+} levels, STIM and Orai proteins redistribute respectively and accumulate in clusters visualized as "puncta". Clusters accumulate in the ER-PM junctions where STIM can bind Orai, opening the channels and allowing Ca^{2+} influx into the cytosol (Lewis, 2007) (Fig. 4).

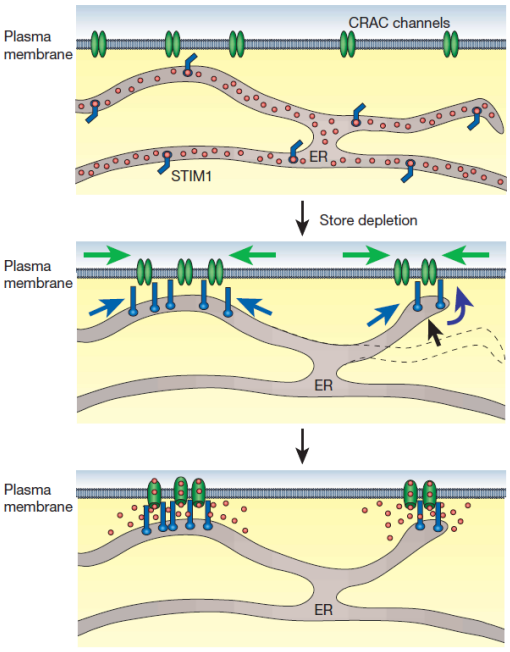

Figure 4. **Molecular choreography of SOCE**. In resting cells with replete Ca^{2+} stores (top panel), STIM and Orai are dispersed throughout the ER and plasma membrane, respectively. Store depletion (middle panel) causes STIM to accumulate at locations where the ER is juxtaposed to the plasma membrane. At the same time, Orai clusters accumulates in regions of the plasma membrane directly opposite to the STIM1 clusters. Interaction beteween STIM and Orai proteins activate de Ca^{2+} channel allowing calcium entry into the cytosol (bottom panel). From (Lewis, 2007).

3.1 Mitochondrial modulation of SOCE

Ca^{2+} entry through SOC channels can decline by i) the deactivation process, due to store refilling, or ii) Ca^{2+}-dependent inactivation. SOC channels have two types of Ca^{2+}-dependent

inactivation: i) fast Ca^{2+}-dependent inactivation, which is due to Ca^{2+} binding at a site within less than 10 nm of the pore (Lee et al., 2009, Derler et al., 2009) and ii) slow Ca^{2+}-dependent inactivation, which could be modulated by mitochondria.

Modulation of SOCE by mitochondria has been extensively investigated and results obtained vary in different cells types (Fonteriz et al., 2016). The condition of energized mitochondria has been found to be necessary to maintain the SOC channel activity (Hoth et al., 2000, Hoth et al., 1997, Gilabert and Parekh, 2000), but the molecular basis of mitochondrial maintenance of SOCE activity is not entirely clear. Nevertheless, it is thought that mitochondria prolong Ca^{2+} influx through SOC channels by buffering Ca^{2+}, preventing Ca^{2+}-dependent inactivation. In fact, a series of reports have shown that sustained SOCE requires normal mitochondrial Ca^{2+} uptake (Valero et al., 2008, Nunez et al., 2006, Malli et al., 2003). Similarly, knocking down MCU decreased Ca^{2+} entry through SOCE (Samanta et al., 2014, Tang et al., 2015, Deak et al., 2014) but see (Fonteriz et al., 2016). In this case, the proximity of mitochondria to SOC channels would be a critical point. According to this idea, several studies reported that mitochondria move closer to PM after ER depletion (Quintana et al., 2006, Quintana et al., 2007, Schwindling et al., 2010). However, mitochondrial subcellular location with respect to SOC channels appears to be highly variable among different cell types (Watson and Parekh, 2012) and the important for SOCE of mitochondrial motility has been questioned in other works (Naghdi et al., 2010, Frieden et al., 2004, Giacomello et al., 2010).

In addition, mitochondria may regulate SOCE by other mechanisms, as pyruvate release (Bakowski and Parekh, 2007), ATP production (Huang et al., 2014, Montalvo et al., 2006, Parekh, 2008) or Ca^{2+}-independent mechanisms (Singaravelu et al., 2011).

3.2 Neuronal SOCE

The presence of the SOCE mechanism in neurons has been questioned (Lu and Fivaz, 2016), since these cells have other major pathways, as VGCCs or receptor operated channels, to permit Ca^{2+} inflow from the external medium (Grienberger and Konnerth, 2012). But, in the last few years, SOCE activity has been observed in hippocampal (Emptage et al., 2001, Baba et al., 2003, Kann et al., 2012, Sun et al., 2014, Samtleben et al., 2015), cortical (Berna-Erro et al., 2009, Klejman et al., 2009, Gruszczynska-Biegala et al., 2011), cerebellar (Baba et al., 2003, Hartmann et al., 2014), sensory (Gemes et al., 2011) and dorsal horn neurons (Xia et al., 2014). Moreover, two independent groups found that STIM1 directly modulates depolarization-induced opening of the voltage-gated Ca^{2+} channel $Ca_{V1.2}$ (Park et al., 2010, Wang et al., 2010).

Neuronal SOCE is thought to perform different roles in resting neurons: the refilling of ER-Ca^{2+}, which is continuously emptying at rest (Samtleben et al., 2015), regulation of neuronal gene

expression (Lalonde et al., 2014), and the maturation and maintenance of dendritic spines (Sun et al., 2014, Korkotian et al., 2017). Other roles of SOCE during neuronal activity have been proposed. First by Baba et al., who found that SOCE contributes to elevate dendritic Ca^{2+} concentration during tetanic stimulation and participates in long-term potentiation (LTP) process in hippocampal slices (Baba et al., 2003). More recent findings suggest that SOCE may control neuronal Ca^{2+} dynamics during synaptic activity in different neurons. For example, a direct link between SOCE and AMPAR-dependent Ca^{2+} signal has been reported (Gruszczynska-Biegala et al., 2016); a mechanism that associates activation of postsynaptic NMDARs and L-types Ca^{2+} channels with signaling by the ER-Ca^{2+} sensor STIM1 has been proposed (Dittmer et al., 2017), and STIM1 has also been proposed to be a key regulator of Ca^{2+} signaling downstream metabotropic glutamate receptors (mGluRs) stimulation (Hartmann et al., 2014, Hou et al., 2015).

Moreover, deregulation of neuronal SOCE has been linked to Alzheimer´s and Huntington´s disease (Popugaeva et al., 2015, Sun et al., 2014, Wu et al., 2016, Zhang et al., 2015), among others neurological disorders (Moccia et al., 2015).

4. Muscarinic acetylcholine receptors. Role in modulating membrane excitability

The brain is highly innervated by cholinergic neurons and acetylcholine (ACh) modulates numerous brain functions (Prado et al., 2017). Cholinergic neurons from the basal forebrain provide the major input to the whole cortex, hippocampus, thalamus and amygdala (Woolf, 1991). ACh is an excitatory neurotransmitter in the peripheral nervous system (PNS) that plays an essential role in the neuromuscular junction. Instead, it acts as a neuromodulator in the central nervous system (CNS), where it may change neuronal excitability, alter presynaptic release of neurotransmitters or coordinate the firing of groups of neurons (Picciotto et al., 2012).

ACh signals through two classes of receptors: nicotinic acetylcholine receptors (nAChR), which are ligand-gated transmembrane channels (Picciotto et al., 2000) and muscarinic acetylcholine receptors (mAChR), which are G-protein coupled receptors (GPCRs). Different muscarinic receptors vary according to the Gα protein to which they are bound. M_1, M_3, and M_5 receptors are coupled to $G\alpha_{q/11}$, and so their activation upregulates phospholipase C-β (PLCβ), inositol triphosphate (IP_3), and calcium as downstream second messengers (Figure 5). The M_2 and M_4 receptors are coupled to $G\alpha_{i/o}$, which causes inhibition of cAMP production (Eglen, 2006).

Cholinergic stimulation has an essential role in modulating the intrinsic firing pattern of cortical neurons (Krnjevic, 1993). In the postsynaptic density, ACh acting via mAChRs may trigger membrane depolarization using different mechanisms: i) the modulation of a number of K^+ conductances (Giessel and Sabatini, 2010, Young et al., 2005, Buchanan et al., 2010) and/or

ii) the activation of nonselective cation conductances, as it has been shown in the persistent firing evoked by muscarinic receptors activation (Egorov et al., 2002, Andrade, 1991). The nonselective TRPC channels play a central role in activity-dependent plateau potentials and persistent activity induced by cholinergic agonists (Zhang et al., 2011). These functions, are mediated by the mAChRs coupled to $G\alpha_{q/11}$, probably by M_1-type receptors, which are the most abundant subtype in cortex and are mainly localized to cell bodies and neurites, consistent with a role as major postsynaptic muscarinic receptors (Levey et al., 1991).

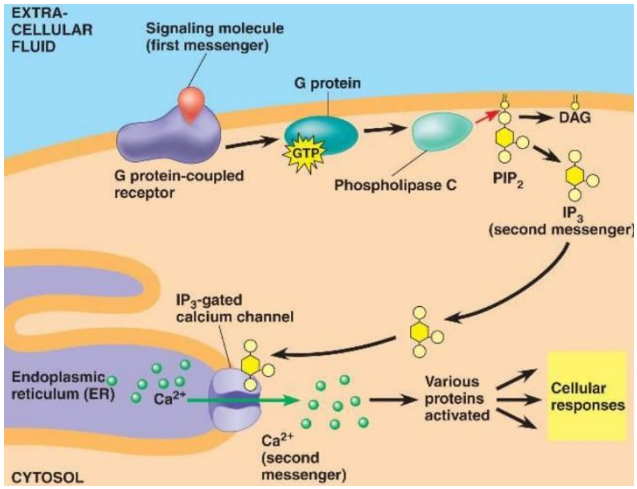

Figure 5. $G\alpha_{q/11}$ signaling pathway. Stimulation of mAChRs M1, M3, or M5, activates $G\alpha_{q/11}$ protein, which activates phospholipase C-β (PLCβ). Phospholipase C cleaves phophatidyl-inositol-4,5-bisphosphate (PIP_2) found in the plasma membrane into the soluble inositol-trisphophate (IP_3) and the membrane resident diacylglycerol (DAG). IP_3 triggers ER-Ca^{2+} depletion through its interaction with IP_3 receptors (or IP_3-gated Ca^{2+} channels) in the ER plasma membrane.

The molecular mechanism of membrane depolarization by mAChRs stimulation is not clear and it has been investigated in cultured neurons showing spontaneous Ca^{2+} oscillations (Nash et al., 2004, Young et al., 2005). Spontaneous oscillations of intracellular Ca^{2+} concentrations have been observed in neuronal cultures without external stimuli (Ogura et al., 1987, Numakawa et al., 2002, Murphy et al., 1992) and also in cerebral cortex of young rats *in vivo* (Kerr et al., 2005). These Ca^{2+} oscillations during embryonic and postnatal periods are implicated in the development of neural circuits in the central nervous system (Spitzer et al., 1995, Feller, 1999, Zhang and Poo, 2001, Spitzer et al., 2000, Burbridge et al., 2014). In cultured neurons, these periodic and spontaneous Ca^{2+} transients result from action potential firing among synaptically connected neurons, since simultaneous recordings of membrane potentials and intracellular Ca^{2+} revealed that each Ca^{2+} transient correlates to a burst of action potentials (Opitz et al., 2002, Bacci et al., 1999). Accordingly, they depend on synaptically released glutamate. The ability of muscarinic agonist to increase spontaneous Ca^{2+} transients has been associated to a direct modulation of neuronal excitability by mAChRs coupled to $G\alpha_{q/11}$, in which stimulation of PLCβ activity and depletion of plasma membrane PIP_2 are required, but do not require Ca^{2+} release from internal stores (Young et al., 2005); similar to the mechanism underlying the nonsynaptic intrinsic persistent firing evoked by muscarinic receptor activation (Zhang et al., 2011).

All these mAChRs functions depend on activation of PLCβ pathway, which finally releases Ca^{2+} from intracellular stores. Although it seems not to be involved in these functions, the depletion of ER-Ca^{2+} could trigger SOCE in the plasma membrane, and its activation could be relevant in the enhanced excitability mediated by muscarinic receptors agonists. In fact, it has been proposed that mAChRs activation utilizes SOCE for the modulation of excitability in hippocampal pyramidal neurons via activation a hyperpolarizing K^+ current (Kann et al., 2012).

5. Metabotropic glutamate receptors. Role in long-term depression

Metabolic glutamate receptors (mGluRs) are GCPRs and provide a mechanism by which glutamate may exert signal via second messenger signaling pathways (Yin and Niswender, 2014). MGluRs are classified into three groups based on sequence homology and G-protein coupling. Group I includes mGluR1 and 5, group II includes mGluR2 and 3, and finally, group III are formed by mGluR4, 5, 6, 7 and 8 (Niswender and Conn, 2010).

Group I mGluRs (mGluRs I) are expressed widely through the CNS, and are localized postsynaptically in a perisynaptic zone surrounding the ionotropic glutamate receptors (Lujan et al., 1996). The canonical signaling pathway linked with the stimulation mGluRs I is the activation of PLCβ, IP_3 generation and Ca^{2+} release (Abe et al., 1992, Aramori and Nakanishi, 1992) (Figure 5). At excitatory synapses, activation of mGluRs I occurs in response to strong activity and triggers many functions modulating the synaptic transmission in different brain regions (Luscher and Huber, 2010). Accordingly, stimulation of these receptors is known to induce the two major forms of long-lasting synaptic plasticity: long-term potentiation (LTP) and long-term depression (LTD), mechanisms that underlie processes of learning and memory formation along with other physiological processes (Collingridge et al., 2010). Activation of mGluRs I using electrical or pharmacological stimulation ((S)-3,5-dihydroxyphenylglycine (DHPG)) leads to LTD of excitatory synapses (mGluR-LTD) in many brain regions. However, the molecular mechanism is not well understood. Independent studies differ on how PLCβ pathway and Ca^{2+} rise in postsynaptic neuron are involved in mGluR-LTD, and their role seems to vary depending on the induction protocol and the brain region (Gladding et al., 2009, Luscher and Huber, 2010). In hippocampal neurons, mGluR-dependent LTD induced by DHPG (DHPG-LTD) occurs independently of PLCβ/IP_3-mediated Ca^{2+} release or PKC activity (Mockett et al., 2011, Fitzjohn et al., 2001, Schnabel et al., 1999, Kim et al., 2015) but see (Sethna et al., 2016), whereas mGluR-LTD induced by electrical activity depends on intracellular Ca^{2+} rise (Oliet et al., 1997, Otani and Connor, 1998) and the presence of ER in the dendritic spines (Holbro et al., 2009). In cerebellum, the activation of PLCβ/IP_3 pathway and Ca^{2+} release is absolutely required for mGluR-LTD (Kano

et al., 2008, Miyata et al., 2000). Moreover, although mGluR-LTD takes place in many brain regions, most studies have focused on hippocampal neurons.

As mentioned before, a role of SOCE in synaptic plasticity has been proposed (Moccia et al., 2015, Majewski and Kuznicki, 2015). Indeed, stimulation of mGluRs I and PLCβ activation, could lead to SOCE activation, and this would be consistent with STIM1 being a key regulator of Ca^{2+} signaling downstream metabotropic glutamate receptors stimulation (Hartmann et al., 2014, Hou et al., 2015). In the light of these facts, one of the purposes of this Doctoral Thesis was to study the relationship between mGluRs I and SOCE and the possible role of SOCE in mGluR-LTD in mouse cortical neurons.

OBJECTIVES

GDAP1 is a protein located in the outer mitochondrial membrane and mutations in *GDAP1* gene are involved in several forms of Charcot-Marie-Tooth disease. Although GDAP1 has been found to participate in different cellular functions, the mechanism underlying the pathology of CMT is not known and therefore we set the following objectives:

1. To study the effect of GDAP1 depletion and *GDAP1* pathological missense mutations in Ca^{2+} homeostasis in human neuroblastoma SH-SY5Y cell line.
2. To investigate consequences of the disruption of Ca^{2+} homeostasis in mitochondrial functions, specifically in energy production by mitochondria.

Having found that store-operated calcium entry (SOCE) is impaired in GDAP1 deficiency and that both SOCE existence and functions in neurons are controversial, we proposed the following objectives:

3. To study the presence of SOCE pathway in mice primary cortical neurons.
4. To explore the role of mitochondria in modulating SOCE activity in cortical neurons.
5. To investigate the role of SOCE in the response to physiological stimuli:

    5.1. To study the role of SOCE in muscarinic acetylcholine receptors stimulation and functional consequences of mAChRs activation on mitochondrial functions.

    5.2. To study the role of SOCE in metabotropic glutamate receptors stimulation and its implication in mGluRs-evoked long term depression (LTD) in cortical neurons.

MATERIALS & METHODS

1. Animals

Wild-type or Aralar-deficient mice both with a mixed C57BL6/Sv129 genetic background were used. AGC1/Aralar-deficient mice have been generated by gene trapping by Lexicon Pharmaceuticals and described in (Jalil et al., 2005). The mice were housed in a humidity- and temperature-controlled room on a 12 h light/dark cycle, receiving water and food *ad libitum*. All the experimental protocols used in this study were approved by the local Ethics Committees at the Center of Molecular Biology Severo Ochoa and Autonoma University (UAM) of Madrid, and were performed in accordance with European regulations (EU directive 2010/63/EU). All efforts were made to minimize animal suffering.

2. Genotypes

Genotype was determined, as previously described (Jalil et al., 2005), by PCR using genomic DNA obtained from tail or embryonic tissue samples (Nucleospin tissue kit, Macherey-Nagel). The following primers were used for genomic DNA amplification: sense primers mAra3_ LTRF3 (5´-GTTCTCTAGAAACTGCTGAGG- 3´) that detects only mutated allele, and mAra int 13F1 (5'-GATGTGAGAACTCACCAGTGT-3') that detects wild-type allele, and antisense primer mAra int 13B (5´-ACCACCACCAGCGTGTCAGC- 3´) that detects both wild-type and mutant alleles. PCR mixtures were preincubated at 94 °C for 5 min, followed by 30 cycles of amplification at 94 °C for 30 s, 58 °C for 30 s, and 72 °C for 60 s; the process was finished with an incubation at 72 °C for 5 min. Wild-type (271 bp) and mutant (406 bp) fragments were separated by electrophoresis on a 1.5 % agarose gel.

3. Cell lines and cultures

Human neuroblastoma SH-SY5Y and mouse neuroblastoma Neuro-2a (N2a) cells were grown in DMEM-F12 (Gibco, Invitrogen) with 10% fetal bovine serum (FBS) (Gibco, Invitrogen), 2 mM L-glutamine and 100 mg/ml penicillin-streptomycin. Human HEK293T cells were grown in DMEM with 10% FBS, 2 mM L-glutamine, 1% nonessential amino acids and 100 mg/ml penicillin-streptomycin. The cultures were maintained at 37 °C in a humidified atmosphere of 5% CO_2. For stable control and *GDAP1*-KD cell clones, both in SH-SY5Y and HEK293T cell lines, 2 μg/ml puromycin was added to maintain the selection. The cultures were maintained at 37 °C in a humidified atmosphere of 5% CO_2.

4. Primary neuronal culture

Cortical neuronal cultures were prepared from E15-E16 mouse embryos as described earlier (Ramos et al., 2003, Pardo et al., 2006). To study the role of ARALAR, individual E15-E16 embryos were obtained from crosses between C57BL6/Sv129 Aralar$^{+/-}$ mice, and non-brain tissue was used for determination of *Aralar* genotype. Cerebral cortices were removed free of meninges, cut into small pieces, and enzymatically dissociated in phosphate-buffered saline (PBS) containing 1 % bovine serum albumin (BSA), 0.4 mg/ml papain (Roche), and 6 mM glucose and then mechanically dissociated, in the presence of DNase (Roche), by using glass pipettes of different pore size. Dissociated cells were collected by centrifugation (340 g, 5 min) and plated on poly-L-lysine and laminin-coated pretreated glass coverslips in medium containing 20% horse serum for 3 h. After this time, medium was completely replaced by serum-free Neurobasal medium supplemented with 2% B27, 1% glutamax (all from Gibco, Invitrogen) and 100 mg/ml penicillin-streptomycin. Cultures were maintained at 37ºC in a humidified atmosphere of 5% CO_2. The culture medium was partially replaced every 2nd day. Cultures were used for experimentation between 9 and 12 days *in vitro* (DIV). For electrophysiological experiments, on DIV 5 half of the plating medium was removed from each well and replenished with BrainPhys medium (Bardy et al., 2015) (Stem cell Technologies) supplemented with 2% B27 and 100 mg/ml penicillin-streptomycin.

5. Pharmacological agents

Below, the pharmacological agents used in this thesis and the processes where they participate are listed.

Agents used to mobilize Ca^{2+} from intracellular stores: Thapsigargin (Tg) (Alomone Labs) and 2,5-di-tert-butylhydroquinone (BHQ) (Sigma-Aldrich), both inhibitors of SERCA, the ER-Ca^{2+}-ATPase. Ionomycin (Sigma-Aldrich), an ionophore used in a Ca^{2+}-free medium to compare the ER-Ca^{2+} content upon different treatments.

Agonists: Carbachol (Cch) and ATP (both from Sigma-Aldrich), agonist of acetylcholine and purinergic receptors respectively, (S)-3,5-dihydroxyphenylglycine (DHPG) (Tocris Bioscience), an agonist of group I of metabotropic glutamate receptors. All of them also can mobilize ER-Ca^{2+} via IP_3 signaling.

Metabolic inhibitors: oligomycin (Olig), an ATP synthase blocker, 2,4-dinitrophenol (DNP), an ionophore that dissipates the proton gradient across the mitochondrial membrane and antimycin A (Ant)/rotenone (Rot), inhibitors of complex III and I of the mitochondrial electron transport chain, respectively (all from Sigma-Aldrich).

Ca^{2+} channels antagonists: YM-58483 (Tocris Bioscience) and 2-Aminoethoxydiphenyl borate (2-APB) (Sigma-Aldrich), both SOCE blockers. 6-cyano-7-nitroquinoxaline-2,3-dione (CNQX), an AMPA/Kainate receptors inhibitor; (5S,10R)-(+)-5-Methyl-10,11-dihydro-5H-dibenzo[a,d]cyclohepten-5,10-imine hydrogen maleate (MK-801), a NMDA receptors inhibitor; $NiCl_2$, a low-voltage-activated calcium channels inhibitor (all from Sigma-Aldrich); 2-Methyl-6-(phenylethynyl) pyridine (MPEP), a mGluRs 5 inhibitor and tetrodotoxin (TTX), a voltage-gated sodium channels blocker (both from Tocris Bioscience).

6. Cell transfection

Neuroblastoma SH-SY5Y and N2a cells were transfected using Lipofectamine 2000 (ThermoFisher) according to the manufacturer's instructions. The ratio DNA:Lipofectamine was 1:1 and we used approximately 1µg DNA/10^5 cells. HEK293T cell line was transfected using calcium phosphate following the protocol described in (Jiang and Chen, 2006). Cells were transfected 24h before experimental assays in a free-serum DMEM medium, with the exception of MCU silencing experiments, in which N2a cells were transfected 72 hours before. Primary cortical neurons were transfected with Lipofectamine 2000, with a DNA:Lipofectamine ratio 1:2 and approximately 1µg DNA/ 10^5 cells, in Neurobasal medium 48h before experimental assays.

7. Silencing of *GDAP1* in HEK293T cell line

For the generation of a stable *GDAP1*-silenced HEK293T cell line, we used the pLKO.1 puro vector (MISSION® shRNA, Sigma-Aldrich) containing a hairpin sequence against GDAP1, described in (Pla-Martin et al., 2013), or a non-target control vector (pLKO-NT), containing 5 bp mismatches within the shRNA sequence. Stable gene silencing was attained using the puromycin resistance gene as a selectable marker. To determine the appropriate concentration of puromycin, 2 x 10^5 HEK293T cells were plated in each well of a 6-well plate containing 2 ml of the culture medium with increasing concentrations of puromycin (i.e., 0, 1, 2, 5, 7.5, and 10.0 µg/ml). Medium was replaced with fresh selective medium after 2 days to remove dead cells, and the percentage of survival cells were monitored daily. The optimal antibiotic concentration was 2 µg/ml, it was the lowest concentration that killed 100% of the cells in 3-5 days from the start of puromycin selection. To generate the stable *GDAP1*-silenced clones, HEK293T cells were transfected with the pLKO.1 puro vector containing the hairpin sequence against *GDAP1* or the non-target control vector. *GDAP1*-silenced clonal cell lines were obtained by limiting dilution. The aim of this technique is to isolate individual cells carrying the puromycin resistance gene for selection and to expand these cells in separate wells. To this end, transfected cells were plated at

very low cell density (< 1 cell per well) in 96 well plates, in culture medium containing 2 μg/ml puromycin to select. Puromycin resistant clones were expanded and reached high cell densities in two weeks. Fifteen transfected clones with the pLKO-NT plasmid and twenty-five transfected clones with the pLKO.1 plasmid containing a hairpin sequence specific against GDAP1 were collected and tested for GDAP1 silencing by Western Blot.

8. Plasmids, virus generation and transduction of neurons

In immunofluorescence assays we used pCMV-myc (Clontech) derived vectors for expression of GDAP1 WT or the mutant variants p.R161H and p.T157P, all fused to myc epitope at the C-terminus. In oxygen consumption rate (OCR) experiments we used the IRES-containing bicistronic pCAGIG vector (Clontech) for the simultaneous expression of GDAP1 (WT or mutant variant p.S130C) and green fluorescence protein (GFP), these plasmids were provided by Francesc Palau´s Lab and described in (Pla-Martin et al., 2015, Gonzalez-Sanchez et al., 2017, Pla-Martin et al., 2013).

Knocking down of *Mcu* expression was performed with short-hairpin RNAs (shRNAs), using a recombinant adeno-associated viral (rAAV) vector provided by Hilmar Bading and Giles E. Hardingham and previously described (Qiu et al., 2013). The rAAV contains the U6 promoter driving shRNA expression and also a CaMKII promoter driving mCherry expression to identify infected neurons. The production of adeno-associated virus was done as described in (McClure et al., 2011). The titration of viral stocks was done by infection of primary cortical neurons, they were transduced at DIV 3 with serial dilutions of rAAVs (from 1 μl of undiluted viral stock to $1:10^8$) and were fixed at DIV 9. The infection unit per microliter was obtained counting the number of transduced cells from the three wells that have the highest dilution factor, but still contain infected cells, finding the average and multiplying it by the dilution factor (McClure et al., 2011).

Cortical neurons were transduced with 10^{11} rAAV particles per μl at DIV 3. Infection efficiencies were determined at DIV 9 by analyzing mCherry fluorescence. Approximately, the 80-90% of viable neurons were infected. The level of MCU silencing was determined by western blot using a specific α-MCU antibody.

9. Western blot

Neuro-2a cells and HEK293T clones were cultured in 100 mm Petri dishes and were removed when cells were 90% confluent. Cortical neurons were plated at a density of 1 x 10^6

cells/well on poly-L-lysine and laminin-coated pretreated 6 wells plates. Cells were collected with a scrapper into a homogenization buffer (250 mM Sucrose, 20 mM Hepes, 10 mM KCl, 1.5 mM $MgCl_2$, 1 mM EDTA, 1 mM EGTA, 1 mM DTT, complete protease inhibitor cocktail mini-EDTA free, (Roche); and adjusted to pH 7.4). The samples were homogenized by sonication (10 pulses of 1 second, 4ºC), and were quantified by the Bradford protein assay. In the case of HEK293T, after sonication, two differential centrifugation steps were performed to separate different organelles in order to obtain a mitochondria-enriched fraction (700 g, 10 min and 10.000 g, 15 min.). Aliquots of 30 µg proteins were separated by SDS-PAGE in an appropriate % of SDS acrylamide gel (in relation with the molecular weight of the protein under study) and transferred electrophoretically to nitrocellulose membranes, which were blocked in 5 % (w/v) dry skimmed milk (Sveltesse, Nestle) in Tris-buffered saline (10 mM Tris-HCl pH 7.5, 150 mM NaCl plus 0.05% (v/v) Tween-20) for 1 h, and further incubated with primary antibodies for 1h at room temperature (RT) or overnight (O/N) at 4ºC. Primary antibodies and dilutions used are summarized in Table 1. Secondary antibodies used were IRDye® 800CW goat (polyclonal) anti-rabbit (LI-COR, ref 926-32211) and IRDye® 680LT donkey (polyclonal) anti-mouse (LI-COR, ref 926-68022), and signal fluorescence detection was performed in the Odissey® Imaging system (LI-COR Bioscience), following manufacturer's instructions.

Primary Antibodies	*Dilution*	*Produced in*	*Reference*	*Incubation time*
α-GDAP1	1:1000	Mouse (Polyclonal)	Abnova, H00054332-A01	O.N. 4ºC
α-Mcu	1:500	Rabbit (Polyclonal)	Sigma-Aldrich, HPA016480	1 h RT
α-SCaMC1	1:5000	Rabbit (Polyclonal)	(del Arco and Satrustegui, 2004)	1h RT
α-βATPase	1:5000	Mouse(Monoclonal)	ThermoFisher, A21351	1h RT
α-Orai1	1:200	Rabbit (Polyclonal)	Alomone Labs, ACC-062	O.N. 4ºC
α-Orai2	1:200	Rabbit (Polyclonal)	Alomone Labs, ACC-061	1h R
α-STIM2	1:500	Rabbit (Polyclonal)	Alomone Labs, ACC-064	1h R
α-TRPC1	1:500	Rabbit (Polyclonal)	Alomone Labs, ACC-010	O.N. 4ºC
α-TRPC4	1:500	Rabbit (Polyclonal)	Alomone Labs, ACC-119	1h RT
α-βActin	1:5000	Mouse(Monoclonal)	Sigma-Aldrich, A2172	1h RT

Table 1. Primary antibodies.

10. Measurement of cytosolic Ca^{2+} signals

To recorder cytosolic Ca^{2+} signals, cells lines were plated at a density of 7.5 x 10^4 cells/well on 12 mm coverslips and cortical neurons were plated at 2 x 10^5 cells/well on poly-L-lysine and laminin-coated 12 mm coverslips. Cells were loaded with 5 μM Fura-2AM and 50 μM pluronic acid F.217 (both from Molecular Probes) for 30 min. at 37 °C in HCSS-calcium free (120 mM NaCl, 0.8 mM $MgCl_2$, 5.4 mM KCl, 25 mM HEPES, pH 7.4), 2.5-15 mM glucose medium (for cortical neurons and cell lines respectively), and washed for 30 min. in HCSS, 2 mM $CaCl_2$, 2.5-15 mM glucose. Then, coverslips were mounted on the microscope stage equipped with a 40 X objective and Fura-2AM fluorescence was imaged ratiometrically using alternate excitation at 340 and 380 nm and a 510-nm emission filter at 37 °C, as described earlier (Ruiz et al., 1998). Experiments were performed in HCSS medium containing 2.5-15 mM glucose. The presence or absence of $CaCl_2$ and the specific conditions of the measurements are detailed in each experiment (results section). Additions were made as a bolus with a final volume of 300 μl. Single cell analysis of the changes in cytosolic calcium concentration were expressed as the ratio of fluorescence intensity at 340 (F340) and 380 nm (F380) (F340/F380). Regions of interest (ROIs) were selected covering single cells. Image acquisition and analysis were performed with the Aquacosmos 2.5 software (Hamamatsu).

11. Measurement of plasma membrane and mitochondrial Ca^{2+} signals

To image subplasmalemmal and mitochondrial Ca^{2+} signals, cell lines were plated onto 4-wells Lab-Tek chamber slides (Nunc) at a density of 8.5 x 10^4 cells/well and cortical neurons at 1 x 10^5 cells/well. Cells were transfected with pcDNA-lynD3cpv vector (Addgene, (Palmer et al., 2006)), encoding for ratiometric plasma membrane targeted Ca^{2+} FRET probe, or with Mit-GEM-GECO1 (Addgene, (Zhao et al., 2011)) or pcDNA-4mtD3cpv (Addgene, (Palmer et al., 2006)) both encoding for ratiometric mitochondrial targeted Ca^{2+} FRET probes. Cells were transfected as described before. Experiments were performed in HCSS medium containing 2.5-15 mM glucose (cortical neurons and cell lines respectively), and the presence or absence of $CaCl_2$ and the specific conditions of the measurements are detailed in each experiment (results section). Cells were excited for 100 ms at 436/20 mm and the emitted fluorescence was collected through a dual-pass dichroic CFP-YFP (440/500 nm (CFP) and 510/600 nm (cpV or YFP) alternatively). Images were collected every 5 s using a filter wheel (Lambda 10-2, Sutter Instruments; all filters were from Chroma) and recorded by a Hamamatsu C9100–02 camera mounted on an Axiovert 200M inverted microscope equipped with a 63X/1.4 oil Plan-Apochromat Ph3 objective. ROIs were selected on somas areas and single-cell fluorescence recordings were analyzed using MetaMorph (Universal Imaging) and ImageJ (NIH).

12. Cell sorting

GDAP1-KD neuroblastoma SH-SY5Y cells were cultured in 100 mm Petri dishes and transfected with the bicistronic pCAGIG vector, encoding for GDAP1 (WT or mutant form) and the GFP protein 24 h before the experiment. Cells were collected using trypsin, washed (2 x PBS without Ca^{2+}/Mg^{2+}, and resuspended in sorting buffer (PBS, 5mM EDTA, 25mM Hepes, pH 7.0, 2% fetal bovine serum (FBS)). The concentration of the samples was 1-4 x 10^6 cells/ml and they were filtered with a 70 µm filter before being sorted out with the FACSVantage (BD Biosciences) cell sorter, based on the presence of GFP in the target population. After sorting, the GFP-expressing SH-SY5Y cells were collected in the culture medium.

13. Measurement of cellular oxygen consumption

Cellular oxygen consumption rate (OCR) (pmol/min) was measured using a Seahorse XF24 Extracellular Flux Analyzer (Seahorse Bioscience) (Qian and Van Houten, 2010). Neuroblastoma SH-SY5Y and HEK293T cells were plated in XF24 V7 cell culture at 1.5 × 10^5 cells/well and incubated for 24 h in a 37 °C, 5% CO_2 incubator in culture medium. Primary cortical neurons were plated at 1 × 10^5 cells/well and incubated for 8-10 days in a 37 °C, 5% CO_2 incubator in culture medium. Cells were equilibrated with bicarbonate-free low-buffered DMEM medium (without pyruvate, lactate, glucose, glutamine, and Ca^{2+}) supplemented with 2.5-15 mM glucose (for neurons or cell lines respectively) and 2 mM $CaCl_2$ or 100 µM EGTA in conditions of ± Ca^{2+}, for 1 h immediately before extracellular flux assay. Drugs were prepared in the same medium and were injected from the reagent ports automatically to the wells at the times indicated. Bioenergetics characterization of culture cells was determined through sequential addition of 6 µM oligomycin, 0.25 mM 2,4- dinitrophenol (DNP), and 1 µM antimycin A/1 µM rotenone. This allowed determination of basal oxygen consumption, oxygen consumption linked to ATP synthesis, non-ATP linked oxygen consumption, maximal uncoupled respiration (MUR), and non-mitochondrial oxygen consumption (Brand and Nicholls, 2011). When required, BAPTA-AM (Sigma-Aldrich) loading was performed in Ca^{2+}-free DMEM during 30 min before the experiment. To investigate the consequence of GDAP1 mutants on SOCE-driven stimulation of respiration, *GDAP1*-KD HEK293T cells were cultured in 100 mm Petri dishes and were transfected. 24 h after transfection, cells were seeded in a XF24 V7 cell culture plate and incubated for an additional 24 h in a 37 °C, 5% CO_2 incubator.

14. Immunofluorescence assay

For the study of mitochondrial distribution in neuroblastoma *GDAP1*-KD cells expressing GDAP1 mutated variants, 7 x 10^4 cells were plated onto 12 mm colverslips and were co-transfected with pCMV-myc plasmids for expression of GDAP1 WT or mutant variants along with Orai1::CFP plasmid (Addgene, (Prakriya et al., 2006)) as plasma membrane marker. 24 h upon transfection, cells were washed (1 x PBS) and fixed with 2% paraformaldehyde (PFA) for 10 min and 4% PFA for 10 min. Then, coverslips were washed (2 x PBS) and incubated in PBS with 10 % horse serum (HS) and 0.25 % Triton X-100 for 1h. Afterwards, they were incubated O/N at 4ºC with a mouse monoclonal α-c-myc antibody (Dilution 1:2000, Sigma-Aldrich, St. Louis, MO, USA) for GDAP1-transfected cells and a mouse monoclonal α-βATPase (Dilution 1:2000 Sigma-Aldrich) for transfected cells with empty vector in PBS with 1 % HS and 0.25 % Triton X-100. The secondary antibody, a goat anti-mouse coupled to Alexa Fluor 555 (Dilution 1:5000, ThermoFisher), was incubated for 1-2 h at room temperature prior to mounting with mowiol. Images were taken using the Confocal LSM710 laser scanning microscope from Zeiss. Cells were excited at 458 nm for Orai1::CFP and at 561 nm for Alexa Fluor 555, and the emitted fluorescence was collected between 461-512 nm for CFP and 562–630 nm for Alexa 555. Fifteen-twelve images with 0.12 μm between each were acquired. Images were deconvolved with Huygens software (Scientific Volume Imaging) and analysis was done using ImageJ software (NIH).

15. Mitochondrial distribution analysis

To determine mitochondrial fluorescence profile, a projection of Z-stacks was done for each cell, removing the two upper and lower planes, using ImageJ software. For every cell, 6 - 9 lines of different lengths between opposite plasma membrane covering the majority of mitochondrial network and avoiding the nucleus were drawn (an example is shown in Fig. 6A). Line length was between 8 - 18 μm, depending on cell morphology. Cells and lines were chosen so that, for each condition, the number of lines of each length was similar. Drawn lines were parallel and with a separation of 1,5 μm. Then, the fluorescence profile was calculated in the mitochondrial images (Fig. 6B) using ImageJ software. Mitochondrial fluorescence distribution in subplasmalemal (SP) domains (defined as 2 μm underneath the plasma membrane) and the central zone (the space between the opposite SP domains) was calculated as percent of total fluorescence in each profile, using MATLAB software.

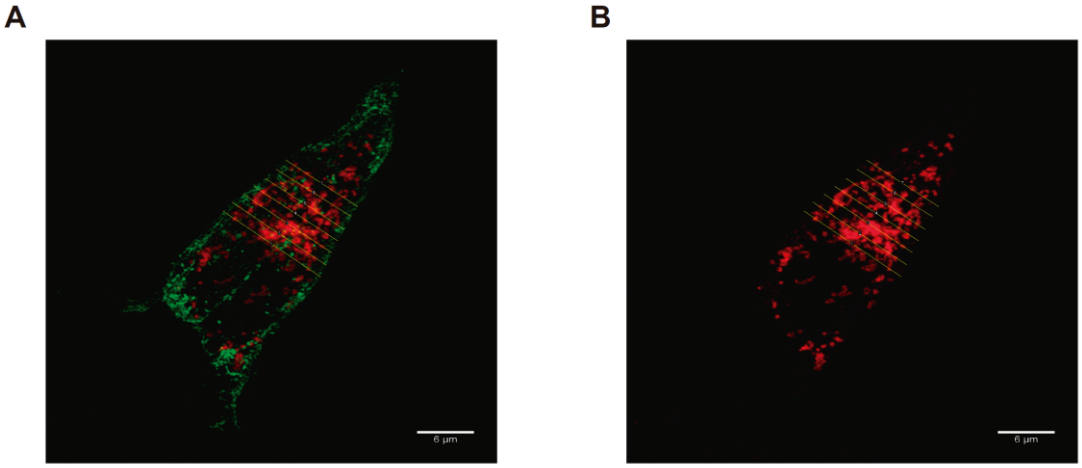

Figure 6. Analysis of mitochondrial distrubution in neuroblastoma *GDAP1*-KD cells. Cells were co-transfected with Orai1::CFP (green), as a plasma membrane marker, and GDAP1 mutant variant, detected using α-c-myc (red), as described before. Lines were drawn using an image in which both PM and mitochondrial markers were shown **(A)** and the fluorescence profile was calculated in the mitochondrial images **(B)**.

16. Gene expression analysis by quantitative real time PCR (qRT-PCR)

Levels of messenger RNA (mRNA) in neurons were determined by quantitative real time PCR, qRT-PCR. Specific primers for PCR amplification of the SOCE genes: *Orai1*, *2* and *3*, *Stim1* and *2*, *Trpc1*, *2*, *3*, *4*, *5*, *6* and *7*, were designed using Universal Probe Library web (https://lifescience.roche.com/en_es/brands/universal-probe-library.html) (Roche), and are summarized in Table 2, together with the amplicons length. All of them are intron-spanning primers, which do not amplify the larger genomic sequence efficiently, and no products are obtained from a possible genomic DNA contamination. The specificity of each pair of primers was tested using Primer-BLAST software (basic local alignment search tool) from NIH (https://www.ncbi.nlm.nih.gov/tools/primer-blast/index.cgi?LINK_LOC=BlastHome), having no mismatch for target genes and at least 4 mismatches for non-target genes.

Cortical neurons were plated at a density of 1 x 10^6 cells/well on poly-L-lysine and laminin-coated pretreated 6 wells plates. 8-9 DIV neurons were trypsinized and collected as a cell pellet, RNA extraction was done with RNeasy mini kit (QIAGEN) following the manufacturer's instructions. 1 µg of total RNA was subjected to first strand cDNA synthesis with Avian Myeloblastosis Virus (AMV) reverse transcriptase (Promega) in 20 µl of reaction using random primers $p(dN)_6$. The cDNA obtained was quantified using the spectrophotometer NanoDrop 1000 (ThermoFisher).

Gene	Forward primer (5´-3´)	Reverse primer (5´-3´)	Amplicon size (nt)
Orai1	tacttaagccgcgccaag	acttccaccatcgctacca	83
Orai2	cacagacgctagccacgag	atgggcacattgagctctg	106
Orai3	cacatctgctctgctgtcg	aggcctggtgggtattcat	84
Stim1	cagggactgtactgaagatgaca	aggtgattatgccgagtcaag	109
Stim2	gagggcgcagagtgtgag	tttagagccatgcggacct	74
Trpc1	tgtggttgtgattgtgctga	tccattctttatcctcatgatttg	89
Trpc2	cccatcgggacctttacc	tcgaaggcggtaggacac	78
Trpc3	ttaattatggtctgggttcttgg	tccacaactgcacgatgtact	91
Trpc4	aaggaagccagaaagcttcg	ccaggttcctcatcacctct	92
Trpc5	ggcgatgcattactctacgc	atcatcagcgtgggaacct	107
Trpc6	tactggtgtgctccttgcag	caaacttcatgaacggtcctc	61
Trpc7	aacgatgaagtcaatgaaggtg	ccagctctcctgtagcctga	107

Table 2. Intron-spanning primers used for qRT-PCR analysis of SOCE genes expression levels.

We performed an absolute quantification using the standard curve method. For quantification of the PCR products, we used the fluorescent dye SYBER-Green (SYBR® Green, Biorad). The parameter analyzed was the Cq: the cycle at which the fluorescence of a sample crosses a threshold line. The Cq value is directly proportional to the number of copies of the gene. A standard curve of each amplicon (from 10 to 10^8 copies) was used and the number of copies of SOCE genes (nº copies/ng cDNA) was obtained by extrapolation. Amplicons were obtained previously by standard PCR using 1 µl of cDNA as template in 25 µl of PCR reaction using the specific primers for each gene, and the amplification protocol was 35 cycles (45 sec. 94 C, 45 sec. 58ºC, 30 sec. 72ºC). 1 µl of amplified fragments was ligated into the pGEM-T cloning vector (Promega) following the manufacturer's instructions and transformed into XL1-Blue competent cells. Recombinant plasmids were isolated and verified by restriction using standard procedures. These plasmids were linearized to be used in the standard curve of the qPCR.

The PCR efficiency was calculated for each pair of specific primers. To this end, 6 serial dilutions of cDNA were used, from 25 ng up to 0.024 ng of cDNA, and the Cq value for each dilution was recorded. The efficiency was calculated from the slopes of the calibration curves (Cq vs. log copy numbers). Only primers designed to amplify *Trpc4* gene shown a decreased efficiency, and it was corrected in the experiment. The melting curve was also analyzed for each gene in order to distinguish primer dimers from the specific amplicon and to assess whether the

qPCR assays have produced single and specific products. All pairs of primers amplified a single product, and no primer dimers were observed.

To performed the qPCR, 2.5 ng of the cDNA synthesized was amplified using the ABI Prism 7900HT real-time PCR System (Applied Biosystems). We used the Power SYBR® Green Master Mix (Applied Biosystem) and the amplification protocol was: hot start (10 min. 95ºC) and 40 amplification cycles (15 sec. 95ºC, 1 min. 60ºC). The number of copies of each gene was directly proportional to Cq value, and it was obtained by extrapolation in the standard curve. All reactions were carried out in triplicates.

17. mEPSCs recording and analysis

Primary cortical neurons were plated at a density of 2 x 10^6 cells/wells on poly-L-lysine and laminin-coated 12 mm coverslips. Voltage-clamp whole-cell recordings were performed in 10-11 DIV cortical neurons. Neurons at 37ºC were continuously perfused with a recording medium containing 120 mM NaCl, 0.8 mM $MgCl_2$, 5.4 mM KCl, 25 mM HEPES, 2.5 mM D-glucose, 2 mM $CaCl_2$ and supplemented with 1 μM TTX to prevent action potential-evoked EPSCs, pH was adjusted to 7.4. Patch electrodes with resistances between 4-6 mΩ were filled with an internal solution containing 115 mM K gluconate, 20 mM KCl, 10 mM HEPES, 2 mM $MgCl_2$, 4 mM Na_2-ATP, 0.3 mM Na_3-GTP, pH adjusted to 7.3 and osmolarity ~290 mOsm. Neurons were voltage-clamped at - 60 mV and mEPSCs were amplified using the Multiclamp 700B amplifier (Molecular Devices). Inter-event interval and mEPSC amplitude were compared during a 2-min baseline period and in 2-min windows 15 minutes after 200 μM DHPG application (5 min). Data were analyzed using Clampfit 10.7 (Molecular Devices). Only events with an amplitude > 8 pA, an exponential decay and a monotonic rising phase, which could be clearly discriminated from the background noise, were considered as mEPSCs.

18. Statistical analysis

Shapiro-Wilk test was applied to determine the distribution of the data. In normal distributions, statistic was performed using the one-way or two-way ANOVA test, following of a *posthoc* Bonferroni test. In non-normal distributions (mEPSC parameters) statistics were performed using the Wilcoxon matched paired test. Significance was **$p < 0.05$, **$p < 0.01$, ***$p < 0.001$ (STATISTICA software, version 7, StatSoft).

RESULTS

1. CHARCOT MARIE TOOTH DISEASE CAUSED BY MUTATIONS IN *GDAP1* GENE

Previous findings of our laboratory carried out in collaboration with Francesc Palau´s research group suggests that Ca^{2+} homeostasis could be disturbed by GDAP1 deficiency. Therefore, we decided to study in depth Ca^{2+} homeostasis in SH-SY5Y cell line and how depletion and different mutations of GDAP1 could affect this highly controlled equilibrium. To this aim we used a *GDAP1*-KD stable human neuroblastoma SH-SY5Y cell line (Pla-Martin et al., 2013). Experiments were performed in wild-type cells (named hereafter SH-SY5Y), in control cells containing the non-target control vector (named pLKO-NT), and in *GDAP1*-KD clone, with approximately 80% of protein reduction (clone G4 in (Pla-Martin et al., 2013)).

1.1 Store-operated calcium entry (SOCE) is reduced in *GDAP1*-KD SH-SY5Y cells

The emptying of ER-Ca^{2+} stores activates Ca^{2+} entry through low-conductance plasmalemmal channels that are regulated by the level of Ca^{2+} stored in the ER, a process named store-operated calcium entry (SOCE) (Putney, 1986). To study this process, we performed the known Ca^{2+} addback protocol, in which ER-Ca^{2+} is depleted in a Ca^{2+}-free medium and then Ca^{2+} is added to the external medium. We used thapsigargin (Tg, 7 μM), an inhibitor of SERCA, the ER Ca^{2+}-ATPase that allows net Ca^{2+} leak from ER. We observed that Ca^{2+} readmission after ER-Ca^{2+} depletion, i.e. SOCE activity, quantified as ΔRatio (maximum value of fura-2 ratio after Ca^{2+} addition minus fura-2 ratio before Ca^{2+} addition), was much smaller in *GDAP1*-silenced cells (1.08 ± 0.13) than in control cells (pLKO-NT: 1.4 ±0.1) (Fig. 7 A, B). These findings revealed an effect of GDAP1 deficiency on SOCE in neuroblastoma cell line.

As mitochondria exert a control on SOCE activity in different cell types, we investigated whether the decreased SOCE could be associated with an impairment on mitochondrial Ca^{2+} uptake in response to SOCE-mediated Ca^{2+} signal. To study this possibility, we used a genetically encoded Ca^{2+} sensor targeted to mitochondria, the FRET probe GEM-GECO 1 (Zhao et al., 2011). We used the same protocol as in experiment shown in figure 7A, we depleted the ER-Ca^{2+} using 10 μM 2,5-di-tert-butylhydroquinone (tBuBHQ) (Jardin et al., 2008), an inhibitor of SERCA, and then we added 2 mM Ca^{2+} to the external medium. We quantified the mitochondrial Ca^{2+} uptake as ΔRatio × s^{-1}, and we found a robust increase in the GEM-GECO 1 ratio which was decreased in the *GDAP1*-KD cells (pLKO-NT: 2.89 ± 0.33 vs. *GDAP1*-KD: 1.78 ± 0.17) (Fig. 7 C, D). This was not due to a defect in Ca^{2+} uptake in mitochondria, as GDAP1 deficiency did not change Ca^{2+} transport kinetics or total retention capacity in mitochondria from digitonin-permeabilized cells (Pla-Martin et al., 2013). Indeed, GDAP1 re-expression in *GDAP1*-KD cells restores capacitative calcium entry (Fig. 7 E). These results suggested that the decrease in SOCE activity associated with GDAP1 deficiency could be due, at least in part, to an impaired handling by mitochondria

of calcium entering through SOCE, which may result in its Ca^{2+}-dependent inactivation due to misregulation of mitochondrial dynamics and distribution processes.

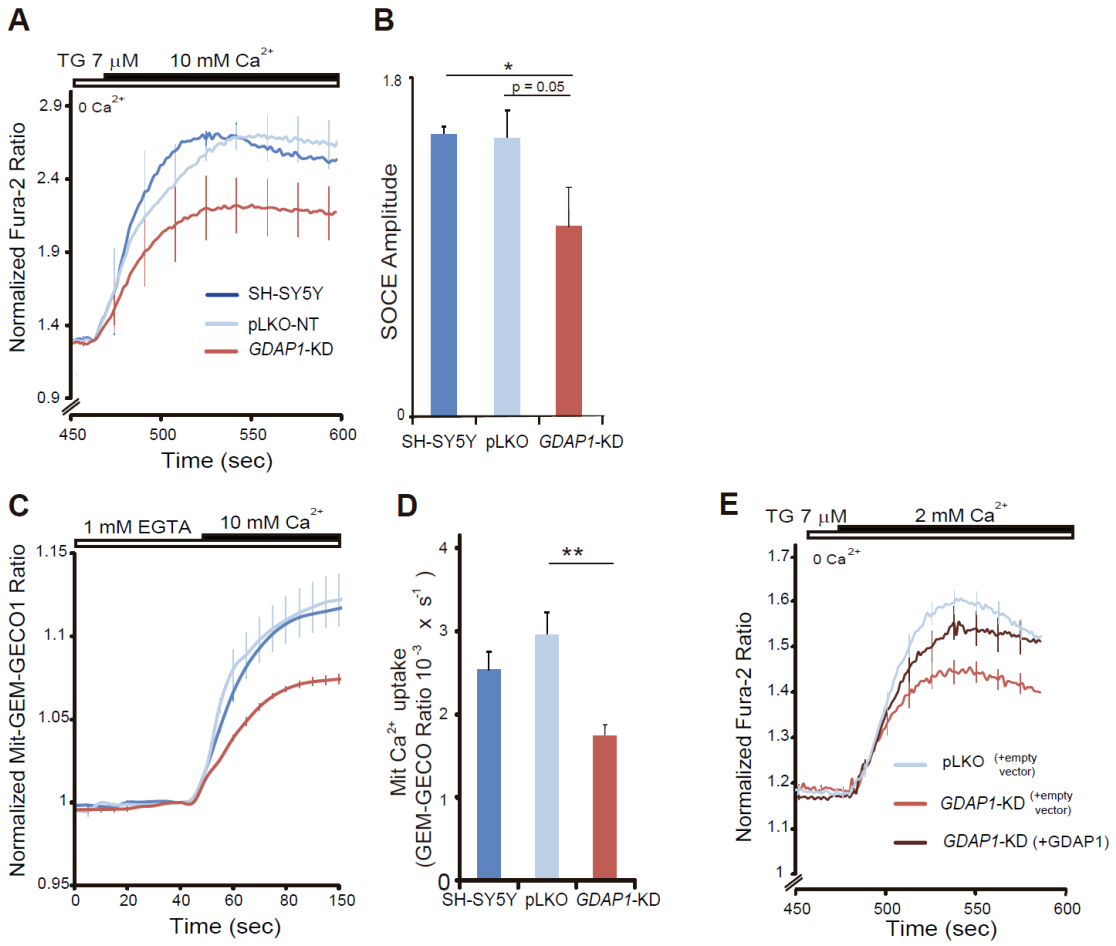

Figure 7. SOCE impairment in *GDAP1*-silenced SH-SY5Y cells. (**A**) Fura-2 $[Ca^{2+}]_i$ signals upon re-addition of 10 mM Ca^{2+} after stimulation 6 min before with 7 µM Tg in Ca^{2+}-free medium in wild-type, control and *GDAP1*-KD clone cells. (**B**) Quantification of SOCE amplitude as ΔRatio (F340/F380) ± SEM for each cell line. Data were obtained averaging at least 120 cells from no less than 4 independent experiments. (**C**) GEM-GECO 1 mitochondrial calcium signals upon re-addition of 10 mM Ca^{2+} after stimulation with 10 µM tBuBHQ in 1 mM EGTA medium in wild-type, control and *GDAP1*-KD clone cells. (**D**) Quantification of increase in Mit-GEM-GECO 1 ratio × s^{-1}. Data were obtained from at least 20 cells from 3 to 10 experiments and three different platings. (**E**) Fura-2 $[Ca^{2+}]_i$ signals upon re-addition of 2 mM Ca^{2+} after stimulation 6 min before with 7 µM Tg comparing control, *GDAP1*-KD (both expressing an empty-vector) and *GDAP1*-KD cells overexpressing GDAP1 WT protein. Cells were transfected 24 h prior to Ca^{2+} measurements. Data were obtained from 4-5 experiments. All data are normalized to the initial values and are expressed as mean ± SEM. Means were compared using one-way ANOVA, *p < 0.05, **p < 0.01, ***p < 0.001, *posthoc* Bonferroni test.

1.2 Mitochondrial Ca^{2+} uptake regulates SOCE activity in neuroblastoma cells

To investigate the role of mitochondrial Ca^{2+} uptake in modulation of SOCE in neuroblastoma cells, we studied the effect of MCU knockdown with the use of mouse-directed sequences kindly provided by Dr. Giles Hardingham and Dr. Hilmar Bading. A mouse neuroblastoma cell line, Neuro-2a, was used. Cells were transfected with plasmids containing *Mcu*-directed small hairpin RNA (shRNA) or non-target control sequence (scrambled) along with mCherry, to identify transfected cells (Qiu et al., 2013), and studied 72 hours later. This resulted in a drop of MCU protein levels to 56.2 ± 8.3% of control values (Fig. 8 A). Cytosolic Ca^{2+} signals evoked by ATP were the same in scrambled or *Mcu*-KD cells (Fig. 8 B). However, Ca^{2+} uptake in mitochondria (Ca_{mit}) in response to these signals, studied with 4mt-D3cpv, a FRET calcium probe targeted to the mitochondrial matrix (Palmer et al., 2006), was quite different. We observed that Ca^{2+} uptake in *Mcu*-KD was much lower than in scrambled mitochondria (Scr 0.56 ± 0.09 vs. *Mcu*-KD 0.32 ± 0.02 ΔRatio, *p < 0.05) (Fig. 8 B).

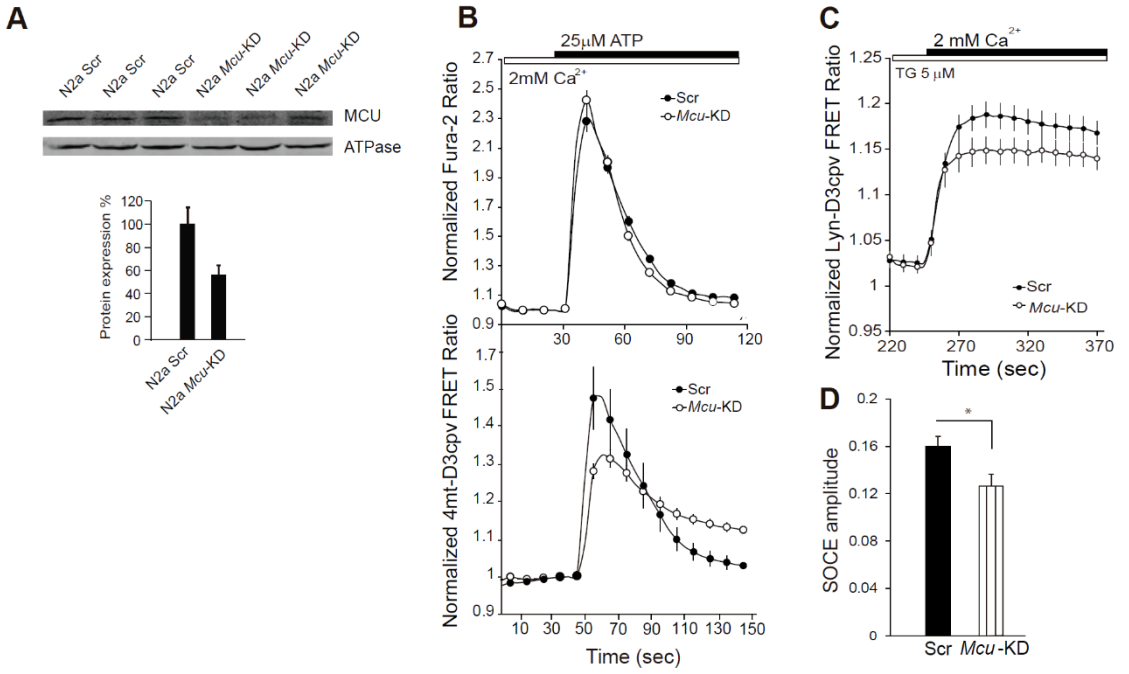

Figure 8. Mitochondria regulate SOCE activity in neuroblastoma cells. (**A**) Analysis of MCU levels by Western blot. Protein extracts were obtained 72 hours after transfection of N2a cells with either shScr or shMcu. Primary antibodies used were α -MCU and α -β ATPase as a control. MCU protein levels drop to 56, 2 ± 8, 3% of control values. (**B**) Fura-2 $[Ca^{2+}]_i$ signals and 4mt-D3cpv mitochondrial calcium signals in N2a cells transfected with shScr or shMcu upon addition of 25 μ M ATP where indicated. (**C**) Lyn-D3cpv subplasmalemmal Ca^{2+} signals were measured in N2a cells transfected with shScr or shMcu upon addition of 2 mM Ca^{2+} in Ca^{2+}-free medium containing 5 μM thapsigargin (Tg). Data were obtained from 3 independent experiments (n = 9–16 cells). (**D**) Quantification of SOCE amplitude as ΔRatio (F510/F440) ± SEM for each condition. All data are normalized to the initial values and are expressed as mean ± SEM. Means were compared using one-way ANOVA, *p < 0.05, **p < 0.01, ***p < 0.001, *posthoc* Bonferroni test.

We next studied the effects of MCU silencing on Ca^{2+} entry through SOCE channels. To this aim, we used the genetically encoded calcium indicator Lyn-D3cpv which is targeted to the plasma membrane (Palmer et al., 2006) in order to study changes in Ca^{2+} at the plasma membrane boundary, i.e, the site of SOCE. Figure 8 C and D show that Ca^{2+} inflow upon SOCE activation with thapsigargin was reduced in *Mcu*-KD cells compared with scrambled sequences (Scr 0.16 ± 0.01 vs. *Mcu*-KD 0.12 ± 0.01).

1.3 SOCE decrease by *GDAP1* silencing in SH-SY5Y cells is due to an impairment in mitochondrial handling of Ca^{2+} entry through SOCE

Having shown that mitochondria regulate SOCE activity in neuroblastoma cells, to determine whether decreased SOCE in SH-SY5Y *GDAP1*-KD cells is due to an impairment in mitochondrial Ca^{2+} handling, we studied Ca^{2+} influx through SOC channels in control and *GDAP1*-KD cells in presence of 0.25 mM 2,4-dinitrophenol (DNP), which collapses the mitochondrial membrane potential and prevents mitochondrial Ca^{2+} uptake. We found that in control pLKO-NT cells, DNP exposure caused a decreased SOCE amplitude (1.41 ± 0.04 and 1.01 ± 0.04 in absence or presence of DNP, respectively), which was reduced to the level of *GDAP1*-KD cell line (1.14 ± 0.04) (Fig. 9 A, B). In contrast, DNP exposure did not affect the amplitude of SOCE in *GDAP1*-KD cells (1.14 ± 0.05).

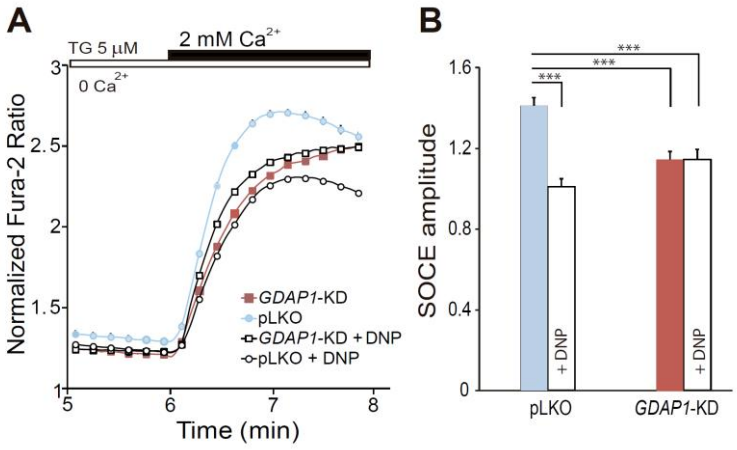

Figure 9. Fail in mitochondrial handling of Ca^{2+} entry through SOCE by GDAP1 deficiency. (**A**) SOCE response in control pLKO-NT and *GDAP1*-KD neuroblastoma cells, in presence or absence of DNP (0.25 mM). Fura-2 $[Ca^{2+}]_i$ signals were measured upon addition of 5 µM Tg in Ca^{2+}-free medium and 2 mM $CaCl_2$ where indicated. DNP was added 2 min before Ca^{2+} addition. (**B**) Quantification of SOCE amplitude as ΔRatio (F340/F380) ± SEM for each cell line and condition. Data were obtained averaging at least 120 cells from at least 4 independent experiments. All data are normalized to the initial values and are expressed as mean ± SEM. Means were compared using two-way ANOVA, *p < 0.05, **p < 0.01, ***p < 0.001, *posthoc* Bonferroni test.

Interestingly, DNP treatment in human SH-SY5Y neuroblastoma cells caused a decrease in SOCE activity to 71.5 ± 2.8% of control values, and MCU silencing in mouse N2a neuroblastoma cells resulted in a similar decrease to 79 ± 6% of the levels in control cells treated with scrambled sequences. These results are consistent with the hypothesis that GDAP1 deficiency prevents adequate handling of SOCE-driven Ca^{2+} inflow, thereby causing a decrease in SOCE.

1.4 SOCE stimulates mitochondrial respiration in neuroblastoma cells and Ca^{2+} signaling is required

We have shown that neuroblastoma SH-SY5Y cell line can experience substantial Ca^{2+} influx through SOC channels. The role of Ca^{2+} in tuning ATP production to ATP demand in excitable cells has been known for a long time (Hayakawa et al., 2005, Glancy and Balaban, 2012, Jouaville et al., 1999), and recently, Ca^{2+} has been shown to cooperate in adjusting coupled respiration to ATP demand under the workloads induced by carbachol, high K^+ depolarization or veratridine in neurons (Llorente-Folch et al., 2013, Rueda et al., 2014). We analyzed whether SOCE-driven Ca^{2+} signals stimulate mitochondrial respiration in control pLKO-NT SH-SY5Y cells. The Seahorse XF24 technique was used to analyze oxygen consumption rate (OCR) in intact cells. To this end, SOCE was activated by carbachol, which mobilizes ER-Ca^{2+} through activation of IP_3 receptors, followed by the addition of 2 mM $CaCl_2$. We observed a strong stimulation of respiration by Ca^{2+}, which resulted in 30.39 ± 2.43 % increase over basal levels (Fig. 10 A), mainly coupled respiration, as it was largely inhibited by oligomycin (Fig. 10 B). In the absence of external Ca^{2+} (vehicle), the increase in OCR was not observed (Fig. 10 A). SOCE-induced stimulation of respiration was smaller than the maximal respiration obtained after uncoupler addition (Fig. 10 C).

We next studied whether SOCE-stimulated respiration was due to an increase in ATP demand or through a direct effect of cytosolic Ca^{2+} on oxidative phosphorylation. To this end, we preincubated control neuroblastoma cells with different concentrations of BAPTA-AM, a rapid intracellular Ca^{2+} chelator (Abramov and Duchen, 2008) before measuring SOCE-stimulated respiration. BAPTA loading prevents cytosolic Ca^{2+} signals but does not change Ca^{2+} inflow through SOCE channels and thereby maintains the SOCE-induced workload (Llorente-Folch et al., 2013). In BAPTA-AM (50 and 25 μM) loaded cells Ca^{2+} stimulation of respiration was completely abolished during the first 3 min after Ca^{2+} readmission (Fig. 10 D), and the OCR stimulation observed thereafter was much lower in the presence of the chelator than in its absence (Control: 51.53 ± 6.19 % vs. 50 μM BAPTA-AM: 8.25 ± 2.39 % or 25 μM BAPTA-AM: 11.02 ±3.38 %, 6 min after stimulation) (Fig. 10 E). A low chelator concentration (10 μM) had smaller, yet significant effects on Ca^{2+} stimulation respiration (Control: 38.56 ± 5.88 % vs. 10 μM

BAPTA-AM: 16.28 ± 2.88 %, 3 min after stimulation) (Fig. 10 D, E). Therefore, the results indicate that Ca^{2+} signaling itself through regulation of mitochondrial respiration is required to couple respiration to SOCE activity.

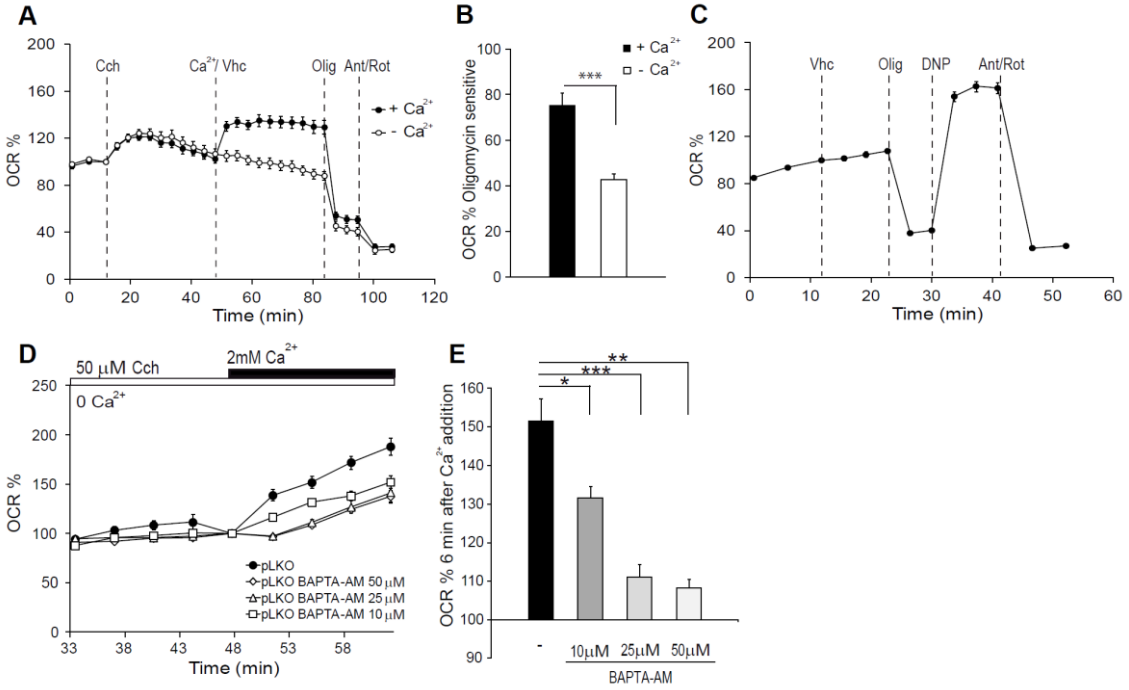

Figure 10. SOCE stimulates mitochondrial respiration in neuroblastoma cells. (**A**) Oxygen consumption rate expressed as percentage of basal OCR in control pLKO-NT cells showing the sequential injection of carbachol (Cch, 50 µ M), vehicle (Veh) or Ca^{2+} (2 mM) and metabolic inhibitors: oligomycin (Olig, 6 µM) and antimycin A/rotenone (Ant/Rot, 1µ M/1 µM) at the indicated time points. (**B**) Quantification of oligomycin sensitive OCR expressed as percentage of basal OCR in control pLKO cells. The effect of calcium was significant (n = 27, obtained from at least 8 independent experiments). (**C**) Oxygen consumption rate expressed as percentage of basal OCR in control pLKO-NT cells at the time of vehicle addition. Sequential injection: vehicle, oligomycin, 2-4 dinitrophenol (DNP, 0.25 mM) and antimycin A/rotenone at the indicated time points. (**D**) SOCE-stimulation of respiration in absence or presence of BAPTA-AM (50, 25 or 10 µM). Oxygen consumption rate expressed as percentage of OCR after carbachol addition (Cch, 50 µ M) in Ca^{2+}-free medium. (**E**) Quantification of % OCR 6 min after calcium addition, (n = 3–12, from at least 3 independent experiments). All data are expressed as mean ± SEM. Means were compared using one-way ANOVA, *p < 0.05, **p < 0.01, ***p < 0.001, *posthoc* Bonferroni test.

1.5 GDAP1 silencing impairs SOCE-driven stimulation of respiration

We next tested the effect of *GDAP1*-KD on SOCE-stimulated mitochondrial respiration. For this purpose, stimulation of OCR was determined in the control and *GDAP1*-KD cells similarly to that described in section 1.4. We found that OCR stimulation caused by Ca^{2+} re-addition after ER-Ca^{2+} mobilization by carbachol was clearly lower in *GDAP1*-KD than control pLKO-NT cells

(Fig. 11 A). Ca^{2+}-dependent stimulation of respiration 3 min after Ca^{2+} addition, a time at which the SOCE-induced by carbachol increase in $[Ca^{2+}]_i$ levels off (Fig. 11 B), was 27.9 ± 2.4% above the initial values in control cells and 16.0 ± 0.7% in GDAP1 deficient cells (Fig. 11 A, C). Interestingly, the increase in respiration caused by carbachol addition in a Ca^{2+}-free medium is also reduced in the *GDAP1*-KD cells (Fig. 11 A, D), a result explained by lower ER-Ca^{2+} levels observed in *GDAP1*-KD cells (Pla-Martin et al., 2015).

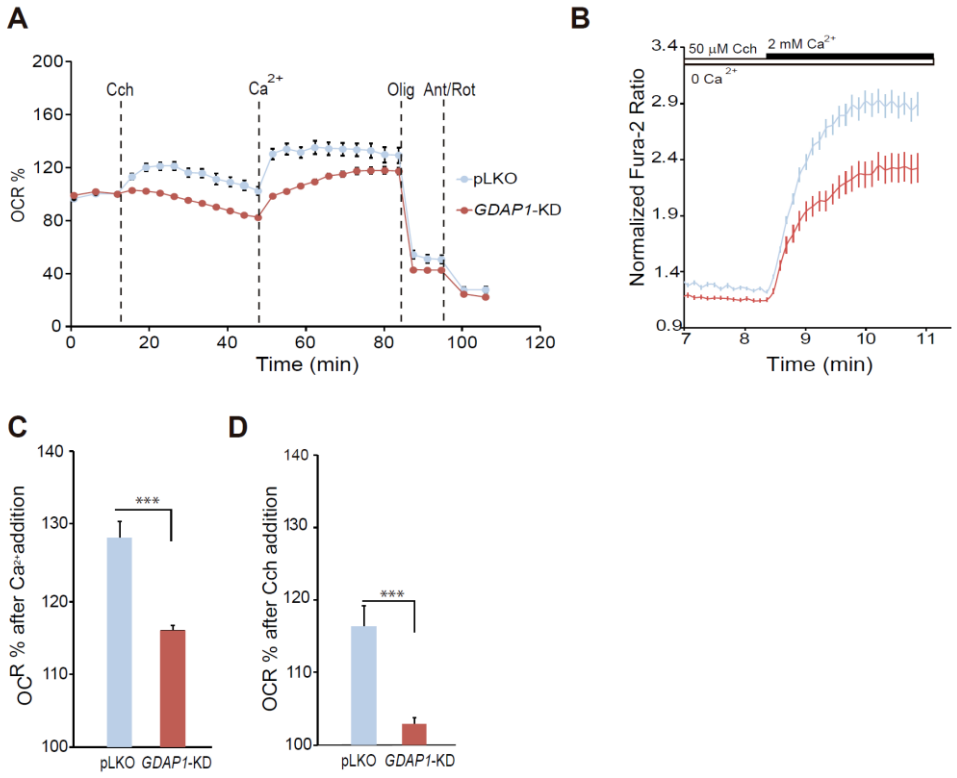

Figure 11. SOCE-stimulated respiration is reduced in *GDAP1*-KD cells. (**A**) Oxygen consumption rate expressed as percentage of basal OCR in control pLKO and *GDAP1*-KD cells, showing the sequential injection of carbachol (Cch, 50 µ M), Ca^{2+} (2 mM) and metabolic inhibitors. (**B**) Fura-2 $[Ca^{2+}]_i$ signals upon addition of 2 mM Ca^{2+} in Ca^{2+}-free medium with 50 µM carbachol. Data were obtained from 3 independent experiments (n = 65-80 cells). (**C, D**) Quantification of % OCR 6 min after carbachol addition and 3 min after calcium addition respectively. Data were obtained from at least 8 independent experiments (n = 27–50). All data are normalized to the initial values and are expressed as mean ± SEM. Means were compared using one-way ANOVA, ***p < 0.001, *posthoc* Bonferroni test.

1.6 Clinical GDAP1 mutations: Recessive GDAP1 mutations located in the α-loop domain fail to restore SOCE and SOCE-stimulated respiration in *GDAP1*-KD cells

GDAP1 has two GST domains separated by a region called α-loop, and a C-terminus containing one or two transmembrane domains (TM). The α-loop is the protein domain where caytaxin and RAB6B interact (Pla-Martin et al., 2013). This suggests that mutations in the α-loop

or even in the GST domains could affect the interaction with other protein partners, while mutations in the TM domain may be related to failures in mitochondrial anchoring as proposed previously (Wagner et al., 2009). In a previous study performed in Francesc Palau´s Lab to address the role of these GDAP1 mutant proteins in restoring SOCE activity in *GDAP1*-KD cells, a battery of dominant and recessive missense mutations located along the whole protein (summarized in scheme 1) were overexpressed in *GDAP1*-KD cells and the effect on SOCE was tested. The results of this investigation showed that the effect of GDAP1 on SOCE activity was different depending on the type of mutation (Gonzalez-Sanchez et al., 2017). In brief, recessive mutations located outside α-loop, in TM or GST domains, had the same effect on SOCE as wild-type GDAP1, they did not show any impairment of SOCE activity. Overexpression of GDAP1 dominant mutations in the α-loop region or in a GST domain, caused a significant increase in SOCE activity compared to wild type GDAP1, suggesting a gain of function of these mutations. And finally, recessive mutations located inside the α-loop, as p.S130C, were unable to compensate for the lack of GDAP1 in SOCE activity, indicating a complete loss of function.

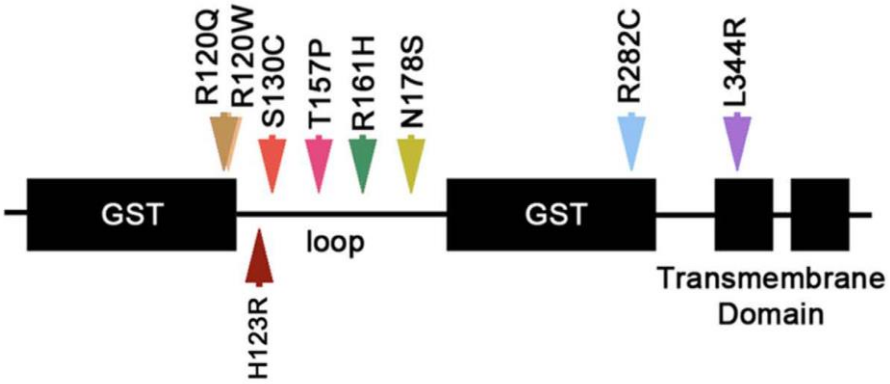

Scheme 1. Schematic view of the GDAP1 missense mutations selected. GDAP1 dominant mutations: p.R120W, p.H123R, p.T157P. GDAP1 recessive mutations located in the α-loop: p.S130C, p.R161H, p.N178S. GDAP1 recessive mutations located outside the α-loop: p.L344R, p.R282C, p. R120Q.

Regarding these results, we proposed to test the effect of recessive GDAP1 mutations located in the α-loop on SOCE-stimulated respiration in *GDAP1*-KD, since they showed to be unable to restore SOCE activity in these cells. Mutated variants were expressed using a bicistronic pCAGIG vector, which expressed also GFP, and allowed us to select the cells expressing the p.S130C mutant variant. To analyze the OCR in an intact cell population we used the Seahorse XF24 technique, which requires a large number of almost pure transfected cells to make reliable experiments. The yield of neuroblastoma *GDAP1*-KD transfection, using different reagents, was very low (15-30 % of positive cells, judged by GFP fluorescence). To use them in OCR

experiment, cells needed to be sorted out in a cell sorter, based on the presence of GFP in the target population (Fig. 12 A, B).

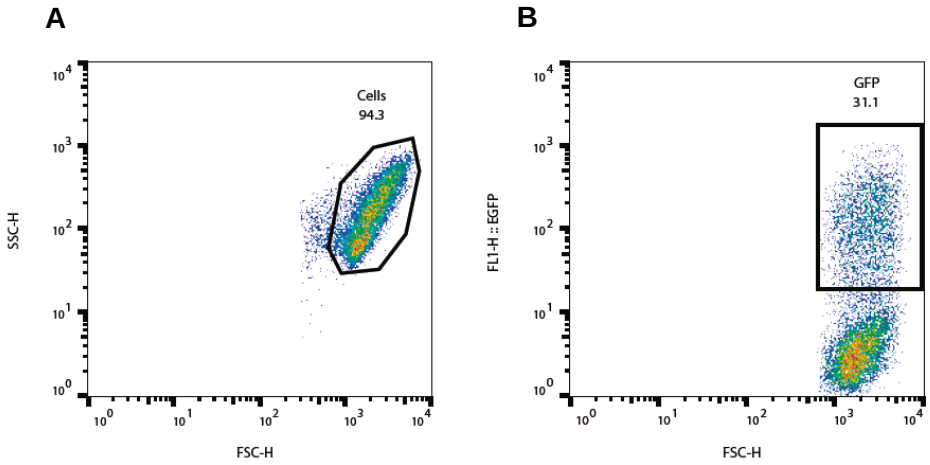

Figure 12. Sorting experiment of pLKO-NT cells transfected with the control empty bicistronic pCAGIG vector. (**A**) Flow cytometry scatter plot of forward scatter (FSC-H) versus side scatter (SSC-H) showing the cell population sorted out. (**B**) Flow cytometry scatter plot of forward scatter (FSC-H) versus GFP fluorescence scatter, showing that the 30% of sorted cells were GFP positive.

However, the results after sorting were not successful, even though we used two different sorters, (at CBMSO and CNB facilities) and conditions. This was due to the large occurrence of electronic aborts and sorting conflicts (the percentage of abort was between 40-50%) whereby target and non-target cells were thrown away and not processed. These problems may be due to cell aggregation and were not solved by decreasing the sample rate and/or modifying the sorting buffer. The purity of final samples was also low (values between 70-80%). In sum, we could not obtain enough GFP positive neuroblastoma cells to carry out respiration experiments.

Therefore, we generated a stable *GDAP1*-KD HEK293T cell line using the pLKO.1 pure vector (see materials and methdos), with about 70% reduction in GDAP1 protein levels and a control HEK293T cell line containing the corresponding empty vector (pLKO-NT) (Fig. 13 A). HEK293T cell line has substantial Ca^{2+} influx through SOCE channels (Roos et al., 2005) and it has been used widely to study SOCE mechanism. To determine the effect of recessive GDAP1 mutations on SOCE-stimulated respiration in *GDAP1*-KD HEK293T cells, we expressed GDAP1 p.S130C variant, together with wild type GDAP1 or empty vector as controls. The percentage of cells expressing the vector with different constructions (judged by GFP fluorescence) was about 90%, and therefore, adequate for studies of respiration. SOCE was assayed using the same protocol, addition of 10 μM tBuBHQ in a Ca^{2+}-free medium followed by 2 mM $CaCl_2$ addition, which resulted in a substantial SOCE-driven stimulation of mitochondrial respiration (32.93 ±

4.47 % increase over basal levels, 3 min after addition) (Fig. 13 B, C). Re-expression of WT GDAP1 protein increased SOCE-driven OCR in the *GDAP1*-KD cells (27.23 ±7.13 %) while the p.S130C variant failed to restore the SOCE-driven stimulation in respiration. In fact, SOCE-driven respiration was not different from that of *GDAP1*-KD cells transfected with empty vector (5.31 ± 3.73 % vs. 7.90 ±2.19 %, respectively) (Fig. 13 D, E). These results suggest that the effects of recessive mutations in the α-loop domain on the SOCE activity could cause a reduced SOCE-driven stimulation of mitochondrial respiration.

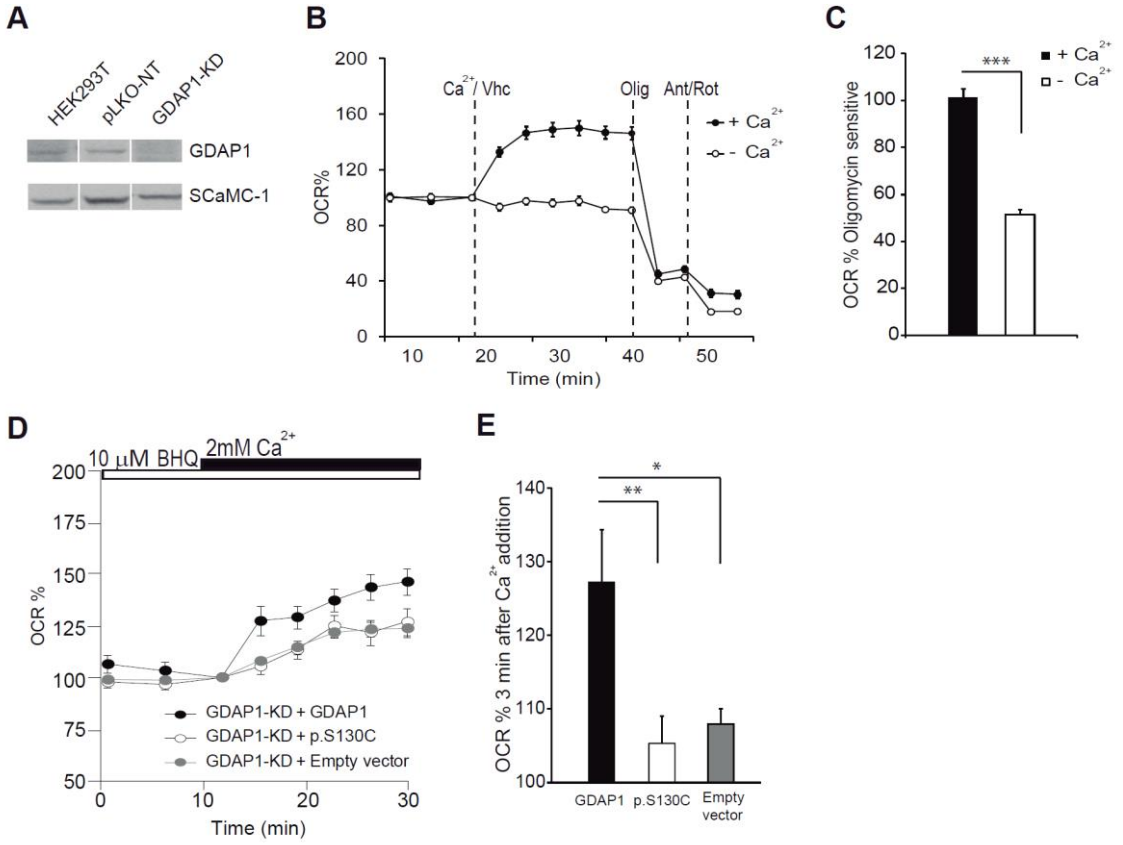

Figure 13. Recessive GDAP1 mutation p.S130C fails to recover SOCE stimulation of respiration in HEK293T *GDAP1*-KD cells. (**A**) Western blot analysis of GDAP1 levels in mitochondrial fractions. Primary antibodies used were α -GDAP1 and α -SCaMC-1 as a control. The experiment was repeated twice with similar results. (**B**) SOCE-stimulation of respiration in HEK293T cells. Oxygen consumption rate expressed as percentage of basal OCR in HEK293T cells treated with 10 μM BHQ in Ca^{2+}-free medium, showing the sequential injection of 2 mM Ca^{2+} or vehicle (Vhc) and metabolic inhibitors: oligomycin (Olig, 6 μM) and antimycin A/rotenone (Ant/Rot, 1μM/1 μM). (**C**) Oligomycin sensitive OCR expressed as percentage of basal OCR in both conditions. The effect of calcium was statistically significant (n = 11 from at least 3 independent experiments). (**D**) SOCE stimulation respiration in HEK293T *GDAP1*-KD expressing WT GDAP1 protein, recessive GDAP1 mutant p.S130C or empty vector. Oxygen consumption rate expressed as percentage of basal OCR in cells treated with 10 μM BHQ in Ca^{2+}-free medium. (**E**) Quantification of % OCR 3 min after calcium addition. Data were obtained from at least 4 independent experiments (n = 10–20). All data are expressed as mean ± SEM. Means were compared using one-way ANOVA test. *p < 0.05, **p < 0.01, ***p < 0.001, *posthoc* Bonferroni test.

1.7 Impaired mitochondrial localization at the subplasmalemmal domain in GDAP1 mutants

Early findings revealed that the failure in mitochondrial Ca^{2+} uptake was a cause, and not a consequence, of the reduced SOCE activity in SH-SY5Y *GDAP1*-KD cells (Pla-Martin et al., 2013). The study of mitochondrial localization in relation to subplasmalemmal domain (SP, defined as 0–2 μ m from plasma membrane) during SOCE activation showed that in control cells, after SOCE activation mitochondrial moved towards subplasmalemmal domains. However, the mitochondria of *GDAP1*-KD cells were mobilized to the plasma membrane to a lesser extent (Pla-Martin et al., 2013).

In order to address the mechanisms whereby the different mutations affect SOCE activity, we studied the localization of mitochondria in relation to SP microdomains (0–2 μ m from plasma membrane) in basal conditions and after ER-Ca^{2+} depletion with Tg in a Ca^{2+}-free medium in neuroblastoma cells expressing dominant (p.T157P) or recessive (p.R161H) mutations in the α –loop domain. To this end, *GDAP1*-KD human neuroblastoma cells were co-transfected with WT GDAP1 or mutant variants (p.T157P or p.R161H), and Orai1::CFP expression vector, used to mark the plasma membrane. 24 hours later, cells were fixed after 10 min of vehicle or Tg treatment. The c-myc epitope from GDAP1-c-myc expression vectors served as marker for mitochondria in immunofluorescence assays. In *GDAP1*-KD cells transfected with empty vector, mitochondria were marked with α -β ATPase. The mitochondrial fluorescence distribution between opposite plasma membranes within the SP and the central cell zones was analyzed as explained in Materials and Methods. And, in agreement with the previous findings, after ER-Ca^{2+} mobilization, mitochondria from *GDAP1*-KD cells expressing an empty vector failed to localize at SP, resulting in a similar mitochondrial distribution in basal and SOCE-activation conditions (Fig. 14 A, B). Re-expression of WT GDAP1 protein allowed mitochondria to be positioned in SP after ER-Ca^{2+} depletion (Fig. 14 A,g,h and B), while overexpression of the recessive mutation p.R161H, located in the α-loop domain, had an effect similar to silencing of GDAP1, no relocation of mitochondria to SP (Fig. 14 A,k,l, B). Mitochondria from cells overexpressing the dominant mutation did not relocalize to SP after ER-Ca^{2+} depletion (Fig. 14 B) but showed a surprisingly higher percentage of mitochondria close to SP under basal conditions (Fig. 14 A,m). This difference was more pronounced in the interval from 0 to 1 μ m from the plasma membrane (Fig. 14 C), and suggests that this abnormal mitochondrial localization, closer to plasma membrane, may be associated with the higher SOCE activity caused by the dominant mutant.

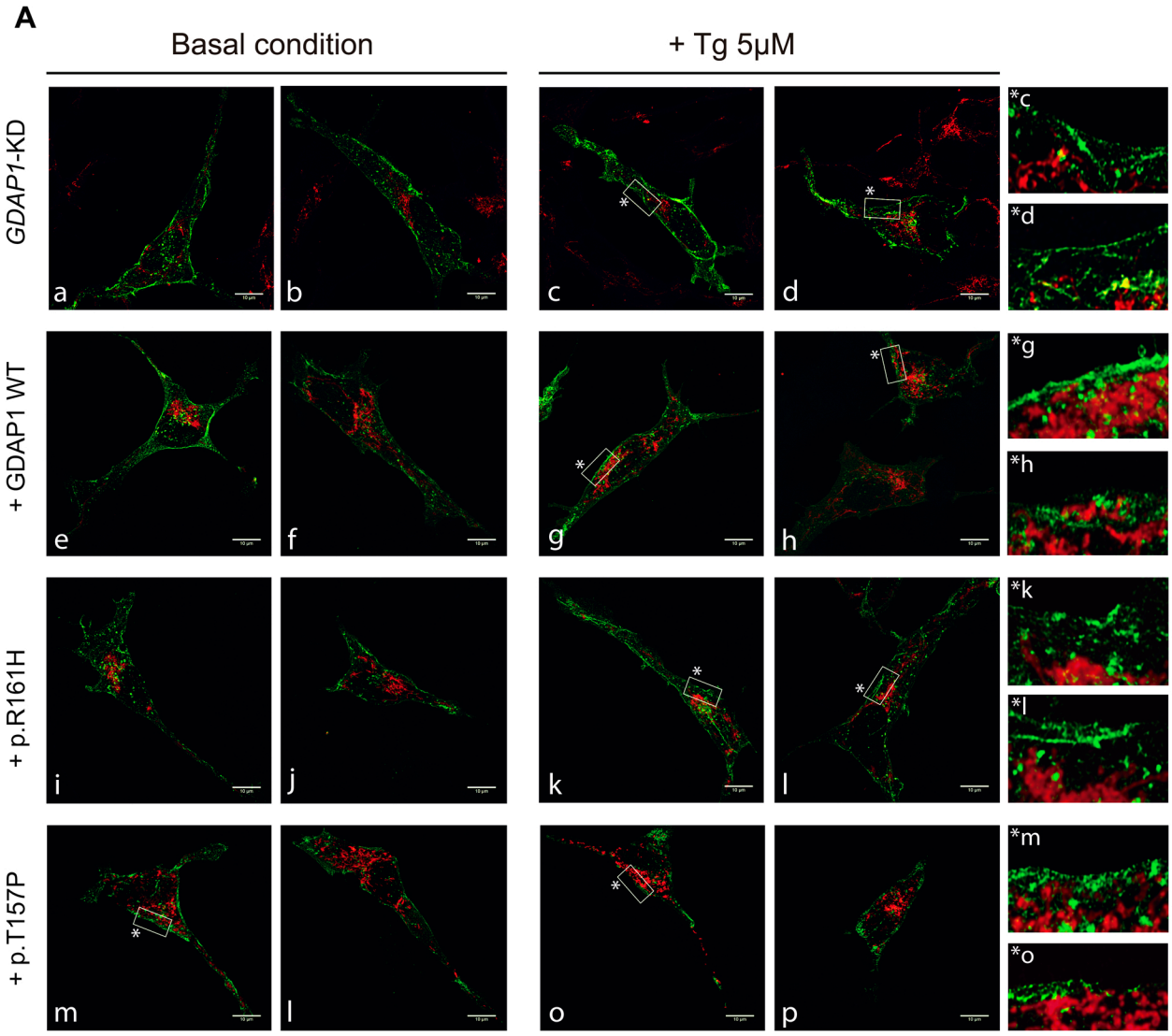
A
Basal condition
+ Tg 5µM
GDAP1-KD
+ GDAP1 WT
+ p.R161H
+ p.T157P
a
b
c
d
*c
*d
e
f
g
h
*g
*h
i
j
k
l
*k
*l
m
l
o
p
*m
*o

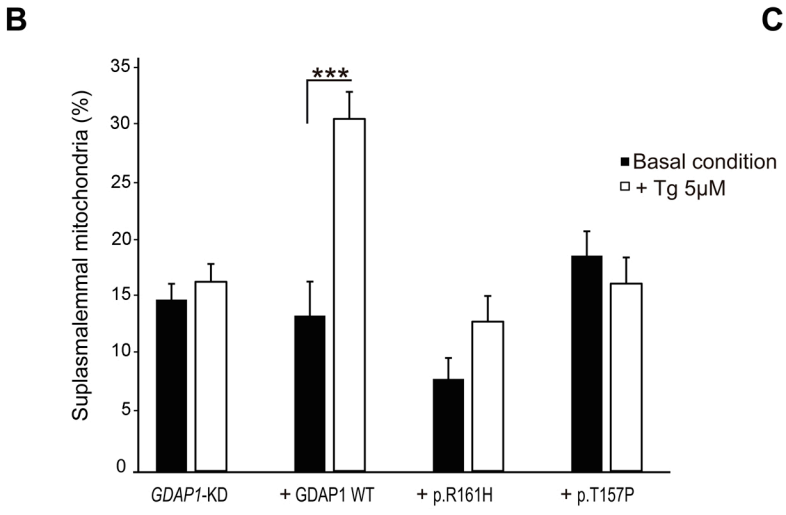
B
Suplasmalemmal mitochondria (%)
35
30
25
20
15
10
5
0
***
Basal condition
+ Tg 5µM
GDAP1-KD
+ GDAP1 WT
+ p.R161H
+ p.T157P

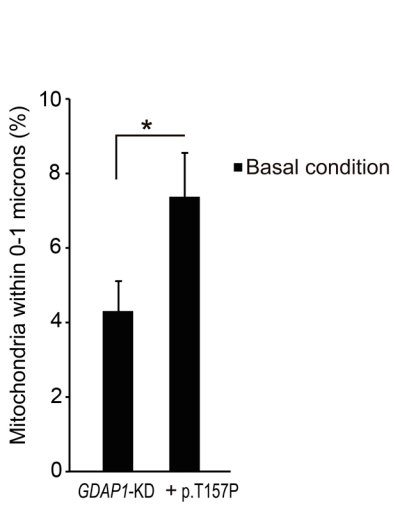
C
Mitochondria within 0-1 microns (%)
10
8
6
4
2
0
*
Basal condition
GDAP1-KD
+ p.T157P

Figure 14. **Mitochondrial network distribution in basal and SOCE activated conditions**. (**A**) Confocal images of *GDAP1*-KD neuroblastoma cells transfected with empty vector (mitochondria marked with α -β ATPase, red signal), GDAP1 WT or mutant proteins (marked with α -c-myc, red signal) and Orai1::CFP (green signal) in basal conditions and after ER-Ca^{2+} mobilization with 5 μM Tg in Ca^{2+}-free medium. Cells were fixed after 10 min of vehicle or Tg treatment. Two images of each cell type and condition are shown. High resolution images of vehicle- (only in the case of dominant mutation) or Tg-treated cells are also shown on the right panel side. Bars indicate 10 μm. (**B**) Quantification of mitochondrial fluorescence distribution in basal conditions and after depletion of ER calcium stores with 5 μM Tg in Ca^{2+}-free medium. Fluorescence distribution at the subplasmalemmal (SP) domains (defined as 2 μm underneath the plasma membrane) and the central zone (the space between the opposite subplasmalemmal domains) were calculated as indicated in Materials and Methods. Fluorescence distribution in 7–9 cells per treatment and genotype is shown. (**C**) Quantification of mitochondrial fluorescence distribution obtained for mitochondria located 0–1 μm away from the plasma membrane. Results are expressed as mean ± SEM. Data were analyzed using two-way (**B**) or one way (**C**) ANOVA and *posthoc* Bonferroni tests. *$p < 0.05$, **$p < 0.01$, ***$p < 0.001$.

2. STORE-OPERATED CALCIUM ENTRY IN CORTICAL NEURONS

The presence of the SOCE mechanism in neurons has been widely discussed (Lu and Fivaz, 2016), since these cells have other major pathways, VGCC or receptor operated channels, to permit Ca^{2+} inflow from external medium (Grienberger and Konnerth, 2012). But currently, the existence of SOCE has been documented in different excitable cells, such as neurons and skeletal, cardiac or smooth muscle cells (Moccia et al., 2015, Pan et al., 2014). The purpose of the present work was to evaluate SOCE in cortical neurons along with the role of this mechanism in the response to physiological stimuli, as activation of muscarinic receptors and metabotropic glutamate receptors. To this aim we used primary cortical neurons of 8-12 days *in vitro* (DIV) from control C57BL/6Sv129 mice.

2.1 Store-operated Ca^{2+} entry is induced in cortical neurons after store depletion

To assess the presence of SOCE pathway in primary cortical neurons, we depleted ER stores using 1 µM thapsigargin (Tg), the sarco/endoplasmatic reticulum Ca ATPase (SERCA) inhibitor, in a medium with 1 µM tetrodotoxin (TTX), in order to prevent neuronal activity. Tg application resulted in an increase in cytosolic calcium, quantified as area under the curve (A.U.C., ΔRatio·min) (Fig. 15 A black line, B). To determine whether Ca^{2+} entered the cell through SOC channels we applied widely used SOCE blockers along with Tg particularly. 2-APB (2-aminoethoxydiphenyl borate) and YM-58483 (also called BTP2) (Xia et al., 2014, Prakriya and Lewis, 2015). YM-58483 is highly specific and has been shown not to interfere with VGCC (Xia et al., 2014), and 2-APB is a commonly used bimodal SOCE modulator which decreases SOCE activity at high concentrations and also inhibits IP_3 signaling (Prakriya and Lewis, 2015). Tg-induced cytosolic Ca^{2+} signal was maintained during the recording time in the absence of SOCE inhibitors (0.35 ± 0.04 ΔRatio·min) but rapidly decreased in the presence of 10 µM YM-58483 (0.12 ± 0.01) or 50 µM 2-APB (0.20 ± 0.03), consistent with a block of Ca^{2+} entry through SOC channel (Fig. 15 A, B).

In addition, to eliminate the possibility that neuronal activity contributed to this calcium signal, cytosolic Ca^{2+} levels were recorded in the presence of an inhibitor cocktail containing 10 µM CNQX (an AMPA/Kainate receptor inhibitor), 10 µM MK-801 (NMDA receptor inhibitor) and 5 µM MPEP (a metabotropic glutamate receptor inhibitor) to block excitatory action of ionotropic and metabotropic glutamate receptors, 10 µM TTX to block voltage-gated sodium channels, and 50 µM $NiCl_2$ to block low-voltage-activated calcium channels. The inhibition cocktail was present during the whole experiment and figure 15 C shows that the cytosolic Ca^{2+} increase triggered by emptying ER-Ca^{2+} was similar both in the absent and the presence of the inhibitory cocktail (0.35±0.04 vs. 0.39±0.05).

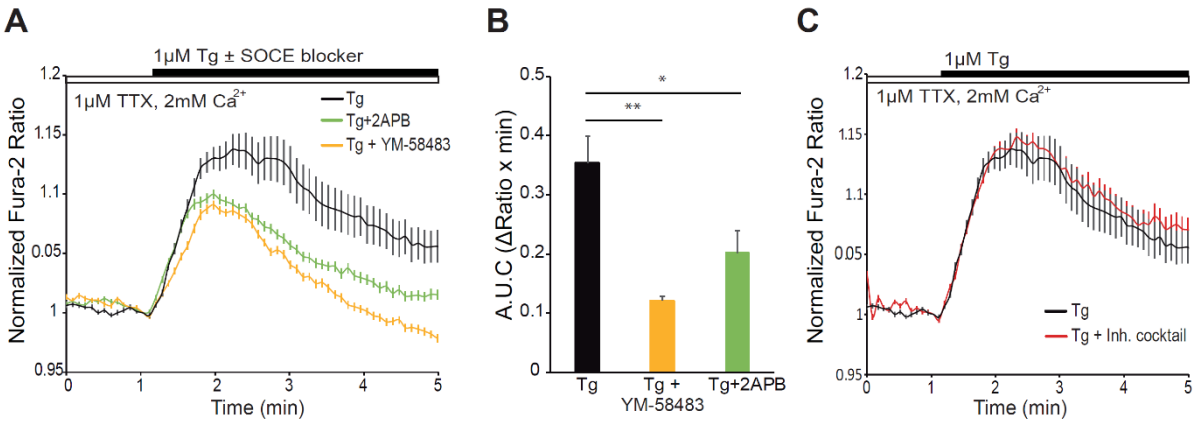

Figure 15. SOCE activity in primary cortical neurons. (**A**) Fura-2 $[Ca^{2+}]_i$ signals in cortical neurons in HCSS medium containing 2 mM $CaCl_2$ and 1 µM TTX, upon addition of 1 µM Tg ± 10 µM YM-584836 or 50 µM 2-APB where indicated. (**B**) Quantification of area under SOCE curve (A.U.C, ΔRatio·min). Data were obtained from 3 independent experiments (n=3). (**C**) Fura-2 $[Ca^{2+}]_i$ signals in cortical neurons in HCSS medium containing 2 mM $CaCl_2$ and 1 µM TTX ± inhibitory cocktail (10 µM CNQX, 10 µM MK-801, 5 µM MPEP, 50 µM $NiCl_2$), upon addition of 1 µM Tg. Data were obtained from 3 independent experiments (n=3). All data are normalized to the initial values and are expressed as mean ± SEM. Means were compared using one-way ANOVA, *p < 0.05, **p < 0.01, ***p < 0.001, *posthoc* Bonferroni test.

2.2 SOC channels proteins are expressed in mice cortical neurons

The molecular identity of SOCE has been shown to be different depending on the neuronal type. Different proteins have been implicated in SOCE, Orai and Trpc family as calcium channels located in plasma membrane and Stim family as calcium sensor in ER-membrane. To determine the molecular identity of SOCE in mice cortical neurons, we first investigated the mRNA levels of the different isoforms of the SOCE components Orai, Stim and Trpc family. To this aim, we performed a RT-qPCR in 8 DIV cultured cortical neurons from four embryos. The profiles obtained for each embryo were quite similar to one another. We found that the isoforms forming the pore channel with highest mRNA levels were Orai1, Orai2, Trpc1 and Trpc4, and the levels of Stim1 and Stim2 were similar (Fig. 16 A).

Protein levels of the SOCE components with highest mRNA levels were investigated by Western Blot. As positive controls, we used the human neuroblastoma SH-SY5Y and HEK293T cell lines, which are known to express these proteins (Olianas et al., 2014, Ong et al., 2015). We observed a band at 50 kDa with the ORAI1 antibody, a single band at 110 kDa with the TRPC4 antibody and a band at 90 kDa with the STIM2 antibody. However, we did not observe the bands corresponding to ORAI2 and TRPC1 proteins (Fig. 16 B). These results show that in cultured cortical neurons, ORAI1, STIM2 and TRPC4 were the predominant members of their respective families, in agreement with previous reports in cortical and others neurons from CNS (Korkotian

et al., 2016, Berna-Erro et al., 2009, Steinbeck et al., 2011). Therefore, these isoforms may have a role in Ca^{2+} homeostasis in these cells.

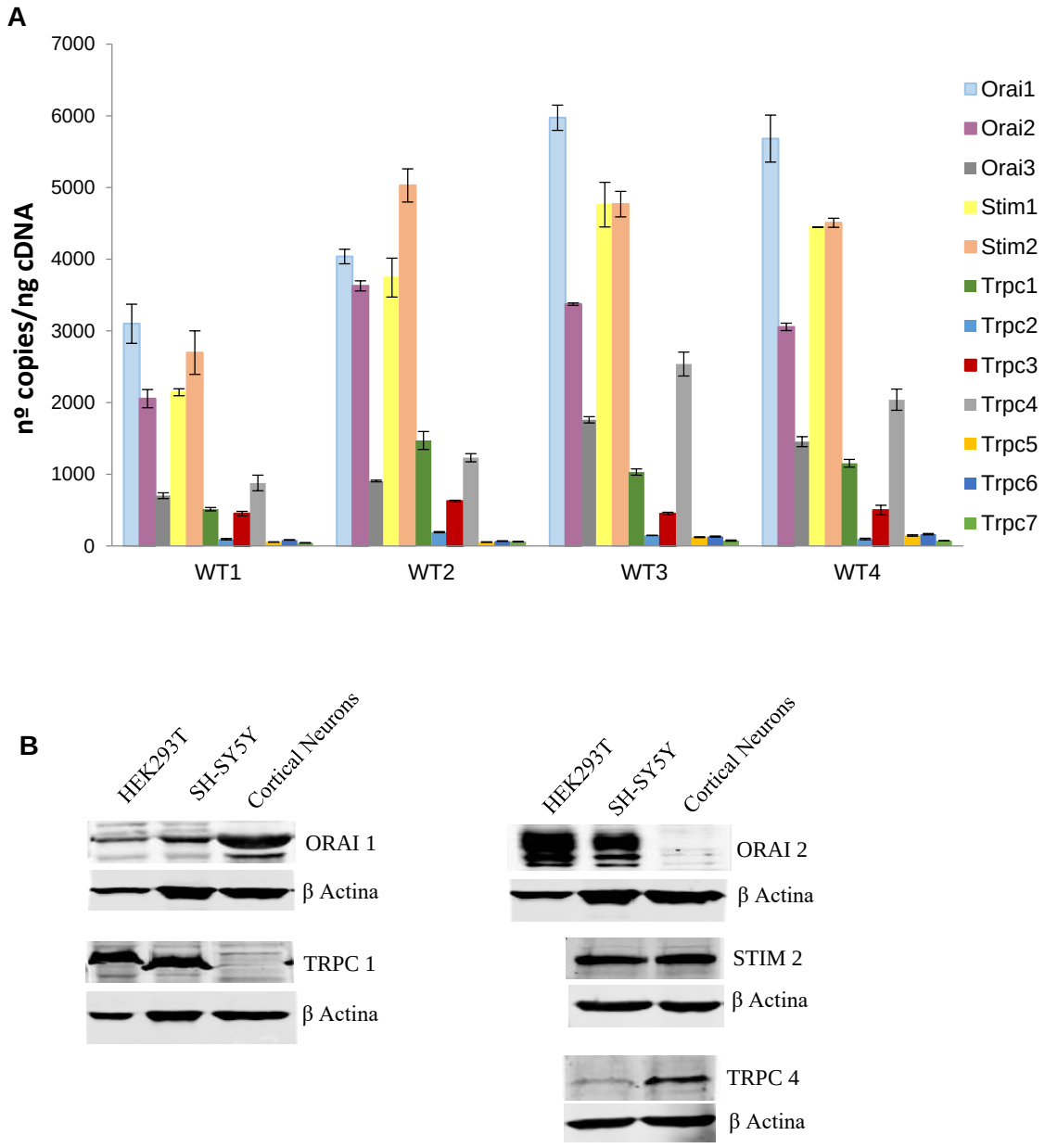

Figure 16. SOC channel proteins. (**A**) RT-PCR of DNA complementary from primary cortical neurons obtained from four embryos with *Orai 1-3, Stim 1, 2* and *Trpc 1-7* specific primers (**B**) Western Blot analysis of ORAI 1, ORAI 2, STIM 2, TRPC 1 and TRPC 4 levels. Protein extracts were obtained from HEK293T cells, SH-SY5Y cells and 8-9 DIV cortical neurons. Primary antibodies used were α-Orai1, α-Orai2, α-Stim2, α-Trpc1, α-Trpc4 and α -β Actina as a control.

2.3 Modulation of SOCE by mitochondria in cortical neurons

Mitochondrial handling of Ca^{2+} entry through SOC channels has been shown to regulate SOCE activity by preventing Ca^{2+}-dependent slow inactivation (Singaravelu et al., 2011, Quintana and Hoth, 2012, Deak et al., 2014, Samanta et al., 2014) and our results in neuroblastoma cells shown in this thesis. But, results obtained using different cells types show no modulation of SOCE by mitochondrial Ca^{2+} handling, arguing that the close apposition between plasma and ER membranes occurring during SOCE activation prevents mitochondria from getting close to the Ca^{2+} channels at the plasma membrane (Fonteriz et al., 2016, De Stefani et al., 2016, Giacomello et al., 2010).

To address whether calcium uptake in mitochondria may control SOCE in mouse cortical neurons, we first silenced MCU and then studied the effect of MCU silencing on SOCE, by investigating the effect of MCU silencing on the increase in cytosolic Ca^{2+} after ER-Ca^{2+} depletion by Tg. To this aim, neurons were transduced at 3 DIV with recombinant adeno-associated virus (rAAV) containing MCU-directed small hairpin RNA (shRNA) or non-target control sequence (scrambled) along with mCherry to identify infected neurons. Experiments were performed at DIV 9-10. Analysis by Western Blot show a 64.5 ± 10.4 % decrease in MCU protein level (Fig. 17 A). Next, we confirmed that MCU silencing was effective, after studying NMDA-driven Ca^{2+} entry in mitochondria, since it has been shown to decrease in MCU-silenced neurons (Qiu et al., 2013). We measured changes in mitochondrial Ca^{2+} levels using the genetically coded calcium indicator 4mt-D3cpv targeted to mitochondrial matrix (Palmer et al., 2006). Figure 17 B and C show the dramatic reduction of NMDA-driven mitochondrial Ca^{2+} peak in MCU-silenced neurons, quantified as area under the curve (A.U.C., ΔRatio·min), compared to control (scrambled) (0.45 ± 0.14 vs. 1.59 ± 0.31, respectively).

Then, we investigated if SOCE was affected by MCU knockdown, Fig 17 D and E show that there was no difference in the SOCE-induced cytosolic Ca^{2+} signal obtained in scrambled- and MCU silenced-neurons (0.34 ± 0.10 vs. 0.32 ± 0.08, respectively). Therefore, this result indicates that, in cortical neurons in primary culture, mitochondria do not modulate SOCE activity.

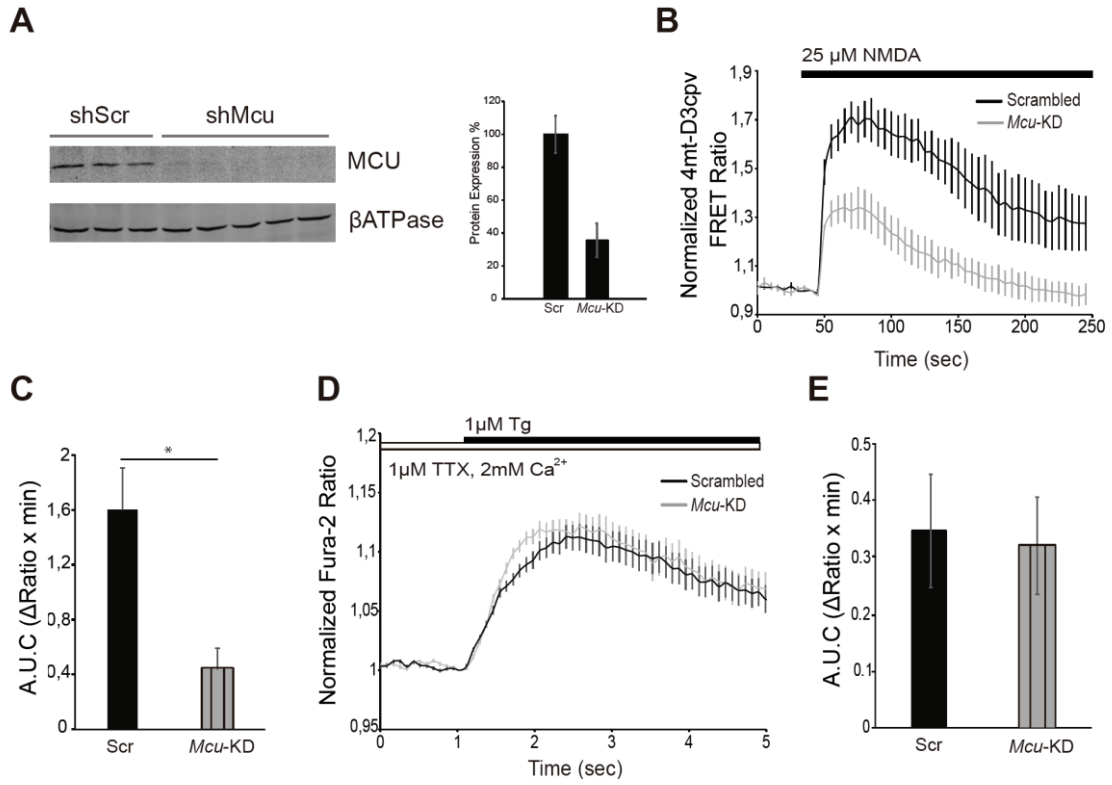

Figure 17. Mitochondrial modulation of SOCE. (**A**) Western Blot analysis of MCU levels. Protein extracts were obtained 6-7 days after infection of cortical neurons with either rAAV containing shScr or shMcu. Primary antibodies used were α -MCU and α -β ATPase as a control. MCU protein levels drop to 35.5 ± 10.9% of control values. (**B**) 4mt-D3cpv mitochondrial calcium signals in scrambled or *Mcu*-KD neurons upon addition of 25 µ M NMDA where indicated. (**C**) Quantification of area under the curve after 25 µM NMDA addition (ΔRatio·min). Data were obtained from 4 independent experiments (n=11-15). (**D**) Fura-2 $[Ca^{2+}]_i$ signals in scrambled or *Mcu*-KD neurons in HCSS medium containing 2 mM $CaCl_2$ and 1 µM TTX, upon addition of 1 µM Tg where indicated. (**E**) Quantification of area under SOCE curve (ΔRatio·min). Data were obtained from 3 independent experiments (n=3) (p = 0.84). All data are normalized to the initial values and are expressed as mean ± SEM. Means were compared using one-way ANOVA, *p < 0.05, **p < 0.01, ***p < 0.001, *posthoc* Bonferroni test.

3. ROLE OF STORE-OPERATED CALCIUM ENTRY IN ACETILCHOLINE RECEPTOR FUNCTION

Acetylcholine receptors (AchR) are integral membrane proteins that respond to the binding of acetylcholine, a neurotransmitter. They can be classified into two groups: nicotinic acetylcholine receptors (nAChR, also known as "ionotropic" acetylcholine receptors) and muscarinic acetylcholine receptors (mAChR, also known as "metabotropic" acetylcholine receptors). Activation of M1, M3 and M5 mAChR, all G-protein coupled-receptors, cause the hydrolysis of phosphatidylinositol 4,5-biphosphate (PIP_2) to generate inositol 1,4,5-triphosphate (IP_3) and diacylglycerol (DAG). An increase in IP_3 levels triggers Ca^{2+} release from internal stores, which could activate SOC channels, and Ca^{2+} entry through these channels could be involved in mAChR-driven Ca^{2+} signaling.

3.1 Activation of acetylcholine receptors by carbachol modulates cytosolic Ca^{2+} only when neurons exhibit spontaneous synaptic activity

First, we investigated the capacity of the agonist of acetylcholine receptor, carbachol (Cch), to modulate cytosolic calcium through mobilizing Ca^{2+} from the ER, and subsequent SOCE opening. To this aim, 8-9 DIV primary cortical neurons were loaded with Fura-2 AM and 250 µM carbachol was added in the presence of 1 µM TTX in order to avoid any response except the activation of AChRs. Similar to previous reports in neurons, activation of mAChRs did not change significantly cytosolic Ca^{2+} levels (Fig. 18 A), indicating that they did not have the ability to activate IP_3R and mobilize intracellular Ca^{2+} (Delmas et al., 2002, Delmas et al., 2004). However, it has been shown that the most effective activation of IP_3R is achieved when IP_3 and Ca^{2+} are presented together (Berridge, 1998). In agreement with this notion, del Rio et al., found that mAChRs can mobilize Ca^{2+} from ER in neurons when they are previously depolarized, due to the large amount of Ca^{2+} that enters by depolarization (del Rio et al., 1999). Therefore, the assumption was made that this situation could lead to SOCE activation. To test this possibility, we performed experiments in the absence of TTX. Mouse cortical neurons plated at high density (150.000 cells/cm^2) and cultured for 8-9 DIV show spontaneous Ca^{2+} activity in the absence of TTX. This activity consists of repetitive Ca^{2+} transients which occurred at the same time in all recorded neurons (Fig. 18 B, time 0-5 min). Treatment of these neurons with the AMPA/Kainate receptor antagonist CNQX (10 µM), the NMDA receptor antagonist MK-801 (10 µM) or the Na^+ channel blocker TTX (1 µM) abolished the spontaneous Ca^{2+} activity (Fig. 18 B), indicating that they depend upon a burst of action potentials (Opitz et al., 2002, Bacci et al., 1999, Young et al., 2005). We found that, in these neurons, Cch addition enhanced the spontaneous Ca^{2+} activity of the whole neuronal network and it was maintained while Cch was present (Fig. 18 C, D).

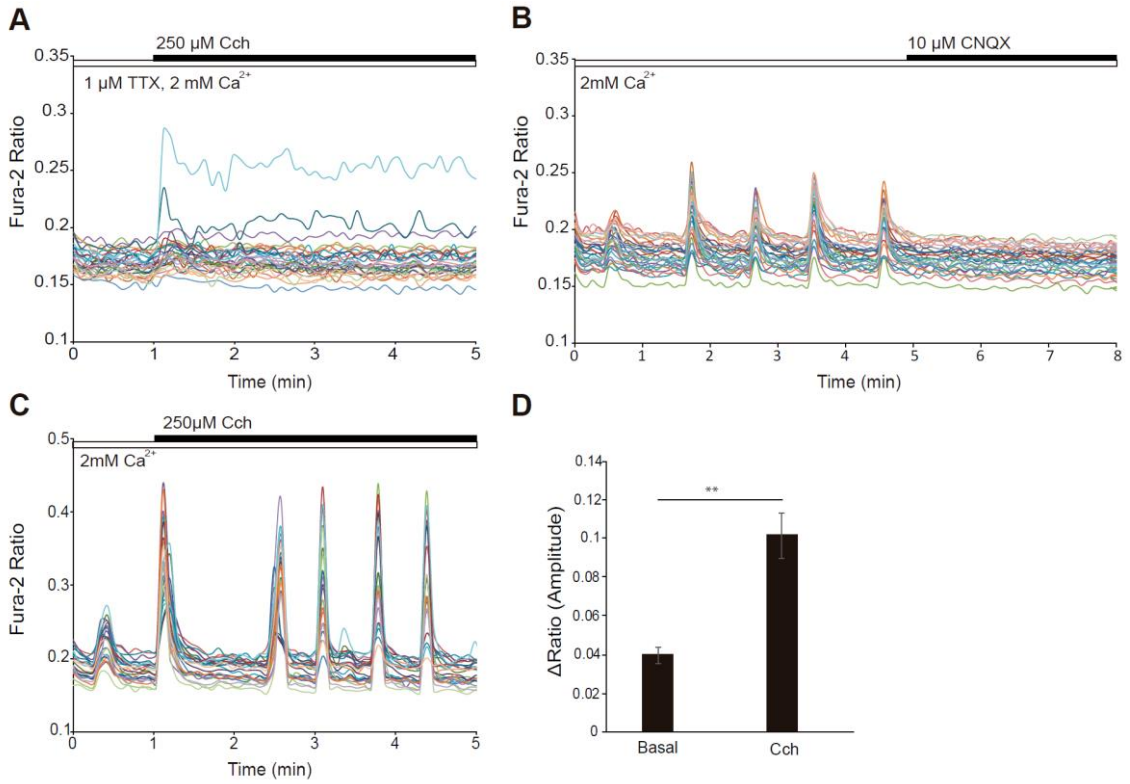

Figure 18. Cch-enhanced spontaneous Ca^{2+} oscillations. (**A**) Fura-2 $[Ca^{2+}]_i$ signals in cortical neurons in HCSS medium containing 2 mM $CaCl_2$ and 1 µM TTX, upon addition of 250 µM Cch where indicated. (**B**) Fura-2 $[Ca^{2+}]_i$ signals in neurons in HCSS medium containing 2 mM $CaCl_2$, upon addition of 10 µM CNQX where indicated. Similar results were obtained using 10 µM MK-801 or 1 µM TTX. (**C**) Fura-2 $[Ca^{2+}]_i$ signals in neurons in HCSS medium containing 2 mM $CaCl_2$, upon addition of 250 µM Cch where indicated. All graphs show a representative experiment; each trace corresponds to a single neuron from the same recording field. (**D**) Quantification of peak amplitude as ΔRatio (F340/F380) ± SEM comparing basal spontaneous Ca^{2+} oscillations to Cch-enhanced Ca^{2+} oscillations. Data were obtained from 6 independent experiments. Means were compared using one-way ANOVA, **p < 0.01, *posthoc* Bonferroni test.

3.2 Cch-enhanced spontaneous Ca^{2+} activity depends on SOCE activation

Next, we investigated if SOCE could be involved in Cch-induced enhanced Ca^{2+} activity. To this end, we studied Cch-enhanced Ca^{2+} transients in the presence of the SOCE inhibitor YM-58483. Interestingly, we found that when Cch was added along with 10 µM YM-58483 no Cch-induced potentiation was observed (Fig. 19 A). The first Ca^{2+} transient after Cch addition was unchanged but the subsequent transients progressively decreased in magnitude (72.4 ± 9.0 % decrease in presence of YM-58483) and frequency (within a fixed time interval of 4 min: 7.4 ± 0.9 peaks when Cch was added alone and 3 ± 1 peaks when Cch was added along with YM-58483) (Fig. 19 B, C). As control, we studied the effect of SOCE blocker on basal spontaneous Ca^{2+} activity, finding no effect on cytosolic Ca^{2+} (Fig. 19 D). This result indicates that SOCE is

not involved in basal spontaneous Ca^{2+} oscillations, which take place in the absence of TTX, but it is activated upon AChRs stimulation.

Moreover, Ca^{2+} oscillations enhanced by Cch depend on synaptic activity since they were totally prevented by TTX and the AMPA/kainate antagonist (CNQX) or NMDA antagonist (MK-801) (Fig. 19 E), in agreement with previous results (Nash et al., 2004, Young et al., 2005). It is likely that SOCE activation following ER-Ca^{2+} mobilization by muscarinic receptors agonists is essential in order to maintain the enhanced Ca^{2+} transients.

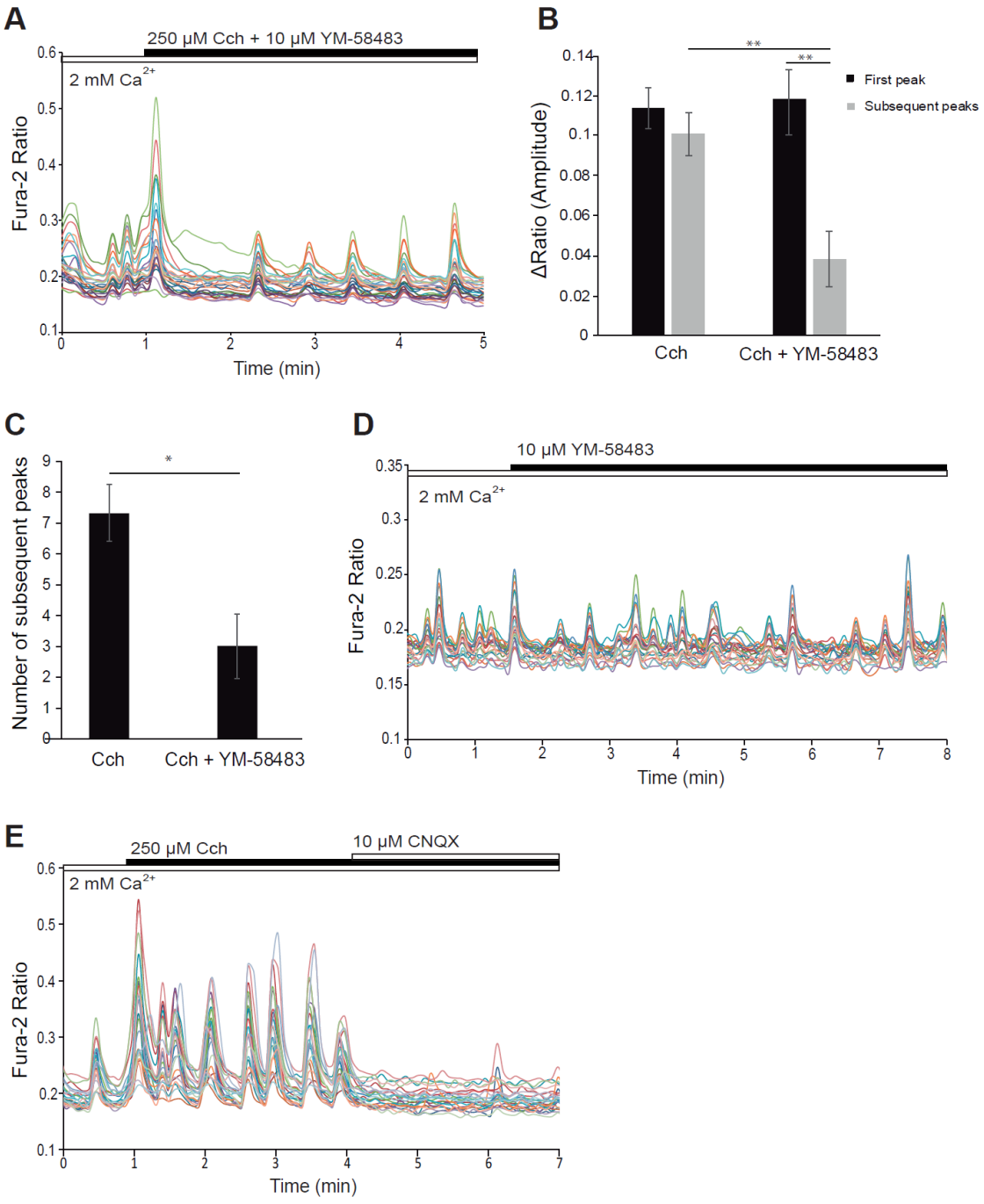

Figure 19. Cch-enhanced spontaneous Ca^{2+} activity depends on SOCE. (**A**) Fura-2 $[Ca^{2+}]_i$ signals in cortical neurons in HCSS medium containing 2 mM $CaCl_2$ upon addition of 250 μM Cch together with 10 μM YM-58483 where indicated. (**B**) Quantification of peak amplitude as ΔRatio (F340/F380) ± SEM comparing the first peak (black) to the mean of the subsequent peaks within a fixed time interval of 4 min after 250 μM Cch addition (grey) in presence or absence of 10 μM YM-58483. Data are expressed as mean ± SEM and were obtained from 6 independent experiments. Means were compared using two-way ANOVA, $^{**}p < 0.01$, *posthoc* Bonferroni test. (**C**) Quantification of the number of subsequent peaks in a fixed time interval (4 min after Cch addition). Data are expressed as mean ± SEM and were obtained from 6 independent experiments. Means were compared using one-way ANOVA, $^{*}p < 0.05$, *posthoc* Bonferroni test. (**D**) Fura-2 $[Ca^{2+}]_i$ signals in cortical neurons in HCSS medium containing 2 mM $CaCl_2$ upon addition of 10 μM YM-58483 where indicated. (**E**) Fura-2 $[Ca^{2+}]_i$ signals in cortical neurons in HCSS medium containing 2 mM $CaCl_2$ upon addition of 250 μM Cch and then 10 μM CNQX where indicated. Similar results were obtained using 10 μM MK-801 or 1 μM TTX. All graphs show a representative experiment; each trace corresponds to a single neuron from the same recording field.

3.3 Ca^{2+} influx through SOCE is involved in the maintenance of ER-Ca^{2+} levels, but ER-Ca^{2+} levels do not have any impact on Cch-enhanced spontaneous Ca^{2+} activity

Ca^{2+} entry through SOC channels has been shown to be necessary for the refilling of ER-Ca^{2+}, which in neurons is continuously emptying at rest (Samtleben et al., 2015). To study the impact of SOCE inhibition in the ER-Ca^{2+} levels, cortical neurons were treated with the SOCE blocker YM-58483 (10 μM) in medium containing 2 mM $CaCl_2$ during different time intervals (from 5 to 60 min). Then, we measured ER-Ca^{2+} levels in neurons loaded with Fura2-AM applying 1 μM ionomycin in a calcium-free medium. SOCE inhibition was found to decrease Ca^{2+} levels of the ER, but the decrease was similar (approximately 25% decrease) in the different time intervals (Fig. 20 A, B). As other pathways for Ca^{2+} entry are active during these experiments (TTX is not present), these results reveal a role of Ca^{2+} influx through SOCE in maintenance of ER-Ca^{2+} levels, setting a minimal limit of specific SOCE effects on about 25% of ionomycin-releasable ER-Ca^{2+}.

Having shown that SOCE is essential for the proper maintenance of ER-Ca^{+2} levels in cortical neurons, we studied if mobilization of Ca^{2+} from ER was a necessary step for the ability to enhance Ca^{2+} oscillations by Cch. To test this hypothesis, we pre-treated neurons with the sarco/endoplasmatic reticulum Ca^{2+} ATPase (SERCA) inhibitor Tg (1 μM), in order to avoid the replenishment of ER-Ca^{2+}. Tg pre-treatment did not affect neither the amplitude of the Ca^{2+} transients enhanced by Cch (Fig. 20 C, D) nor the number of subsequent peaks (within a fixed time interval of 4 min after Cch addition) (Fig. 20 E). In agreement with previous reports (Young et al., 2005), the mechanism of the enhanced Ca^{2+} signals does not rely on Ca^{2+} mobilization from intracellular stores.

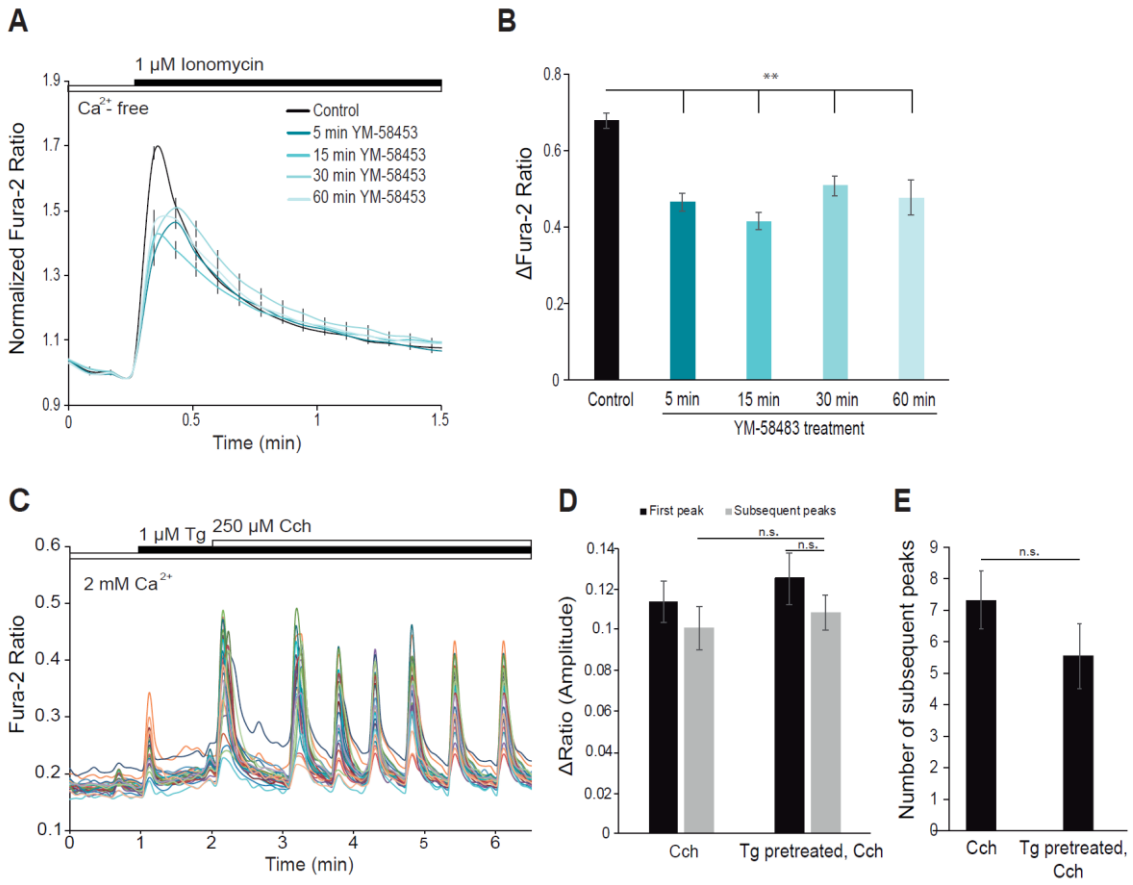

Figure 20. Impairment of ER-Ca^{2+} uptake by SOCE inhibition does not impact on Cch-enhanced Ca^{2+} signals. (**A**) Fura-2 $[Ca^{2+}]_i$ signals in control and pre-treated neurons with 10 µM YM-58483 during different time intervals upon addition of 1 µM ionomycin in a Ca^{2+}-free medium where indicated. Data are expressed as mean ± SEM. (**B**) Quantification of Ca^{2+} peak as ΔRatio (F340/F380) ± SEM after ionomycin addition. Data were obtained from 5-7 independent experiments for each condition. Means were compared using one-way ANOVA, **p < 0.01, *posthoc* Bonferroni test. (**C**) Fura-2 $[Ca^{2+}]_i$ signals in cortical neurons in HCSS medium containing 2 mM $CaCl_2$ upon addition of 1 µM Tg and 250 µM Cch where indicated. Representative experiment, each trace corresponds to a single neuron from the same recording field. (**D**) Quantification of peak amplitude as ΔRatio (F340/F380) ± SEM comparing the first peak (black) to the mean of the subsequent peaks within a fixed time interval of 4 min after 250 µM Cch addition (grey) in control and Tg (1 µM) pre-treated neurons. Data were obtained from 5 independent experiments (n=5). Means were compared using two-way ANOVA, *posthoc* Bonferroni test. (**E**) Quantification of the number of subsequent peaks in a fixed time interval (4 min after Cch addition) comparing control to Tg pre-treated neurons. Data are expressed as mean ± SEM and were obtained from 5-6 independent experiments. Means were compared using one-way ANOVA (p = 0.11), *posthoc* Bonferroni test.

3.4 The inhibition of Cch-enhanced Ca^{2+} activity by blocking SOCE is not due exclusively to a decrease of neurotransmitter release

The SOC channel proteins have been shown to localize both in presynaptic and postsynaptic densities (de Juan-Sanz et al., 2017, Korkotian et al., 2014). Because Ca^{2+} oscillations enhanced

by Cch depend upon a burst of action potentials, and therefore, they depend on presynaptic glutamate release (Bacci et al., 1999), we investigated if the inhibition of SOCE resulted in an impairment of glutamate release. To address this point, neurons were pretreated with the glutamate transport inhibitor DL-Threo-β-Benzyloxyaspartic acid (DL-TBOA), in order to maintain glutamate levels in the synaptic cleft thus bypassing any regulatory effect on glutamate release. We found that, in this situation, the addition of Cch triggered an increase in the amplitude and frequency of Ca^{2+} transients (compared with the spontaneous Ca^{2+} activity before DL-TBOA addition), an effect which was abolished when the SOCE blocker YM-58483 was present. In fact, the SOCE inhibitor had the same effect in the absence or presence of DL-TBOA (section 3.2), a progressive decrease in amplitude and frequency of Ca^{2+} oscillations (Fig. 21 A, B). These results suggest that SOCE plays a role in the postsynaptic site, along with mAChRs stimulation, but, we cannot exclude a possible function of SOCE in the presynaptic density.

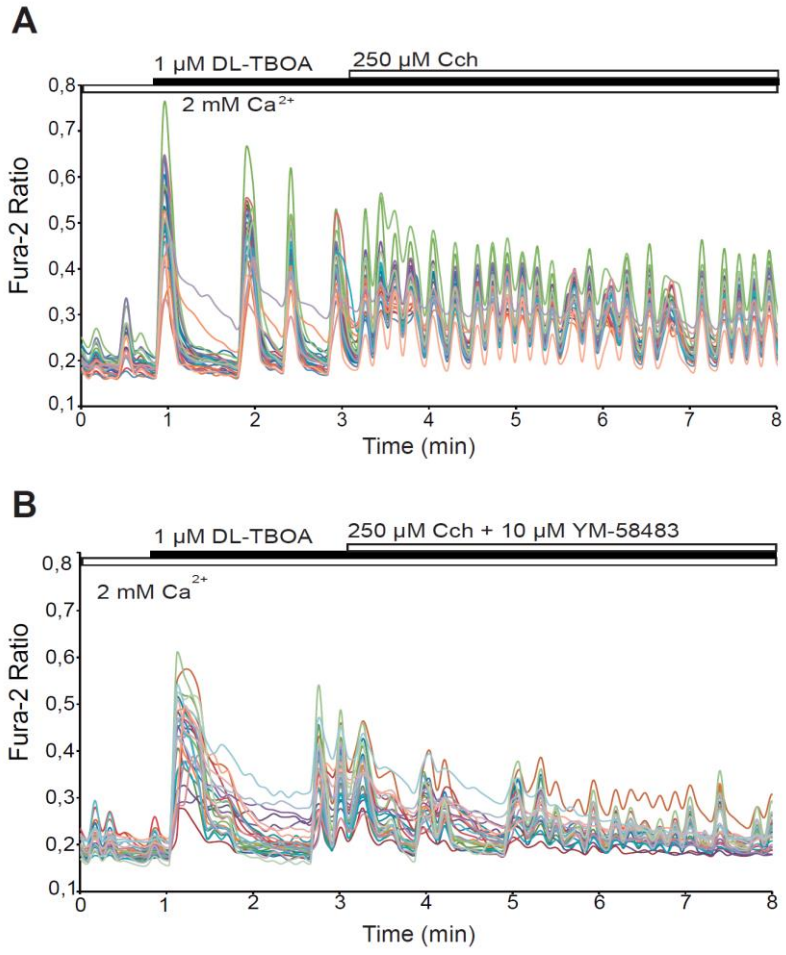

Figure 21. SOCE and neurotransmitters release. (**A**) Fura-2 $[Ca^{2+}]_i$ signals in cortical neurons in HCSS medium containing 2 mM $CaCl_2$ upon addition of 1 µM DL-TBOA and 250 µM Cch ± 10 µM YM-58483 where indicated. Representative experiments, each trace corresponds to a single neuron from the same recording field. Experiments were repeated three times with similar results.

3.5 Carbachol-enhanced Ca^{2+} oscillations stimulate mitochondrial respiration and this stimulation depends on SOCE activation

In excitable cells, Ca^{2+} regulates cell function both by activation of ATP consumption (contraction, movement, ion transport, Ca^{2+} pumps) (ter Keurs, 2012, Carafoli, 1987) and by activating ATP production through stimulation of oxidative phosphorylation. Ca^{2+} regulation of oxidative phosphorylation occurs by a) Ca^{2+} entering into mitochondrial matrix through the mitochondrial calcium uniporter (MCU) complex (Kamer and Mootha, 2015) and the activation of matrix dehydrogenases and complex V, F_1F_0-ATPsynthase (Balaban, 2009, Glancy and Balaban, 2012) and b) through Ca^{2+} activation of mitochondrial metabolite transporters, the aspartate-glutamate carriers (AGCs) and the ATP-Mg^{2+}/Pi transporters (SCaMCs) (del Arco and Satrustegui, 1998, del Arco and Satrustegui, 2004, Fiermonte et al., 2004, Satrustegui et al., 2007), by its action in the intermembrane space. In a previous work, we demonstrated that Ca^{2+} cooperates in adjusting coupled respiration to ATP demand under the workloads induced by carbachol, high K^+ depolarization or veratridine in neurons (Llorente-Folch et al., 2013, Rueda et al., 2014, Llorente-Folch et al., 2015). However, these responses are still unknown in neurons showing spontaneous Ca^{2+} activity. To investigate if the increase in Ca^{2+} transients induced by Cch impacted on mitochondrial respiration in neurons with spontaneous Ca^{2+} activity, we used the Seahorse XF24 technique. Oxygen consumption rate (OCR) changes in intact primary neuronal cultures in 2.5 mM glucose (a concentration close to that normally present in cerebral extracellular fluid in vivo (Lewis et al. 1974)), during exposure to 250 µM Cch, showed that mitochondrial respiration was stimulated upon Cch addition, which resulted in 15.27 ± 1.79 % increase over basal levels (Fig. 22 A, black line). We next studied if Cch-stimulated respiration was affected by the inhibition of SOCE. Interestingly, the increase in OCR induced by Cch was strikingly reduced when Cch was added together with the SOCE blockers 2-APB or YM-58483 (8.97 ± 1.70 % and 6.11 ± 0.97 % respectively) (Fig. 22 A, B).

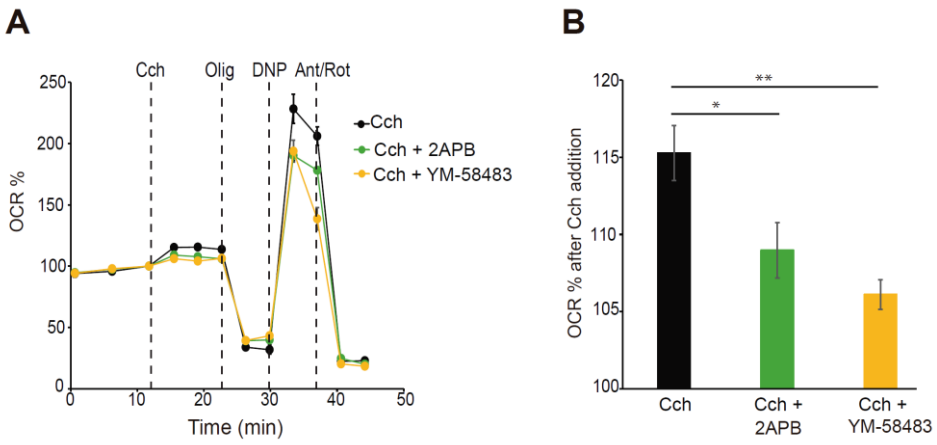

Figure 22. Stimulation of respiration by Cch depends on SOCE activity. (**A**) Oxygen consumption rate expressed as percentage of basal OCR in intact cortical neurons showing the sequential injection of 250 μM Cch ± 50 μM 2-APB or 10 μM YM-584836, and metabolic inhibitors: 6 μM oligomycin (Olig), 0.5 mM 2,4-dinitrophenol (DNP) and 1 μM/1 μM antimycin A/rotenone (Ant/Rot) at the indicated time points. (**B**) Quantification of percentage of respiratory stimulation (% OCR 3 min after carbachol addition) in absence or presence of SOCE blockers. Data were obtained from 3 independent experiments (n = 9-12). All data are normalized to the initial values and are expressed as mean ± SEM. Means were compared using one-way ANOVA, *p < 0.05, **p < 0.01, posthoc Bonferroni test.

3.6 Cch stimulation of mitochondrial respiration is independent of MCU pathway

Having shown that Cch-enhanced Ca^{2+} transients stimulate mitochondrial respiration, we analyzed the different pathways by which Ca^{2+} regulates OXPHOS: by activating metabolite transport in mitochondria, or after Ca^{2+} entry in mitochondria through MCU. First, we investigated if Ca^{2+} reaches mitochondria after Cch stimulation. We measured changes in mitochondrial Ca^{2+} levels using the calcium indicator 4mt-D3cpv targeted to mitochondrial matrix (Palmer et al., 2006), and we observed a robust Ca^{2+} peak in mitochondria after addition of 250 μM Cch, quantified as area under the curve (A.U.C., ΔRatio·min) (0.50 ± 0.16) (Fig. 23 A black line, B). Interestingly, the Ca_{mit} peak was strongly reduced when SOCE was inactivated, applying 10 μM YM-58483 (0.14 ± 0.06) or 50 μM 2-APB (0.04 ± 0.09), together with Cch (Fig. 23 A, B).

Based on these results, we studied the effect of MCU silencing on Cch-stimulated respiration. To address this issue, neurons were infected with rAAV containing MCU-directed small hairpin RNA (shRNA) or non-target control sequence (scrambled) along with mCherry to identify transduced neurons. We found that Cch-driven mitochondrial Ca^{2+} was totally absent in MCU-silenced neurons (Fig. 23 C), while the cytosolic Ca^{2+} enhanced effect evoked by Cch were the same in both scrambled or *Mcu*-KD neurons. No significant differences were found neither in amplitude (comparing the first peak after Cch addition and the mean of the subsequent ones) nor number of peaks after Cch addition (Fig. 23 D, E, F, G). Basal respiration rates were similar in scrambled- and MCU silenced-neurons (Fig. 23 H), and similarly, the stimulation of mitochondrial respiration by Cch was not affect by MCU silencing, OCR reached 13.57 ± 1.05 % in scrambled and 12.46 ± 1.52 % in *Mcu*-KD neurons over basal levels upon Cch addition (Fig. 23 I, J).

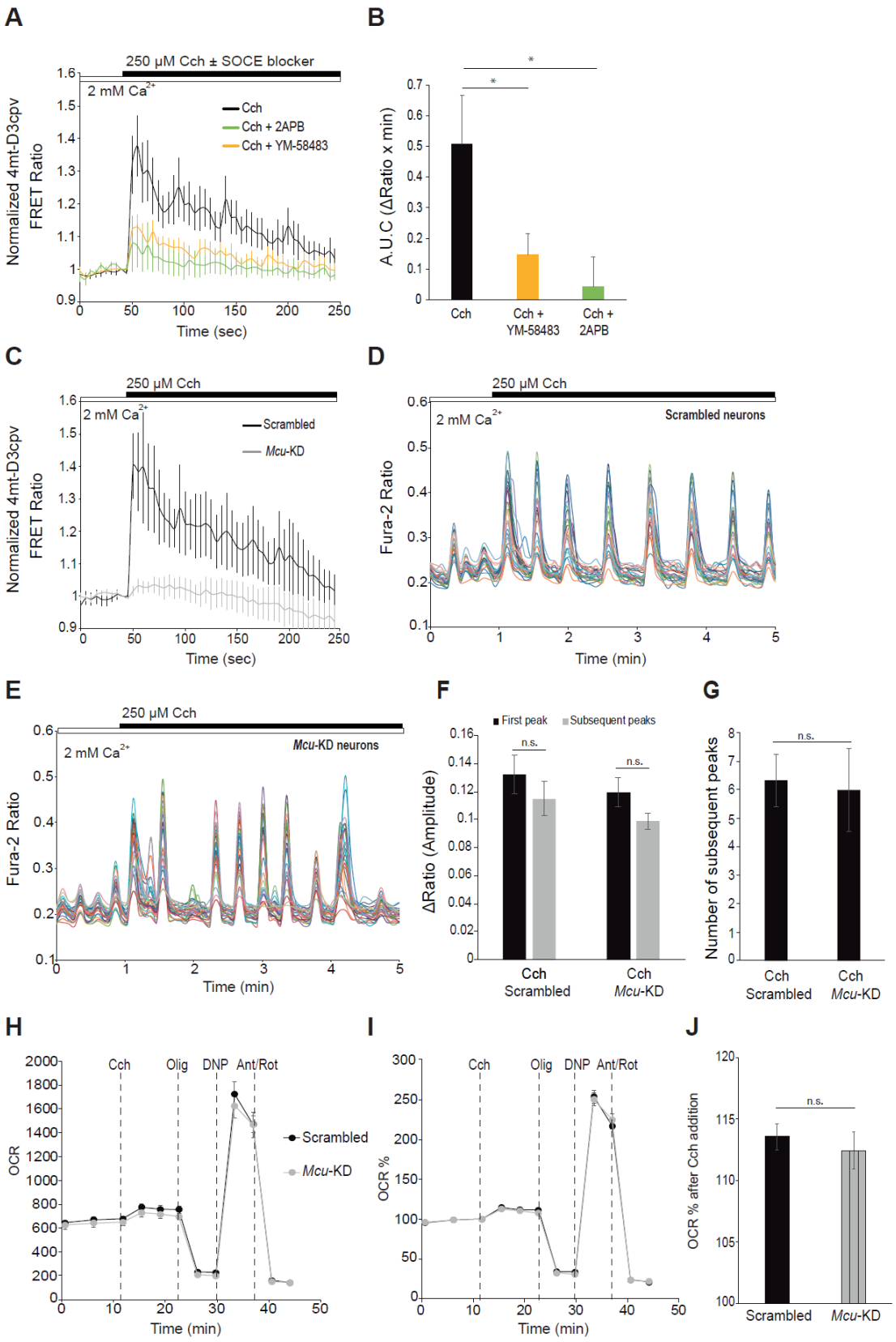

Figure 23. Cch-stimulated respiration is independent on MCU pathway. (**A**) 4mt-D3cpv mitochondrial calcium signals in cortical neurons upon addition of 250 µM Cch ± 10 µM YM-58483 or 50 µM 2-APB where indicated. Data are normalized to the initial values and are expressed as mean ± SEM. (**B**) Quantification of area under the curve after

250 μM Cch addition (ΔRatio·min). Data were obtained from 3 independent experiments (n = 10-15 cells). Data are expressed as mean ± SEM and means were compared using one-way ANOVA, *p < 0.05, **p < 0.01, *posthoc* Bonferroni test. (**C**) 4mt-D3cpv mitochondrial calcium signals in scrambled or *Mcu*-KD neurons upon addition of 250 μM Cch where indicated. Data are normalized to the initial values and are expressed as mean ± SEM. Data were obtained from 3 independent experiments (n = 8-11 cells). (**D, E**) Fura-2 $[Ca^{2+}]_i$ signals in scrambled (**D**) or *Mcu*-KD (**E**) neurons in HCSS medium containing 2 mM $CaCl_2$ upon addition of 250 μM Cch where indicated. Representative experiments, each trace corresponds to a single neuron from the same recording field. (**F**) Quantification of peak amplitude as ΔRatio (F340/F380) ± SEM comparing the first peak (black) to the mean of the subsequent peaks after 250 μM Cch addition (grey) in scrambled (p = 0.21) and *Mcu*-KD (p = 0.26) neurons. Data were obtained from 3 independent experiments (n = 3). Means were compared using two-way ANOVA, *posthoc* Bonferroni test. (**G**) Quantification of the number of subsequent peaks in a fixed time interval (4 min after Cch addition). Data are expressed as mean ± SEM and were obtained from 3 independent experiments. Means were compared using one-way ANOVA, p = 0.86, *posthoc* Bonferroni test. (**H**) Oxygen consumption rate (pmol/min) in scrambled and *Mcu*-KD neurons showing the sequential injection of 250 μM Cch, and metabolic inhibitors: 6 μM Olig, 0.5 mM DNP and 1 μM/1 μM Ant/Rot at the indicated time point. (**I**) Oxygen consumption rate expressed as percentage of basal OCR in scrambled and *Mcu*-KD neurons showing the sequential injection of 250 μM Cch, and metabolic inhibitors at the indicated time points. (**J**) Quantification of percentage of respiratory stimulation (% OCR 3 min after carbachol addition) in scrambled and MCU-silenced neurons. Data were obtained from 3 independent experiments (n = 9-12). Means were compared using one-way ANOVA, p = 0.31, posthoc Bonferroni test.

3.7 Cch stimulation of mitochondrial respiration depends on ARALAR-MAS pathway

Ca^{2+} activation of mitochondrial metabolite transporters occurs by the action of Ca^{2+} on the external side of the inner mitochondrial membrane. There are two metabolite transporters present in neurons, the ATP-Mg^{2+}/Pi exchanger SCaMC-3/Slc25a23 and the aspartate-glutamate exchanger Aralar/AGC1/Slc25a12, a component of the malate-aspartate shuttle. SCaMC-3 has been shown to participate in the stimulation of respiration only at high workloads, whereas ARALAR is needed to maintain basal OCR in intact neurons (Llorente-Folch et al., 2013, Rueda et al., 2014). In addition, the lack of ARALAR was found to prevent the full complete stimulation of respiration in response to Cch addition in lower density cultures than those used in the present study, which did not present spontaneous Ca^{2+} activity. Moreover, in low density cultures, Cch-driven Ca^{2+} signals failed to reach mitochondria (Llorente-Folch et al., 2013), suggesting that the fact that Ca^{2+} reaches mitochondria in these cultures depends on glutamate-dependent Ca^{2+} signals which are enhanced by Cch.

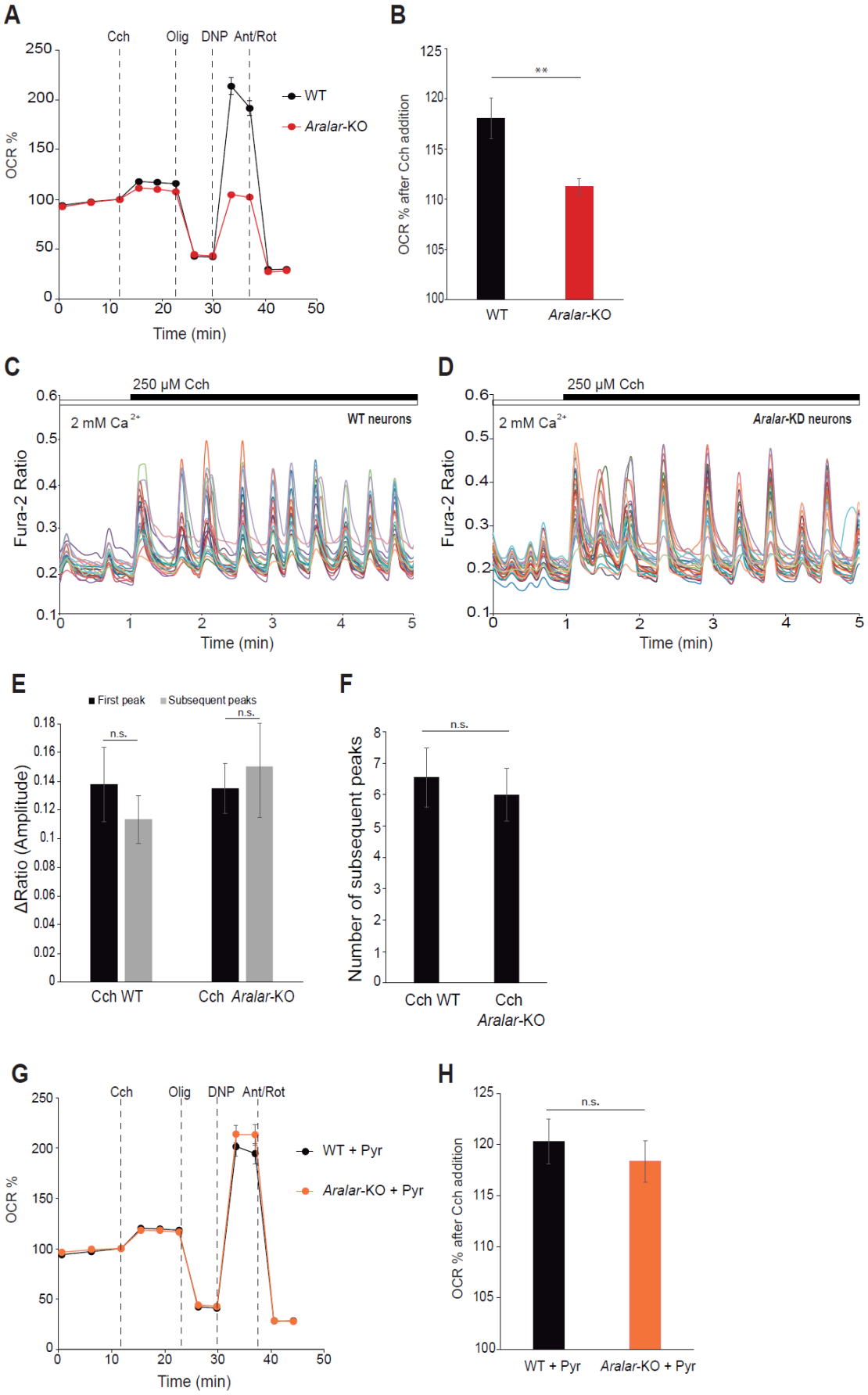
A
Cch
Olig
DNP
Ant/Rot
OCR %
WT
Aralar-KO
Time (min)
B
OCR % after Cch addition
**
WT
Aralar-KO
C
250 µM Cch
2 mM Ca2+
WT neurons
Fura-2 Ratio
Time (min)
D
250 µM Cch
2 mM Ca2+
Aralar-KD neurons
Fura-2 Ratio
Time (min)
E
First peak
Subsequent peaks
n.s.
n.s.
ΔRatio (Amplitude)
Cch WT
Cch Aralar-KO
F
n.s.
Number of subsequent peaks
Cch WT
Cch Aralar-KO
G
Cch
Olig
DNP
Ant/Rot
OCR %
WT + Pyr
Aralar-KO + Pyr
Time (min)
H
n.s.
OCR % after Cch addition
WT + Pyr
Aralar-KO + Pyr

Figure 24. **Cch stimulation of mitochondrial respiration depends on ARALAR-MAS pathway**. (**A**) Oxygen consumption rate expressed as percentage of basal OCR in WT and *aralar*-KO neurons showing the sequential injection of 250 μM Cch, and metabolic inhibitors: 6 μM Olig, 0.5 mM DNP and 1 μM/1 μM Ant/Rot at the indicated time points. (**B**) Quantification of percentage of respiratory stimulation (% OCR 3 min after carbachol addition) in WT and ARALAR-deficient neurons. Data were obtained from 6 independent experiments (n = 21-15). Means were compared using one-way ANOVA, **p < 0.01, *posthoc* Bonferroni test. (**C, D**) Fura-2 $[Ca^{2+}]_i$ signals in WT (**C**) and *aralar*-KO (**D**) neurons in HCSS medium containing 2 mM $CaCl_2$ upon addition of 250 μM Cch where indicated. Representative experiments, each trace corresponds to a single neuron from the same recording field. (**E**) Quantification of peak amplitude as ΔRatio (F340/F380) ± SEM comparing the first peak with the mean of the subsequent peaks after 250 μM Cch addition in WT (p = 0.45) and *aralar*-KO neurons (p = 0.71). Data were obtained from 5 independent experiments. Means were compared using two-way ANOVA, *posthoc* Bonferroni test. (**F**) Quantification of the number of subsequent peaks in a fixed time interval (4 min after Cch addition). Data are expressed as mean ± SEM and were obtained from 5 independent experiments. Means were compared using one-way ANOVA, ***p < 0.001, *posthoc* Bonferroni test. (**G**) Oxygen consumption rate expressed as percentage of basal OCR in WT and *aralar*-KO neurons in 2mM pyruvate medium showing the sequential injection of 250 μM Cch, 6 μM Olig, 0.5 mM DNP and 1 μM/1 μM Ant/Rot at the indicated time points. (**H**) Quantification of percentage of respiratory stimulation (% OCR 3 min after carbachol addition) in WT and ARALAR-deficient neurons in 2mM pyruvate medium. Data were obtained from 3 independent experiments (n = 14-13). Means were compared using one-way ANOVA, p = 0.53, *posthoc* Bonferroni test.

Under the present culture conditions, the Cch-enhanced glutamate Ca^{2+} signals reach mitochondria through the MCU, and having shown that the MCU is not required for Cch-stimulation of respiration, we investigated the role of ARALAR. Figure 24 A and B show that Cch-stimulation of respiration is reduced by about 40% in the absence of ARALAR (WT neurons: 18.04 ± 1.03 % and KO neurons: 11.03 ± 0.79 % increase over basal levels). It is likely that the remaining stimulation of respiration is due exclusively to Ca^{2+}-stimulated workload, not to Ca^{2+} signaling. We checked the cytosolic Ca^{2+} signals induced by Cch in both genotypes and we found that in both WT and *aralar*-KO neurons Cch had the ability to enhance the spontaneous Ca^{2+} oscillations at the same level (Fig. 24 C, D, E, F). Activation by extramitochondrial Ca^{2+} of ARALAR-MAS results in an increase in NADH production in neuronal mitochondria (Pardo et al., 2006) and it has been proposed that Ca^{2+}-activation of ARALAR functions as a “gas pedal” to increase pyruvate formation (Gellerich et al., 2009, Gellerich et al., 2012, Gellerich et al., 2013). To determine if the lower stimulation of respiration in *aralar*-KO neurons was due to a limitation in substrate supply by mitochondria, we analyzed Cch-stimulated respiration in neurons lacking ARALAR in a medium with 2 mM pyruvate. We found that the Cch-stimulated respiration in *aralar*-KO neurons was restored in the presence of pyruvate (18.37 ± 2.02%) at the level of WT (20.29 ± 2.18%) (Fig. 24 G, H). The lack of ARALAR reflects a limitation in substrate supply to mitochondria, as pyruvate addition abolished the differences in Cch stimulation of OCR between ARALAR-deficient and WT neurons.

4. ROLE OF STORE-OPERATED CALCIUM ENTRY IN METABOTROPIC GLUTAMATE RECEPTOR FUNCTION

Metabotropic glutamate receptors (mGluRs) are members of the G-protein coupled receptor (GPCR) superfamily, and are activated by L-glutamate, the major excitatory neurotransmitter in the central nervous system (CNS). They are widely distributed thought the CNS and play a relevant role for synaptic transmission, activity-dependent synaptic plasticity and higher cognitive functions (Niswender and Conn, 2010). Group I mGluR (mGluR I), form by mGluR1 and 5, is coupled to a variety signaling pathways, the $G\alpha_{q/11}$ protein/phospholipase Cβ (PLCβ)/inositol-3,4,5-triphosphate (IP_3) signal cascades have been considered as the canonical pathway, which leads to Ca^{2+} depletion of ER and activation of protein kinase C (PKC). Similar to AChRs, the decrease of ER-Ca^{2+} levels could activate SOCE in the plasma membrane and it could be involved in mGluR-driven Ca^{2+} signaling and its physiological functions, as mGluR-LTD.

4.1 SOCE is involved in mGluR-driven Ca^{2+} signals

In order to study mGluRs functions, we considered it was relevant to obtain a mature neuronal culture that exhibits synaptic network activity. To this end, cortical neurons were cultured in BrainPhys medium, which has an inorganic salt concentration, glucose level and osmolarity similar to those reported for the brain (Bardy et al., 2015). Neurons grown in this culture medium show higher viability and maintain synaptic activity during more days in culture than in the regular culture medium (Bardy et al., 2015). The experiments were performed at 10-12 DIV in a medium with 1 µM TTX in order to eliminate spontaneous activity. The cytosolic Ca^{2+} signal evoked by application of 200 µM (S)-3,5-dihydroxyphenylglycine (DHPG), a selective agonist of mGluRs I, evoked a rapid increase in cytosolic Ca^{2+} followed by a slow recovery that did not reach baseline during the recording period (Fig. 25 A, black line). To determine the impact of SOCE inhibition on Ca^{2+} response to DHPG, we applied the SOCE blockers along, but not before the agonist of mGluR I, to avoid a drop en ER calcium caused by the inhibitors (Samtleben et al., 2015). Interestingly, we found that the cytosolic Ca^{2+} transient rapidly returned to baseline when 10 µM YM-58483 or 50 µM 2-APB were added together with DHPG (Fig. 25 A, B), as predicted if SOCE was responsible for maintaining Ca^{2+} levels above baseline. The presence of YM-58483 did not affect the initial Ca^{2+} peak evoked by mGluRs, suggesting that SOC channels open secondarily to mGluRs activation and that the first peak involves the ER-Ca^{2+} mobilization by PLCβ pathway. On the other hand, the addition of 2-APB decreased the initial Ca^{2+} peak, consistent with the effect of this compound on IP_3 signaling (Prakriya and Lewis, 2015).

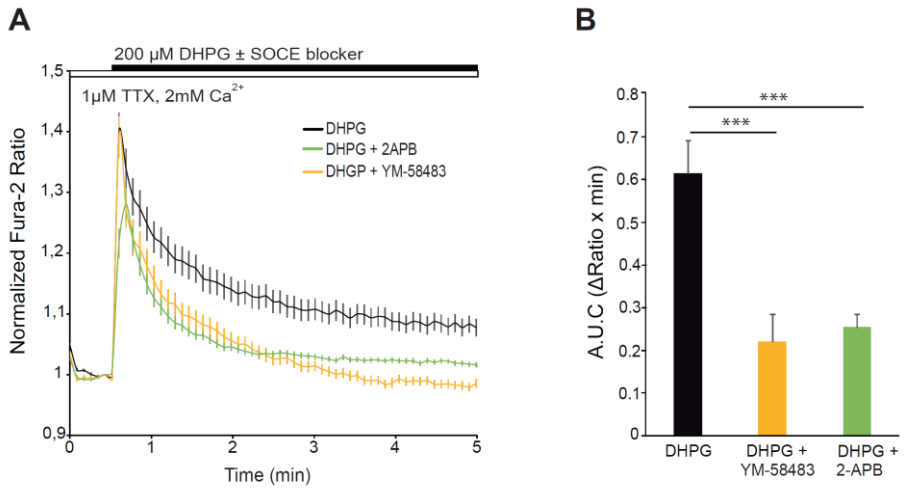

Figure 25. **SOCE is involved in mGluRs-driven Ca^{2+} signal**. (**A**) Fura-2 $[Ca^{2+}]_i$ signals in cortical neurons in HCSS medium containing 2 mM $CaCl_2$ and 1 µM TTX upon addition of 200 µM DHPG ± 10 µM YM-58483 or 50 µM 2-APB where indicated. (**B**) Quantification of area under the curve (ΔRatio·min) after DHPG ± YM-58483 or 2-APB addition. Data were obtained from 3 independent experiments. All data are expressed as mean ± SEM and means were compared using one-way ANOVA, ***$p < 0.001$, *posthoc* Bonferroni test.

4.2 SOCE inhibition impairs DHPG-LTD

Stimulation of group I mGluRs can lead to a reduction of synaptic strength at many synapses. This form of synaptic plasticity is referred to as long-term depression (mGluR-LTD), and it has been demonstrated in diverse brain regions, such as the hippocampus, neocortex, dorsal and ventral striatum, and spinal cord (Bellone et al., 2008, Gladding et al., 2009, Jorntell and Hansel, 2006). This form of LTD can be induced by the application of the group I selective mGluR agonist DHPG (so called DHPG-LTD) (Xiao et al., 2001, Jo et al., 2008), but the underlying molecular mechanism is still poorly understood and appears to depend on the specific neuronal type. Having shown that SOCE was activated after stimulation of group I mGluRs, and was involved in the maintenance of cytosolic Ca^{2+} signal, we investigated if the activation of SOCE could be involved in DHPG-LTD. To address this issue, we carried out a series of experiments in 10-12 DIV primary cortical neurons using electrophysiology techniques. In whole cells recordings, cells were held at -60 mV and miniature excitatory postsynaptic currents (mEPSCs) were recorded with 1 µM TTX in the perfusion solution. We found that bath application of 200 µM DHPG (5 min) caused a 29.3 ± 6.2% long lasting reduction of the evoked EPSC amplitude at 15 minutes after mGluR stimulation (Fig. 26 A, B, E). However, in our experimental model, we did not find any significant effect on the frequency of mEPSCs, suggesting that this type of LTD is predominantly expressed via a postsynaptic mechanism (Fig. 26 A, B, F).

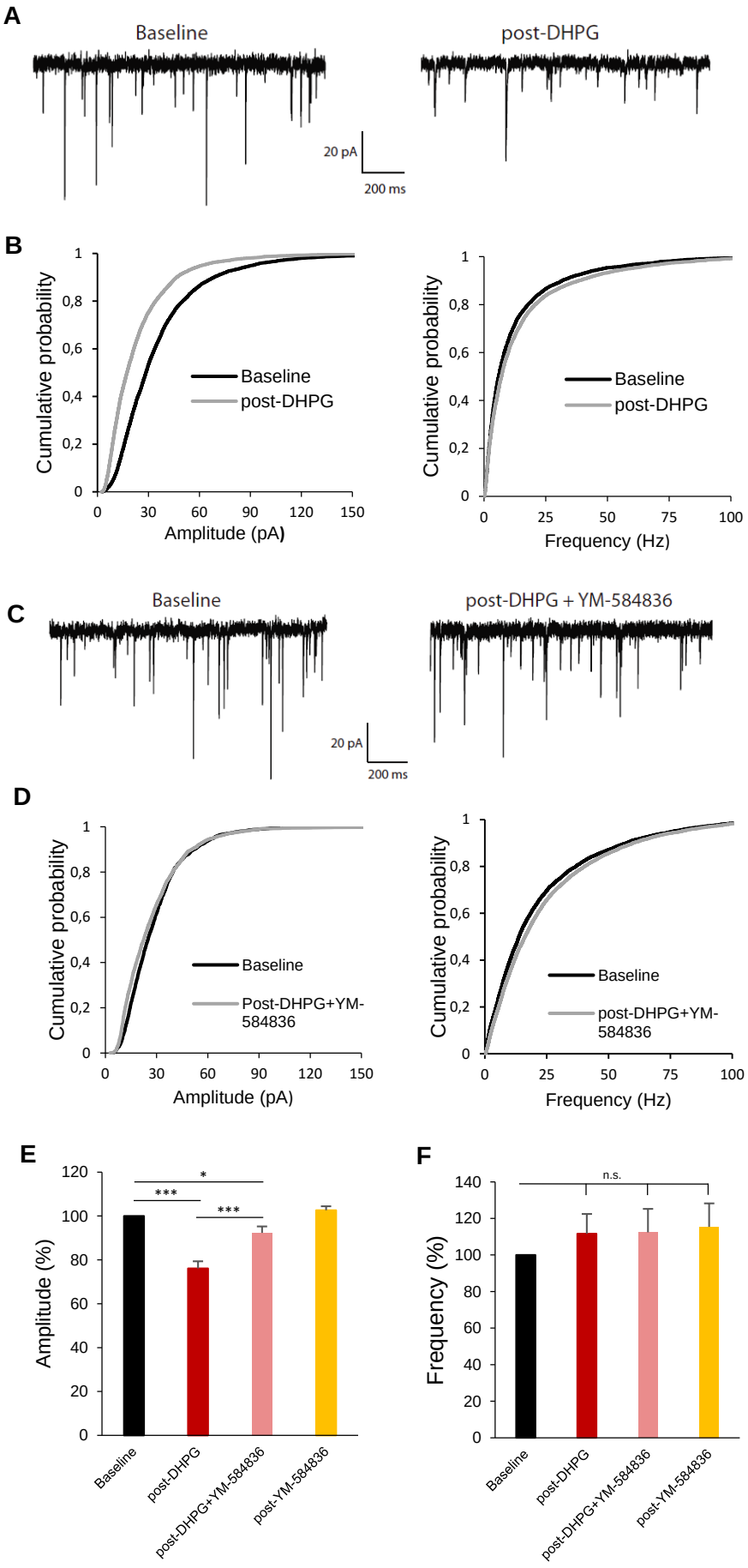
A
Baseline
post-DHPG
20 pA
200 ms
B
Cumulative probability
Baseline
post-DHPG
Amplitude (pA)
Frequency (Hz)
C
Baseline
post-DHPG + YM-584836
20 pA
200 ms
D
Cumulative probability
Baseline
Post-DHPG+YM-584836
post-DHPG+YM-584836
Amplitude (pA)
Frequency (Hz)
E
Amplitude (%)
*
***
***
F
Frequency (%)
n.s.
Baseline
post-DHPG
post-DHPG+YM-584836
post-YM-584836

Figure 26. **DHPG-LTD is reduced by SOCE inhibition.** (**A**) Representative mEPSC recordings from a cortical neuron before and 15 min after 200 µM DHPG application. (**B**) Cumulative probability histograms for amplitude and frequency, showing baseline (2min) and a 2 min interval beginning 15 min after DHPG application. (**C**) Representative mEPSC recordings from a cortical neuron before and 15 min after 200 µM DHPG + 10 µM YM-58483 application. (**D**) Cumulative probability histograms for amplitude and frequency, showing baseline (2min) and a 2 min interval beginning 15 min after DHPG + YM-584836 application. (**E-F**) Mean of mEPSCs amplitude (%) (**E**) and frequency (%) (**F**) comparing baseline (100%) to values obtained 15 min after application of 200 µM DHPG, 200 µM DHPG + 10 µM YM-58483 and 10 µM YM-58483 respectively. Data are expressed as mean ± SEM and were obtained from 6-13 independent experiments. Due to non-normal distribution of mEPSCs parameters, statistics were performed using the Wilcoxon matched pairs test, *$p < 0.05$, ***$p<0,001$.

To investigate the role of SOCE in DHPG-LTD, we studied the effect of the SOCE blocker YM-58483 (10 µM) applied together with DHPG. Interestingly, the long lasting decrease of mEPSCs amplitude was significantly lower (7.7 ± 2.9%) (Fig. 26 C, D, E), but the frequency of mEPSCs was not affected (Fig. 26 F). Five minutes of bath application of 10 µM YM-58483 did not have any effect on the amplitude or frequency of evoked EPSCs (Fig. 26 E, F). All these results suggest that the activation of SOCE after group I mGluRs stimulation is a necessary step for the development of DHPG-LTD in cortical neurons.

DISCUSSION

1. Pathological mechanism underlying *GDAP1*-related CMT disease

Our findings show that GDAP1 is a protein involved in the movement of mitochondria through the cells with a particular and essential role during the store-operated calcium entry (SOCE) process, a Ca^{2+} entry mechanism activated by reduction in ER-Ca^{2+} levels (Putney, 1986). Loss of function mutants generated by gene silencing in cell lines or by genetic disruption in the mouse cause a similar cellular phenotype with regards to calcium homeostasis: a failure to activate store-operated calcium entry after the discharge of intracellular Ca^{2+} stores ((Pla-Martin et al., 2013, Barneo-Munoz et al., 2015) and Martinez-Valero, Doctoral Thesis, 2017). We do not assume any particular molecular composition of SOCE in these cells, and rather agree with a broad definition (Fonteriz et al., 2016), comprising currents with high (I_{CRAC}) or low Ca^{2+} selectivity or even nonselective such as I_{SOC} (Parekh and Putney, 2005), composed by TRP channels, particularly the TRPC subfamily. Thus, homo or heteromeric combinations of different channel subunits involving TRPCs and/or Orai interacting with STIM in the ER would confer them store operated properties.

In this work, we have analyzed the cause and functional consequences of the decrease in SOCE activity caused by GDAP1 deficiency in neuroblastoma cells. We have studied SOCE activity in different neuroblastoma cell lines in which proper mitochondrial Ca^{2+} uptake was prevented by DNP or MCU silencing, and we found the same and limited SOCE response than in GDAP1 deficient cells. In addition, we did not find any effect of treatment with DNP on SOCE in *GDAP1*-KD cells. The proximity of mitochondria to ER-PM junctions has been reported to be a key aspect in its ability to facilitate SOCE (Quintana et al., 2006), and interestingly, we found a smaller number of mitochondria close to plasma membrane (PM) in GDAP1 deficient than in control cells upon SOCE activation. All these results suggest that i) mitochondrial Ca^{2+} uptake regulates SOCE activity in neuroblastoma cells, presumably by preventing its Ca^{2+}-dependent inactivation and ii) a failure to take up Ca^{2+} in mitochondria next to the sites of SOCE channels causes suppression of SOCE in GDAP1 deficient cells. These results agree with previous evidences that suggest that mitochondria move to PM after SOCE activation and are necessary to maintain Ca^{2+} influx across SOC channels (Varadi et al., 2004, Kopach et al., 2011, Quintana and Hoth, 2012, Nunez et al., 2006, Samanta et al., 2014).

We have focused on possible consequences of the reduced SOCE activity in GDAP1 deficient cells, particularly on mitochondrial function and its regulation by calcium. The role of Ca^{2+} in tuning ATP production to ATP demand in excitable cells has been known for a long time (Hayakawa et al., 2005, Glancy and Balaban, 2012, Rizzuto et al., 2012, Jouaville et al., 1999) and has now receiving experimental support in the heart (Kwong et al., 2015, Luongo et al., 2015).

In intact cortical neurons, Ca^{2+} has been shown to cooperate in adjusting coupled respiration to ATP demand under the workloads induced by carbachol, high K^+ depolarization or veratridine (Llorente-Folch et al., 2013, Rueda et al., 2014, Llorente-Folch et al., 2015).

In the present study we have addressed the following issues: i) Is SOCE-driven Ca^{2+} entry involved in stimulating respiration of intact neuroblastoma cells? ii) Is Ca^{2+} signaling (independent of Ca^{2+}-increase in ATP demand) required to upregulate respiration? iii) Is upregulation of respiration affected by GDAP1 deficiency?

i. Our results clearly show that SOCE-driven Ca^{2+} signal results in a stimulation of respiration in neuroblastoma cells. Kann and coworkers (Kann et al., 2012) have shown earlier that SOCE driven Ca^{2+} inflow in hippocampal neurons subsequent to muscarinic receptor stimulation results in mitochondrial depolarization. This may precede the increase in respiration caused by SOCE.

ii. We found that upregulation of respiration is blocked in the presence of BAPTA-AM which prevents Ca^{2+} signaling but not changes in workload (Llorente-Folch et al., 2013), showing that Ca^{2+} signaling itself through regulation of mitochondrial respiration is required to couple respiration to SOCE activity. Ca^{2+} regulation of respiration agrees with the finding of an increase in mitochondrial Ca^{2+} upon SOCE activation and implies matrix and extramitochondrial mechanisms of Ca^{2+} signaling in mitochondria to boost respiration.

iii. Upregulation of respiration by SOCE activation in neuroblastoma cells is impaired by GDAP1 deficiency. Coupling stimulated respiration to SOCE-driven Ca^{2+} signals may involve Ca^{2+} actions on the external side of the inner mitochondrial membrane, where the Ca^{2+} binding domains of Aralar/AGC1 or the ATP-Mg^{2+}/Pi carrier are located, and/or in the matrix, where Ca^{2+}-regulation of mitochondrial dehydrogenases is known to take place (Glancy and Balaban, 2012, Satrustegui et al., 2007). In GDAP1 deficient cells, Ca^{2+} fails to adequately reach the mitochondrial matrix. This suggests an impaired activation of mitochondrial dehydrogenases, resulting in decreased SOCE-stimulated respiration-coupled ATP production. In turn, this will compromise ER-Ca^{2+} levels due to a lower SOCE activity and lower ATP production to feed the ER SERCA pump (Rangaraju et al., 2014). In neuroblastoma SH-SY5Y cells, SOCE stimulation by muscarinic receptor activation induces glucose uptake via activation of AMP kinase subsequent to CAMKII (Olianas et al., 2014) which may feed respiratory substrates for SOCE-stimulated respiration. SOCE-stimulated glucose uptake may also be affected by GDAP1 deficiency, and this may also limit respiratory substrate supply.

The release of ER-Ca^{2+} also stimulates mitochondrial respiration and this stimulation decreased in *GDAP1*-KD cells due to their lower ER-Ca^{2+} levels (Pla-Martin et al., 2015) and Martinez-Valero, Doctoral Thesis, 2017, which may be associated with the impairment of SOCE (Samtleben et al., 2015). Establishing the Ca^{2+} signaling pathways involved in coupling both ER

and SOCE-driven Ca^{2+} signals to respiration will aid to identify potential targets in GDAP1 deficiency. Long-term changes in ER-Ca^{2+} have been shown to regulate the unfolding protein response (UPR) (Krebs et al., 2015) and could be altered by GDAP1 deficiency. It is possible that the decrease in ER-Ca^{2+} may be involved in the altered morphology of embryonic motoneuron ER observed in the *Gdap1*-KO mouse (Barneo-Munoz et al., 2015). It is relevant to mention that ER-Ca^{2+} plays a major role in neurons and synaptic activity. It has been shown to regulate spontaneous neurotransmitter release in synaptic boutons (Emptage et al., 2001, de Juan-Sanz et al., 2017), and metabotropic glutamate receptor-dependent synaptic transmission (Hartmann et al., 2014). A decrease in ER-Ca^{2+} has been observed in all cases of GDAP1 deficiency, *GDAP1*-KD neuroblastoma cells and *Gdap1*-KO mice, and this may be involved in reduced spontaneous neurotransmitter release and/or in a deficit in metabotropic glutamate receptor-dependent synaptic transmission in the PNS neurons affected by CMT disease.

In this study, we have also investigated missense clinical *GDAP1* mutations involved in Charcot-Marie-Tooth disease (*GDAP1*-CMT). *GDAP1*-CMT represents a highly heterogeneous disease characterized by variable clinical spectrum dependent on the mutation, which confers the inheritance pattern of the disease. In general, *GDAP1* recessive mutations are related to a severe form of the disease with early onset, whereas dominant mutations in general produce a mild disease, even sometimes asymptomatic (Cassereau et al., 2011). We found that the recessive mutations located in the α-loop domain, involved in the protein-protein interaction, phenocopy GDAP1 deficiency. Overexpression of these recessive mutations in *GDAP1*-KD cells did not rescue SOCE, ER-Ca^{2+} levels (Gonzalez-Sanchez et al., 2017), and consequently, SOCE-stimulated respiration. The analysis of mitochondrial distribution in cells carrying these recessive mutations has now shown a failure to relocate mitochondria close to plasma membrane under SOCE-activation conditions, and suggests this failure as a likely cause for SOCE impairment. However, neither dominant mutations nor recessive mutations out of the α-loop affected SOCE in the way GDAP1 deficiency does. Interestingly, we observed that cells carrying the dominant mutations had an increase in SOCE amplitude (Gonzalez-Sanchez et al., 2017), which might be related with a bias in mitochondrial distribution towards the plasma membrane under basal conditions, particularly the region within 1μm of the membrane. This bias may be due to an increased interaction of the dominant mutations with RAB6B and caytaxin (Pla-Martin et al., 2013), and may explain an early prevention of SOCE inactivation at the plasma membrane by resident mitochondria. These results suggest that dominant mutations may act through other pathogenic gain of function mechanisms which could be related to elevated ROS and increased apoptosis, as previously described (Niemann, Wagner et al. 2009). Interestingly, an increase in neuronal SOCE activity has been also shown to be detrimental to striatal neurons in a mouse model of Huntington's disease (Wu et al., 2016).

In conclusion, our results suggest that missense *GDAP1* mutations operate by different cellular mechanisms depending on their mode of inheritance and, in the case of recessive mutations, their position. This is in agreement with a previous study in which Niemann and coworkers reported that *GDAP1* mutations could act by different cellular mechanisms depending on their mode on inheritance (Niemann et al., 2009). It is relevant to point out that the recessive forms of CMT involving GDAP1 mutations are severe with an early onset and two of four recessive mutations associated with more severe phenotype (p.P153L and p.R161H) are located in the α-loop domain (Cassereau et al., 2011). Regarding to CMT caused by GDAP1 deficiency and by recessive mutations located in the α-loop domain, we propose the mechanism illustrated in figure 27, which together with the failure in SOCE-driven stimulation of respiration, suggests that the cellular mechanism underlying the pathology in these cases may relate to a Ca^{2+}-dependent bioenergetics failure along with abnormal mitochondrial distribution.

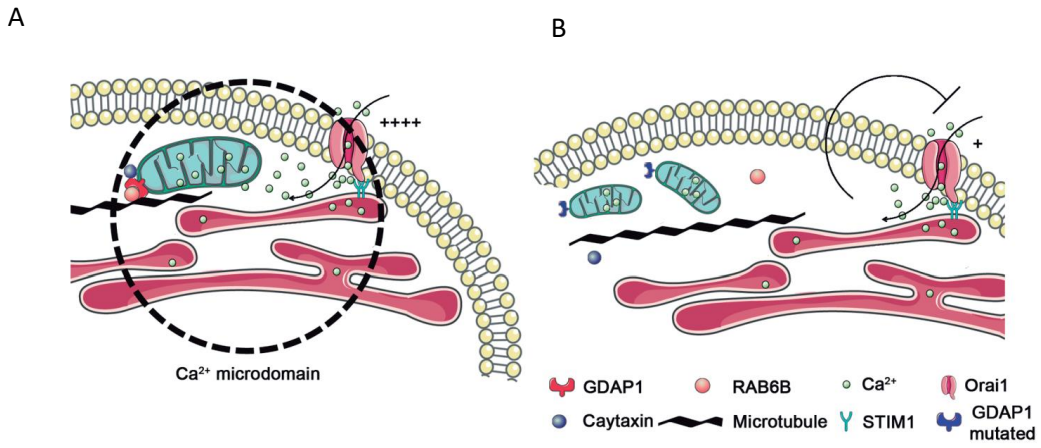

Figure 27. A proposed model for GDAP1 function. (**A**) The scheme shows GDAP1 participation in both retrograde and anterograde movements mediated by RAB6B and caytaxin, respectively, which allows mitochondria to be positioned at Ca^{2+} microdomains between ER and plasma membrane after SOCE activation. (**B**) Mitochondrial movement might be affected by the recessive mutations located in the α-loop. Due to a loss of interaction between GDAP1 and the proteins transport RAB6B and caytaxin, interaction of mitochondria with microtubule network and trafficking could be modified, which might affect the proper mitochondrial localization at the subplasmalemmal microdomains affecting SOCE activity.

2. The existence of SOCE pathway in neurons

SOCE is the main mechanism to replenish intracellular calcium stores in non-excitable cells but its existence in neurons is under debate (Lu and Fivaz, 2016, Putney, 2003), as neurons exhibit other major Ca^{2+} influx pathways through VGCCs and ionotropic glutamate receptors (Grienberger and Konnerth, 2012). Whereas Ca^{2+} entry through SOCs channels has been reported

in different neuronal populations (Emptage et al., 2001, Gemes et al., 2011, Berna-Erro et al., 2009, Xia et al., 2014, Alkhani et al., 2014, Sun et al., 2014), other groups did not find a clear SOCE response in neurons (Park et al., 2010, Garcia-Alvarez et al., 2015a). Different reasons could explain this discrepancy, for example, the use of neurons in different developmental stages, since SOCE has been found to be developmentally regulated in cortical neurons (Bouron et al., 2005). Ca^{2+} signaling in dendritic spines is compartmentalized and relatively isolated from somatic Ca^{2+} signaling (Higley and Sabatini, 2012), so SOCE measurements could vary and be affected by different mechanisms depending on the neuronal compartment (Sun et al., 2014). Finally, another reason could come from the commonly used Ca^{2+} addback protocol to study SOCE, in which neuronal stores are emptied in a Ca^{2+}-free medium, and then Ca^{2+} is added to the external medium. Neurons express multiple Ca^{2+} channels that can be activated in response to changes in extracellular calcium. In the present study, we investigated the existence of SOCE in cortical neurons in a relatively mature state, in a medium containing physiological calcium concentrations. Our results clearly showed a small but maintained increase in cytosolic Ca^{2+} after Tg application, which rapidly returned to basal levels in the presence of SOCE blockers, and was unaltered after adding a cocktail of channel/receptor inhibitors, i.e, all conditions consistent with a bona fide thapsigargin-induced SOCE. We also investigated the molecular players of SOCE in mouse cortical neurons and we found that STIM1 and STIM2 mRNA levels are very similar and we found a high protein level of STIM2 by western blot. Orai1 seems to form the store-operated pore, and in a lesser extent, TRPC4, similar to results reported for cortical and hippocampal neurons (Gruszczynska-Biegala et al., 2011, Korkotian et al., 2017, Klejman et al., 2009, Berna-Erro et al., 2009).

2.1 Modulation of neuronal SOCE by mitochondria

We have studied the mitochondrial modulation of SOCE in two different cell models, in neuroblastoma cell lines and in mouse cortical neurons. The mitochondrial role in SOCE activity has been extensively investigated and several possible mechanisms have been implicated to explain the ability of mitochondria to facilitate SOCE, as Ca^{2+} buffering (Parekh, 2003), ATP production (Montalvo et al., 2006) or pyruvate release (Bakowski and Parekh, 2007). Among them, the capacity of mitochondria to uptake Ca^{2+} in the ER-PM junctions and reduce Ca^{2+}-dependent inactivation of SOCE has been reported in a number of different cell types using different approaches (Valero et al., 2008, Nunez et al., 2006, Malli et al., 2003, Samanta et al., 2014, Tang et al., 2015). Results of this work clearly show that in neuroblastoma cells mitochondrial Ca^{2+} uptake is needed to maintain SOCE activity. However, in mouse cortical neurons we observed that disruption of the capability of mitochondria to uptake Ca^{2+} by *Mcu*

silencing did not affect SOCE activity. This difference could arise from the amount of Ca^{2+} entry through SOCE, much larger in neuroblastoma cells that in cortical neurons. Ca^{2+} influx through SOC channels is mostly buffered by the ER using SERCA, which colocalizes with STIM1 (Jousset et al., 2007). When SOCE-driven Ca^{2+} entry is larger, Ca^{2+} influx may exceed the capacity of subplasmalemmal SERCA and under these conditions mitochondria may play a major role buffering the excess Ca^{2+} and relay it to different ER regions, as proposed before (Jousset et al., 2007, Kopach et al., 2011). We hypothesize that the relatively small Ca^{2+} influx in cortical neurons could be handled by SERCA without needing an extra Ca^{2+} clearance system. However, we cannot completely exclude a role of mitochondria in neuronal SOCE, independent of MCU, since mitochondria may be required to produce local ATP to maintain SERCA activity, a function for which the entry of Ca^{2+} into the mitochondrial matrix is not essential (Llorente-Folch et al., 2013).

3. Activation of neuronal SOCE upon physiological stimuli

Having shown the existence of SOCE in cortical neurons, we sought to determine its physiological role upon stimulation of receptors that trigger ER-Ca^{2+} depletion. In particular, muscarinic acetylcholine receptors and group I of metabotropic glutamate receptors, both linked to the $G\alpha_{q/11}$, which cause activation of phospholipase C-β, IP_3 signaling and calcium release from internal stores. First, we tested the ability of Cch and DHPG, agonists of mAChR and mGluR I respectively, to mobilize Ca^{2+} from the ER, and interestingly, we found that the stimulation of mGluRs I, but not mAChRs, mobilizes Ca^{2+} from the ER. It has been demonstrated in superior cervical ganglion neurons that the lack of coupling of mAChRs to IP_3Rs does not result from its inability or relative inefficiency in stimulating PLC-β (Delmas et al., 2002), so possible reasons for this discrepancy include i) cortical neurons at 9-10 DIV may express a larger number of mGluRs than mAChRs, and the activation of mAChRs does not generate enough IP_3 to activate IP_3R in the ER, ii) different location within signaling microdomains, with mGluRs clustered together with IP_3R while mAChRs distributed along the plasma membrane away from IP_3R clusters (Delmas et al., 2002, Delmas et al., 2004), and iii) in hippocampal neurons, DHPG application has been shown to mobilize intracellular Ca^{2+} from ryanodine-sensitive stores via cyclic adenosine diphosphate ribose (cADPR) (Sohn et al., 2011), and this Ca^{2+} release into the cytosol could enhance the activation of IP_3R (Berridge, 1998). On the other hand, del Rio et al., found that mAChRs can mobilize Ca^{2+} from ER in neurons provided that they were previously depolarized, as the large amount of Ca^{2+} that enters by depolarization sensitizes IP_3R to IP_3 (del Rio, Bevilacqua et al. 1999). In agreement with this, we found that Cch enhanced Ca^{2+} signals in neurons showing spontaneous activity.

3.1 Role of SOCE in mAChRs stimulation

Our findings suggest that SOCE activation is required for the correct function of Cch-enhanced spontaneous Ca^{2+} oscillations. The role of SOCE in this paradigm is not related to the most known function in replenishing the Ca^{2+} stores in cells (Hartmann et al., 2014). In agreement with earlier works (del Rio et al., 1999, Young et al., 2005), we report that previous treatment with Tg did not affect the Cch-enhanced Ca^{2+} signals, suggesting a minor role of Ca^{2+} release from ER in the enhanced cytosolic signals triggered by Cch. Likewise, neither does it appear to be related to an effect on neurotransmitter release, since the inhibition of glutamate reuptake did not change the effects of SOCE blocker on Cch-enhanced spontaneous Ca^{2+} oscillations. The ability of Cch to increase spontaneous Ca^{2+} transients has been associated to a direct modulation of neuronal excitability by mAChRs, in which the depletion of PIP_2 levels in plasma membrane has been proposed to be an essential step to maintain the enhanced neuronal excitability (Zhang et al., 2011, Young et al., 2005) through PIP_2 actions on cation conductances in the plasma membrane which remain unresolved (see below). A possible role of SOCE activation in this process may be the requirement of the ER-Ca^{2+} sensors STIM proteins to migrate to the plasma membrane and interact with other targets involved in controlling the excitability of the plasma membrane. This function has already been proposed previously (de Juan-Sanz et al., 2017). In fact, STIMs proteins are able to interact with PIP_2 in the PM (Bhardwaj et al., 2013), and this interaction may modulate or facilitate PIP_2 depletion. However, the fact that the SOCE blocker used here, YM-58483, which appears to act on the SOCE channel itself (He et al., 2005), completely blocks Cch-stimulated Ca^{2+} transients argues against a role of STIM oligomerization/interaction with PIP_2 in the enhanced excitability conferred by SOCE opening.

Muscarinic stimulation has been shown both to inhibit background potassium currents and to activate a nonselective cation current, and different evidences suggest that membrane depolarization upon mAChRs stimulation is a consequence of nonselective cation current activation (Haj-Dahmane and Andrade, 1996, Yamada-Hanff and Bean, 2013). TRPC channels have been suggested to mediate this current (Tai et al., 2011). Moreover, TRPC channels are able to sustain the membrane depolarization after mAChRs stimulation that supports persistent repetitive firing in entorhinal cortical neurons (Yoshida et al., 2012, Zhang et al., 2011). According to this interpretation, this cation current driving depolarization would be Cch-activated SOCE. Specifically, TRPC1, 4 and 5 or TRPC1+4+5 heteromers, but not TRPC3, 6 or 7, are the channels involved in the action of muscarinic receptors (Zhang et al., 2011). Interestingly, early studies already showed that TRPC1, TRPC4, and TRPC5 can directly interact with STIM1, while conflicting results were found with TRPC3, TRPC6, and TRPC7 (Huang et al., 2006). These results suggest that STIM proteins could be the link between mAChRs stimulation and the opening of TRPCs. In this scenario, we propose that STIM1/STIM2 may also activate Orai1

which could contribute to Ca^{2+} influx alone (Gross et al., 2009), or in a complex with TRPC1, 4 or 5 (Cheng et al., 2011, Kim et al., 2009, Cioffi et al., 2012, Ma et al., 2008) (Fig. 28).

Finally, an alternative mechanism to explain Cch actions includes a role of SOCE in modulating any potassium current, a function proposed previously by Kann et al., (Kann et al., 2012).

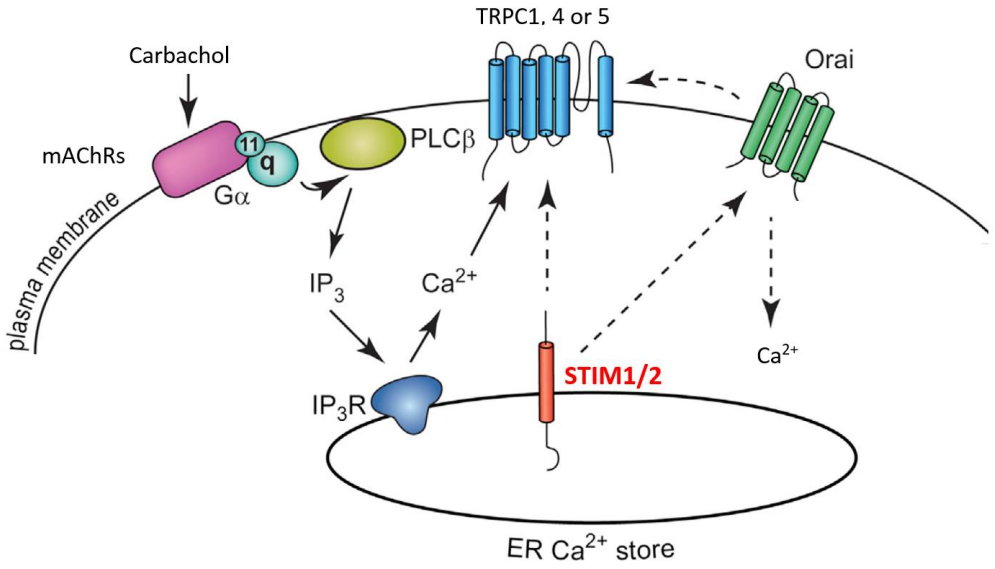

Figure 28. Hypothesis for a role of SOCE in membrane depolarization by mAChRs stimulation. Stimulation mAChRs by carbachol triggers PLC/IP_3 signaling and ER-Ca^{2+} release. Intracellular store depletion activates STIM proteins which migrate to PM and interact with Orai and TRPC channels allowing Ca^{2+} influx into the cytosol. This non-selective Ca^{2+} current has been proposed to underlie the membrane depolarization. Modified from (Hartmann et al., 2014).

3.1.1 Regulation of mitochondrial respiration by mAChRs stimulation

As recent findings have shown that Ca^{2+} signaling cooperates in adjusting coupled respiration to ATP demand under different workloads (Llorente-Folch et al., 2013), in the present study we have also addressed whether the Cch-enhanced Ca^{2+} oscillations boost mitochondrial respiration in cortical neurons. Our results clearly show that the increase in Ca^{2+} oscillations by muscarinic receptors activation stimulates mitochondrial respiration, and it is totally dependent on SOCE activation since it is prevented by the SOCE blockers YM-58483 or 2-APB. We next analyzed the pathways involved in the stimulation of respiration by Ca^{2+}. We found that Ca^{2+} oscillations reach mitochondria, so that Ca^{2+} entry into the matrix and the activation of mitochondrial dehydrogenases (Glancy and Balaban, 2012) could be a relevant mechanism in the stimulation of respiration. Surprisingly, although Ca^{2+} was unable to reach mitochondria in *Mcu*-KD neurons, these *Mcu*-silenced neurons responded to carbachol at the same level than WT. The regulation of mitochondrial respiration by MCU pathway in neurons is still unknown, but our results suggest a

minor role of MCU-driven Ca^{2+} entry in mitochondria in boosting respiration by Cch-enhanced Ca^{2+} oscillations. The limited role of Ca^{2+} entry into the matrix in Ca^{2+}-regulated respiration in intact neurons is consistent with the findings in *Mcu*-KO mice (Pan et al., 2013). *Mcu*-KO mice did not present alterations in basal metabolism at the whole animal level, or any defect in respiration in mouse embryonic fibroblast cultures, even though the Ca^{2+} content in skeletal muscle mitochondria was decreased. Consistent with a role of MCU at high workloads, skeletal muscle peak performance was slightly decreased in *Mcu*-KO mice. However, the presence of compensatory mechanisms that explain the mild effect of MCU deficiency remain to be established and the MCU-driven Ca^{2+} regulation of mitochondrial metabolism could vary in different tissues and cells with changing energy demands.

Ca^{2+} may also regulate mitochondrial respiration from the cytosol, activating the calcium binding mitochondrial carriers (del Arco and Satrustegui, 2004, Satrustegui et al., 2007). We have investigated the role of ARALAR, which activity is needed in low, mild and high workloads, and even to maintain basal OCR in intact neurons (Llorente-Folch et al., 2013, Rueda et al., 2014). Accordingly, we observed that while carbachol has de ability to enhance Ca^{2+} oscillations in both WT and *Aralar*-KO neurons at the same level, *Aralar*-KO neurons were unable to stimulate mitochondrial respiration upon mAChRs activation. The lack of ARALAR reflects a limitation in substrate supply to mitochondria, as pyruvate addition abolished the differences in carbachol-stimulated OCR between *Aralar*-KO and WT neurons. These findings point out an essential role of ARALAR-MAS in coupling the Cch-enhanced Ca^{2+} signals to ATP production in mitochondria.

This link between Ca^{2+} signals and mitochondrial metabolism may be strongly relevant in cholinergic modulation, since it is critical for hippocampal and prefrontal functions (Dutar et al., 1995, Hasselmo, 2006, Hasselmo and Sarter, 2011, Ross et al., 2005), its disruption impairs learning and memory (Green et al., 2005, McGaughy et al., 2005) and has been related to several neuropsychiatric disorders, including schizophrenia, Alzheimer's disease and other forms of senile dementia (Terry and Buccafusco, 2003).

3.2 Role of SOCE in mGluRs stimulation

The other physiological stimulus we investigated was glutamate acting via metabotropic receptors, and we found that group I mGluRs activation using the specific agonist DHPG induces SOCE in mouse cortical neurons through the same signaling pathway than mAChRs (illustrated in Fig. 28). Moreover, SOCE activity is required to maintain the mGluR-driven cytosolic Ca^{2+} signal. This result is in agreement with a previous report in which stimulation of mGluRs I

triggered STIM1 oligomerization and migration to plasma membrane (Ng et al., 2011), the first step needed in SOCE induction (Lewis, 2007). More recent findings point to a central role of STIM proteins as one of the intracellular links between mGluR I and its downstream effectors (Hartmann et al., 2014, Hou et al., 2015).

Metabotropic glutamate receptors are widely distributed throughout the CNS and play a relevant role for synaptic transmission, activity-dependent synaptic plasticity and higher cognitive functions (Niswender and Conn, 2010). Particularly, stimulation of group I mGluRs triggers long-term depression (LTD) of excitatory synaptic strength. In this work, we have observed that SOCE inhibition causes a strong impairment of DHPG-LTD in primary cortical neurons. In relation with SOCE components, STIM1 has been found to control mGluR I-dependent slow excitatory potentials in Purkinje neurons through its action in maintaining the ER-Ca^{2+} levels (Hartmann et al., 2014), and both STIM2 knockout (Yap et al., 2017) and STIM1/STIM2 double knockout mice (Garcia-Alvarez et al., 2015b) have impaired LTP and LTD.

MGluR-LTD has been broadly studied in hippocampus and cerebellum (Luscher and Huber, 2010, Gladding et al., 2009, Jorntell and Hansel, 2006), but less is known about other brain regions. It is not clear if the expression mechanism of DHPG-LTD relies on presynaptic (neurotransmitter release) or postsynaptic (AMPAR internalization) changes (Anwyl, 2006). Moreover, in hippocampal neurons, the expression mechanism of DHPG-LTD depends on the developmental state of the synapse (Nosyreva and Huber, 2005). Our results show a clear reduction in the amplitude, but not in frequency, of mEPSCs 15 minutes after DHPG application, which suggests a postsynaptic mechanism of expression.

In cortical neurons, the strong impairment of DHPG-LTD and the failure to maintain DHPG-driven cytosolic Ca^{2+} signals in the presence of SOCE blockers suggest that SOCE-mediated Ca^{2+} signal might be essential to activate signaling pathways downstream mGluRs stimulation. SOCE-role in mGluRs I stimulation could be due to signaling by calcium influx through SOCs channels or through SOCE's known function in maintaining the ER-Ca^{2+} levels (Samtleben et al., 2015), which are depleted by mGluRs stimulation. According to this idea, it has been demonstrated that ER-Ca^{2+} release from internal stores via IP_3 generation after mGluRs stimulation is required to induce LTD in cerebellum (Kano et al., 2008, Miyata et al., 2000), and in the perirhinal cortex the induction of DHPG-LTD depends on interactions between the neuronal Ca^{2+} sensor protein (NCS-1) and protein interacting with C kinase (PICK1) in a Ca^{2+}-dependent manner (Jo et al., 2008). However, it is relevant to note that the molecular mechanisms seem to differ between brain regions. Indeed, in hippocampus, DHPG-LTD is considered to be independent of PLC/IP_3 pathway and postsynaptic Ca^{2+} (Mockett et al., 2011, Fitzjohn et al., 2001, Schnabel et al., 1999, Kim et al., 2015), but see (Sethna et al., 2016).

Although STIM recruitment and Ca^{2+} influx through SOCs channels has been implicated in several functions in dendritic spines (Sun et al., 2014, Korkotian and Segal, 2017, Korkotian et al., 2017, Brini et al., 2014), we cannot exclude a possible function of STIM proteins outside the canonical SOCE pathway. The activation of the ER-sensors STIM proteins in a SOCE-independent manner was first described in non-excitable cells (Shinde et al., 2013, Lefkimmiatis et al., 2009, Tian et al., 2012), and recently, this behavior has been also found in neurons. Garcia-Alvarez et al., showed that, in hippocampal neurons, STIM2 mediates PKA-dependent phosphorylation and trafficking of AMPARs due to an increase in cAMP levels (Garcia-Alvarez et al., 2015a). Interestingly, a recent work found that STIM1 overexpression in hippocampus does not affect SOCE but impairs both synaptically and chemically induced mGluR-LTD, suggesting that these results are SOCE-independent. (Majewski et al., 2017). However, it is relevant to note that the SOCE blocker used in this study to perform the experiments of DHPG-LTD, YM-58483, seems to exert its action on the channel itself, without interfering with STIM proteins (He et al., 2005), suggesting a relevant role of Ca^{2+} entry through SOC channels in DHPG-LTD.

In conclusion, our findings reveal a close relationship between metabotropic glutamate receptors and SOCE in cortical neurons, and show that SOCE activation is a necessary step in the development of DHPG-driven cytosolic Ca^{2+} signals. Blocking SOCE activation upon mGluRs stimulation prevented DHPG-LTD. Altogether the results suggest that, in cortical neurons SOCE-mediated Ca^{2+} signal could be relevant in generating downstream effects to evoke mGluR-LTD.

CONCLUSIONS

1. In neuroblastoma cell lines, mitochondria modulate SOCE activity. Mitochondrial Ca^{2+} uptake prolongs Ca^{2+} influx through SOC channels, by preventing Ca^{2+}-dependent inactivation.

2. GDAP1 deficiency and recessive GDAP1 mutations located in the α-loop domain impair SOCE activity, by preventing mitochondrial location close to the SOC channels in the plasma membrane, and impairing adequate mitochondrial Ca^{2+} handling needed to sustain SOCE activity in these cells.

3. In human neuroblastoma cell line, Ca^{2+} entry through SOC channels stimulates mitochondrial respiration and Ca^{2+} signaling (independent of Ca^{2+}-increased ATP demand) is required to stimulate respiration.

4. GDAP1 deficiency and recessive GDAP1 mutations located in the α-loop domain fail to stimulate mitochondrial respiration upon SOCE activation, suggesting that a failure in Ca^{2+}-dependent bioenergetics could be a pathological mechanism involved in CMT disease caused by these recessive GDAP1 mutations.

5. SOCE takes place in primary mouse cortical neurons, but it is not modulated by Ca^{2+} handling by mitochondria.

6. Neuronal SOCE is involved in mAChRs functions, and its activation is required for the correct function of carbachol-enhanced spontaneous Ca^{2+} oscillations.

7. The increase in Ca^{2+} oscillations driven by mAChRs activation stimulates mitochondrial respiration. Stimulation depends on SOCE, and ARALAR-malate-aspartate shuttle (MAS), rather than MCU, is the main pathway coupling carbachol-enhanced Ca^{2+} signals to the increase in ATP production in mitochondria.

8. Neuronal SOCE activity is required to maintain the mGluR-driven cytosolic Ca^{2+} signal and to evoke chemically induced mGluR-LTD in cortical neurons.

CONCLUSIONES

1. En líneas celulares de neuroblastoma, la mitocondria modula la actividad SOCE. La captura de Ca^{2+} por parte de la mitocondria prolonga la entrada de Ca^{2+} a través de los canales SOCE, impidiendo su auto-inactivación por Ca^{2+}.

2. La deficiencia de GDAP1 o la expresión de mutaciones recesivas de GDAP1 localizadas en el dominio α-loop disminuyen la actividad del SOCE. Esto es debido a un fallo en la correcta localización de las mitocondrias en zonas cercanas a los canales SOCE en la membrana plasmática, impidiendo así la captura de Ca^{2+} por parte de la mitocondria, función necesaria para el mantenimiento del SOCE en estas células.

3. En la línea celular de neuroblastoma humano, la entrada de Ca^{2+} por los canales SOCE estimula la respiración mitocondrial, y la señalización del Ca^{2+} (de forma independiente al incremento de la demanda de ATP causada por Ca^{2+}) es necesaria para la estimulación de la respiración.

4. La deficiencia de GDAP1 o la expresión de mutaciones recesivas de GDAP1 localizadas en el dominio α-loop impiden la estimulación de la respiración mediada por el SOCE. Esto sugiere que el mecanismo patológico que subyace a la enfermedad de CMT debida a estas mutaciones recesivas podría ser una alteración de la bioenergética dependiente de señales de Ca^{2+}.

5. El SOCE tiene lugar en neuronas corticales primarias de ratón, pero la captura de Ca^{2+} por parte de la mitocondria no participa en su modulación.

6. El SOCE en neuronas corticales está involucrado en funciones de los receptores muscarínicos de acetilcolina. La activación del SOCE es necesaria para el incremento de las señales espontáneas oscilatorias de Ca^{2+} dependiente de la estimulación de los receptores muscarínicos.

7. El incremento en las oscilaciones de Ca^{2+} debido a la activación de los receptores muscarínicos de acetilcolina estimula la respiración mitocondrial. Esta estimulación es dependiente de la activación del SOCE y de la lanzadera ARALAR-MAS, en lugar de MCU, representando la principal vía de acoplamiento entre la señal de Ca^{2+} y el incremento en la producción de ATP en la mitocondria.

8. El SOCE en neuronas corticales está involucrado en funciones de los receptores metabotrópicos de glutamato. La activación del SOCE es necesaria tanto para el mantenimiento de la señal de Ca^{2+} citosólica mediada por estos receptores, como para la correcta obtención de LTD dependiente de los receptores metabotrópicos de glutamato usando estimulación química.

REFERENCES

ABE, T., SUGIHARA, H., NAWA, H., SHIGEMOTO, R., MIZUNO, N. & NAKANISHI, S. 1992. Molecular characterization of a novel metabotropic glutamate receptor mGluR5 coupled to inositol phosphate/Ca2+ signal transduction. *J Biol Chem,* 267**,** 13361-8.

ALBARRAN, L., LOPEZ, J. J., SALIDO, G. M. & ROSADO, J. A. 2016. Historical Overview of Store-Operated Ca(2+) Entry. *Adv Exp Med Biol,* 898**,** 3-24.

ALKHANI, H., ASE, A. R., GRANT, R., O'DONNELL, D., GROSCHNER, K. & SEGUELA, P. 2014. Contribution of TRPC3 to store-operated calcium entry and inflammatory transductions in primary nociceptors. *Mol Pain,* 10**,** 43.

AMBUDKAR, I. S., DE SOUZA, L. B. & ONG, H. L. 2016. TRPC1, Orai1, and STIM1 in SOCE: Friends in tight spaces. *Cell Calcium*.

AMBUDKAR, I. S., ONG, H. L., LIU, X., BANDYOPADHYAY, B. C. & CHENG, K. T. 2007. TRPC1: the link between functionally distinct store-operated calcium channels. *Cell Calcium,* 42**,** 213-23.

AMIGO, I., TRABA, J., GONZALEZ-BARROSO, M. M., RUEDA, C. B., FERNANDEZ, M., RIAL, E., SANCHEZ, A., SATRUSTEGUI, J. & DEL ARCO, A. 2013. Glucagon regulation of oxidative phosphorylation requires an increase in matrix adenine nucleotide content through Ca2+ activation of the mitoc drial ATP-Mg/Pi carrier SCaMC-3. *J Biol Chem,* 288**,** 7791-802.

ANDRADE, R. 1991. Cell excitation enhances muscarinic cholinergic responses in rat association cortex. *Brain Res,* 548**,** 81-93.

ANWYL, R. 2006. Induction and expression mechanisms of postsynaptic NMDA receptor-independent homosynaptic long-term depression. *Prog Neurobiol,* 78**,** 17-37.

AOYAMA, T., HATA, S., NAKAO, T., TANIGAWA, Y., OKA, C. & KAWAICHI, M. 2009. Cayman ataxia protein caytaxin is transported by kinesin along neurites through binding to kinesin light chains. *J Cell Sci,* 122**,** 4177-85.

ARAMORI, I. & NAKANISHI, S. 1992. Signal transduction and pharmacological characteristics of a metabotropic glutamate receptor, mGluR1, in transfected CHO cells. *Neuron,* 8**,** 757-65.

BABA, A., YASUI, T., FUJISAWA, S., YAMADA, R. X., YAMADA, M. K., NISHIYAMA, N., MATSUKI, N. & IKEGAYA, Y. 2003. Activity-evoked capacitative Ca2+ entry: implications in synaptic plasticity. *J Neurosci,* 23**,** 7737-41.

BACCI, A., VERDERIO, C., PRAVETTONI, E. & MATTEOLI, M. 1999. Synaptic and intrinsic mechanisms shape synchronous oscillations in hippocampal neurons in culture. *Eur J Neurosci,* 11**,** 389-97.

BAKOWSKI, D. & PAREKH, A. B. 2007. Regulation of store-operated calcium channels by the intermediary metabolite pyruvic acid. *Curr Biol,* 17**,** 1076-81.

BALABAN, R. S. 2009. The role of Ca(2+) signaling in the coordination of mitochondrial ATP production with cardiac work. *Biochim Biophys Acta,* 1787**,** 1334-41.

BARDO, S., CAVAZZINI, M. G. & EMPTAGE, N. 2006. The role of the endoplasmic reticulum Ca2+ store in the plasticity of central neurons. *Trends Pharmacol Sci,* 27**,** 78-84.

BARDY, C., VAN DEN HURK, M., EAMES, T., MARCHAND, C., HERNANDEZ, R. V., KELLOGG, M., GORRIS, M., GALET, B., PALOMARES, V., BROWN, J., BANG, A. G., MERTENS, J., BOHNKE, L., BOYER, L., SIMON, S. & GAGE, F. H. 2015. Neuronal medium that supports basic synaptic functions and activity of human neurons in vitro. *Proc Natl Acad Sci U S A,* 112**,** E2725-34.

BARNEO-MUNOZ, M., JUAREZ, P., CIVERA-TREGON, A., YNDRIAGO, L., PLA-MARTIN, D., ZENKER, J., CUEVAS-MARTIN, C., ESTELA, A., SANCHEZ-ARAGO, M., FORTEZA-VILA, J., CUEZVA, J. M., CHRAST, R. & PALAU, F. 2015. Lack of GDAP1 induces neuronal calcium and mitochondrial defects in a knockout mouse model of charcot-marie-tooth neuropathy. *PLoS Genet,* 11**,** e1005115.

BAUGHMAN, J. M., PEROCCHI, F., GIRGIS, H. S., PLOVANICH, M., BELCHER-TIMME, C. A., SANCAK, Y., BAO, X. R., STRITTMATTER, L., GOLDBERGER, O., BOGORAD, R. L.,

KOTELIANSKY, V. & MOOTHA, V. K. 2011. Integrative genomics identifies MCU as an essential component of the mitochondrial calcium uniporter. *Nature,* 476**,** 341-5.

BAXTER, R. V., BEN OTHMANE, K., ROCHELLE, J. M., STAJICH, J. E., HULETTE, C., DEW-KNIGHT, S., HENTATI, F., BEN HAMIDA, M., BEL, S., STENGER, J. E., GILBERT, J. R., PERICAK-VANCE, M. A. & VANCE, J. M. 2002. Ganglioside-induced differentiation-associated protein-1 is mutant in Charcot-Marie-Tooth disease type 4A/8q21. *Nat Genet,* 30**,** 21-2.

BENARROCH, E. E. 2010. Neuronal voltage-gated calcium channels: brief overview of their function and clinical implications in neurology. *Neurology,* 74**,** 1310-5.

BENZ, R., KOTTKE, M. & BRDICZKA, D. 1990. The cationically selective state of the mitochondrial outer membrane pore: a study with intact mitochondria and reconstituted mitochondrial porin. *Biochim Biophys Acta,* 1022**,** 311-8.

BERNA-ERRO, A., BRAUN, A., KRAFT, R., KLEINSCHNITZ, C., SCHUHMANN, M. K., STEGNER, D., WULTSCH, T., EILERS, J., MEUTH, S. G., STOLL, G. & NIESWANDT, B. 2009. STIM2 regulates capacitive Ca2+ entry in neurons and plays a key role in hypoxic neuronal cell death. *Sci Signal,* 2**,** ra67.

BERRIDGE, M. J. 1993. Inositol trisphosphate and calcium signalling. *Nature,* 361**,** 315-25.

BERRIDGE, M. J. 1998. Neuronal calcium signaling. *Neuron,* 21**,** 13-26.

BHARDWAJ, R., MULLER, H. M., NICKEL, W. & SEEDORF, M. 2013. Oligomerization and Ca2+/calmodulin control binding of the ER Ca2+-sensors STIM1 and STIM2 to plasma membrane lipids. *Biosci Rep,* 33.

BLACHLY-DYSON, E. & FORTE, M. 2001. VDAC channels. *IUBMB Life,* 52**,** 113-8.

BOURNE, J. N. & HARRIS, K. M. 2012. Nanoscale analysis of structural synaptic plasticity. *Curr Opin Neurobiol,* 22**,** 372-82.

BOURON, A., ALTAFAJ, X., BOISSEAU, S. & DE WAARD, M. 2005. A store-operated Ca2+ influx activated in response to the depletion of thapsigargin-sensitive Ca2+ stores is developmentally regulated in embryonic cortical neurons from mice. *Brain Res Dev Brain Res,* 159**,** 64-71.

BRAND, M. D. & NICHOLLS, D. G. 2011. Assessing mitochondrial dysfunction in cells. *Biochem J,* 435**,** 297-312.

BRANDMAN, O., LIOU, J., PARK, W. S. & MEYER, T. 2007. STIM2 is a feedback regulator that stabilizes basal cytosolic and endoplasmic reticulum Ca2+ levels. *Cell,* 131**,** 1327-39.

BRINI, M., CALI, T., OTTOLINI, D. & CARAFOLI, E. 2013. Intracellular calcium homeostasis and signaling. *Met Ions Life Sci,* 12**,** 119-68.

BRINI, M., CALI, T., OTTOLINI, D. & CARAFOLI, E. 2014. Neuronal calcium signaling: function and dysfunction. *Cell Mol Life Sci,* 71**,** 2787-814.

BROCARD, J. B., TASSETTO, M. & REYNOLDS, I. J. 2001. Quantitative evaluation of mitochondrial calcium content in rat cortical neurones following a glutamate stimulus. *J Physiol,* 531**,** 793-805.

BUCHANAN, K. A., PETROVIC, M. M., CHAMBERLAIN, S. E., MARRION, N. V. & MELLOR, J. R. 2010. Facilitation of long-term potentiation by muscarinic M(1) receptors is mediated by inhibition of SK channels. *Neuron,* 68**,** 948-63.

BURBRIDGE, T. J., XU, H. P., ACKMAN, J. B., GE, X., ZHANG, Y., YE, M. J., ZHOU, Z. J., XU, J., CONTRACTOR, A. & CRAIR, M. C. 2014. Visual circuit development requires patterned activity mediated by retinal acetylcholine receptors. *Neuron,* 84**,** 1049-64.

CAI, Q. & SHENG, Z. H. 2009. Mitochondrial transport and docking in axons. *Exp Neurol,* 218**,** 257-67.

CASSEREAU, J., CHEVROLLIER, A., GUEGUEN, N., DESQUIRET, V., VERNY, C., NICOLAS, G., DUBAS, F., AMATI-BONNEAU, P., REYNIER, P., BONNEAU, D. & PROCACCIO, V. 2011. Mitochondrial dysfunction and pathophysiology of Charcot-Marie-Tooth disease involving GDAP1 mutations. *Exp Neurol,* 227**,** 31-41.

CAVAZZINI, M., BLISS, T. & EMPTAGE, N. 2005. Ca2+ and synaptic plasticity. *Cell Calcium,* 38**,** 355-67.

CIOFFI, D. L., WU, S., CHEN, H., ALEXEYEV, M., ST CROIX, C. M., PITT, B. R., UHLIG, S. & STEVENS, T. 2012. Orai1 determines calcium selectivity of an endogenous TRPC heterotetramer channel. *Circ Res,* 110**,** 1435-44.

CLAPHAM, D. E. 2007. Calcium signaling. *Cell,* 131**,** 1047-58.

CLARAMUNT, R., PEDROLA, L., SEVILLA, T., LOPEZ DE MUNAIN, A., BERCIANO, J., CUESTA, A., SANCHEZ-NAVARRO, B., MILLAN, J. M., SAIFI, G. M., LUPSKI, J. R., VILCHEZ, J. J., ESPINOS, C. & PALAU, F. 2005. Genetics of Charcot-Marie-Tooth disease type 4A: mutations, inheritance, phenotypic variability, and founder effect. *J Med Genet,* 42**,** 358-65.

COLLINGRIDGE, G. L., PEINEAU, S., HOWLAND, J. G. & WANG, Y. T. 2010. Long-term depression in the CNS. *Nat Rev Neurosci,* 11**,** 459-73.

CONTRERAS, L., GOMEZ-PUERTAS, P., IIJIMA, M., KOBAYASHI, K., SAHEKI, T. & SATRUSTEGUI, J. 2007. Ca2+ Activation kinetics of the two aspartate-glutamate mitochondrial carriers, aralar and citrin: role in the heart malate-aspartate NADH shuttle. *J Biol Chem,* 282**,** 7098-106.

CUESTA, A., PEDROLA, L., SEVILLA, T., GARCIA-PLANELLS, J., CHUMILLAS, M. J., MAYORDOMO, F., LEGUERN, E., MARIN, I., VILCHEZ, J. J. & PALAU, F. 2002. The gene encoding ganglioside-induced differentiation-associated protein 1 is mutated in axonal Charcot-Marie-Tooth type 4A disease. *Nat Genet,* 30**,** 22-5.

CHANG, K. T., NIESCIER, R. F. & MIN, K. T. 2011. Mitochondrial matrix Ca2+ as an intrinsic signal regulating mitochondrial motility in axons. *Proc Natl Acad Sci U S A,* 108**,** 15456-61.

CHENG, K. T., LIU, X., ONG, H. L. & AMBUDKAR, I. S. 2008. Functional requirement for Orai1 in store-operated TRPC1-STIM1 channels. *J Biol Chem,* 283**,** 12935-40.

CHENG, K. T., LIU, X., ONG, H. L., SWAIM, W. & AMBUDKAR, I. S. 2011. Local Ca(2)+ entry via Orai1 regulates plasma membrane recruitment of TRPC1 and controls cytosolic Ca(2)+ signals required for specific cell functions. *PLoS Biol,* 9**,** e1001025.

CHOI, S., MALETH, J., JHA, A., LEE, K. P., KIM, M. S., SO, I., AHUJA, M. & MUALLEM, S. 2014. The TRPCs-STIM1-Orai interaction. *Handb Exp Pharmacol,* 223**,** 1035-54.

DAVIES, K. M., ANSELMI, C., WITTIG, I., FARALDO-GOMEZ, J. D. & KUHLBRANDT, W. 2012. Structure of the yeast F1Fo-ATP synthase dimer and its role in shaping the mitochondrial cristae. *Proc Natl Acad Sci U S A,* 109**,** 13602-7.

DE JUAN-SANZ, J., HOLT, G. T., SCHREITER, E. R., DE JUAN, F., KIM, D. S. & RYAN, T. A. 2017. Axonal Endoplasmic Reticulum Ca2+ Content Controls Release Probability in CNS Nerve Terminals. *Neuron,* 93**,** 867-881 e6.

DE STEFANI, D., RAFFAELLO, A., TEARDO, E., SZABO, I. & RIZZUTO, R. 2011. A forty-kilodalton protein of the inner membrane is the mitochondrial calcium uniporter. *Nature,* 476**,** 336-40.

DE STEFANI, D., RIZZUTO, R. & POZZAN, T. 2016. Enjoy the Trip: Calcium in Mitochondria Back and Forth. *Annu Rev Biochem,* 85**,** 161-92.

DEAK, A. T., BLASS, S., KHAN, M. J., GROSCHNER, L. N., WALDECK-WEIERMAIR, M., HALLSTROM, S., GRAIER, W. F. & MALLI, R. 2014. IP3-mediated STIM1 oligomerization requires intact mitochondrial Ca2+ uptake. *J Cell Sci,* 127**,** 2944-55.

DEHAVEN, W. I., JONES, B. F., PETRANKA, J. G., SMYTH, J. T., TOMITA, T., BIRD, G. S. & PUTNEY, J. W., JR. 2009. TRPC channels function independently of STIM1 and Orai1. *J Physiol,* 587**,** 2275-98.

DEL ARCO, A. & SATRUSTEGUI, J. 2004. Identification of a novel human subfamily of mitochondrial carriers with calcium-binding domains. *J Biol Chem,* 279**,** 24701-13.

DEL RIO, E., BEVILACQUA, J. A., MARSH, S. J., HALLEY, P. & CAULFIELD, M. P. 1999. Muscarinic M1 receptors activate phosphoinositide turnover and Ca2+ mobilisation in rat sympathetic neurones, but this signalling pathway does not mediate M-current inhibition. *J Physiol,* 520 Pt 1**,** 101-11.

DELMAS, P., CREST, M. & BROWN, D. A. 2004. Functional organization of PLC signaling microdomains in neurons. *Trends Neurosci,* 27**,** 41-7.

DELMAS, P., WANAVERBECQ, N., ABOGADIE, F. C., MISTRY, M. & BROWN, D. A. 2002. Signaling microdomains define the specificity of receptor-mediated InsP(3) pathways in neurons. *Neuron,* 34**,** 209-20.

DENTON, R. M. 2009. Regulation of mitochondrial dehydrogenases by calcium ions. *Biochim Biophys Acta,* 1787**,** 1309-16.

DERLER, I., FAHRNER, M., MUIK, M., LACKNER, B., SCHINDL, R., GROSCHNER, K. & ROMANIN, C. 2009. A Ca2(+)release-activated Ca2(+) (CRAC) modulatory domain (CMD) within STIM1 mediates fast Ca2(+)-dependent inactivation of ORAI1 channels. *J Biol Chem,* 284**,** 24933-8.

DIONISIO, N., REDONDO, P. C., JARDIN, I. & ROSADO, J. A. 2012. Transient receptor potential channels in human platelets: expression and functional role. *Curr Mol Med,* 12**,** 1319-28.

DITTMER, P. J., WILD, A. R., DELL'ACQUA, M. L. & SATHER, W. A. 2017. STIM1 Ca2+ Sensor Control of L-type Ca2+-Channel-Dependent Dendritic Spine Structural Plasticity and Nuclear Signaling. *Cell Rep,* 19**,** 321-334.

DRAGO, I., PIZZO, P. & POZZAN, T. 2011. After half a century mitochondrial calcium in- and efflux machineries reveal themselves. *EMBO J,* 30**,** 4119-25.

DUTAR, P., BASSANT, M. H., SENUT, M. C. & LAMOUR, Y. 1995. The septohippocampal pathway: structure and function of a central cholinergic system. *Physiol Rev,* 75**,** 393-427.

EGLEN, R. M. 2006. Muscarinic receptor subtypes in neuronal and non-neuronal cholinergic function. *Auton Autacoid Pharmacol,* 26**,** 219-33.

EGOROV, A. V., HAMAM, B. N., FRANSEN, E., HASSELMO, M. E. & ALONSO, A. A. 2002. Graded persistent activity in entorhinal cortex neurons. *Nature,* 420**,** 173-8.

EMPTAGE, N. J., REID, C. A. & FINE, A. 2001. Calcium stores in hippocampal synaptic boutons mediate short-term plasticity, store-operated Ca2+ entry, and spontaneous transmitter release. *Neuron,* 29**,** 197-208.

FELLER, M. B. 1999. Spontaneous correlated activity in developing neural circuits. *Neuron,* 22**,** 653-6.

FERNANDEZ DE SEVILLA, D., NUNEZ, A., BORDE, M., MALINOW, R. & BUNO, W. 2008. Cholinergic-mediated IP3-receptor activation induces long-lasting synaptic enhancement in CA1 pyramidal neurons. *J Neurosci,* 28**,** 1469-78.

FESKE, S., GWACK, Y., PRAKRIYA, M., SRIKANTH, S., PUPPEL, S. H., TANASA, B., HOGAN, P. G., LEWIS, R. S., DALY, M. & RAO, A. 2006. A mutation in Orai1 causes immune deficiency by abrogating CRAC channel function. *Nature,* 441**,** 179-85.

FIERMONTE, G., DE LEONARDIS, F., TODISCO, S., PALMIERI, L., LASORSA, F. M. & PALMIERI, F. 2004. Identification of the mitochondrial ATP-Mg/Pi transporter. Bacterial expression, reconstitution, functional characterization, and tissue distribution. *J Biol Chem,* 279**,** 30722-30.

FITZJOHN, S. M. & COLLINGRIDGE, G. L. 2002. Calcium stores and synaptic plasticity. *Cell Calcium,* 32**,** 405-11.

FITZJOHN, S. M., PALMER, M. J., MAY, J. E., NEESON, A., MORRIS, S. A. & COLLINGRIDGE, G. L. 2001. A characterisation of long-term depression induced by metabotropic glutamate receptor activation in the rat hippocampus in vitro. *J Physiol,* 537**,** 421-30.

FONTERIZ, R., MATESANZ-ISABEL, J., ARIAS-DEL-VAL, J., ALVAREZ-ILLERA, P., MONTERO, M. & ALVAREZ, J. 2016. Modulation of Calcium Entry by Mitochondria. *Adv Exp Med Biol,* 898**,** 405-21.

FRIEDEN, M., JAMES, D., CASTELBOU, C., DANCKAERT, A., MARTINOU, J. C. & DEMAUREX, N. 2004. Ca(2+) homeostasis during mitochondrial fragmentation and perinuclear clustering induced by hFis1. *J Biol Chem,* 279**,** 22704-14.

GARCIA-ALVAREZ, G., LU, B., YAP, K. A., WONG, L. C., THEVATHASAN, J. V., LIM, L., JI, F., TAN, K. W., MANCUSO, J. J., TANG, W., POON, S. Y., AUGUSTINE, G. J. & FIVAZ, M. 2015a. STIM2 regulates PKA-dependent phosphorylation and trafficking of AMPARs. *Mol Biol Cell,* 26**,** 1141-59.

GARCIA-ALVAREZ, G., SHETTY, M. S., LU, B., YAP, K. A., OH-HORA, M., SAJIKUMAR, S., BICHLER, Z. & FIVAZ, M. 2015b. Impaired spatial memory and enhanced long-term potentiation in mice with forebrain-specific ablation of the Stim genes. *Front Behav Neurosci,* 9**,** 180.

GELLERICH, F. N., GIZATULLINA, Z., GAINUTDINOV, T., MUTH, K., SEPPET, E., ORYNBAYEVA, Z. & VIELHABER, S. 2013. The control of brain mitochondrial energization by cytosolic calcium: the mitochondrial gas pedal. *IUBMB Life,* 65**,** 180-90.

GELLERICH, F. N., GIZATULLINA, Z., TRUMBEKAITE, S., KORZENIEWSKI, B., GAYNUTDINOV, T., SEPPET, E., VIELHABER, S., HEINZE, H. J. & STRIGGOW, F. 2012. Cytosolic Ca2+ regulates the energization of isolated brain mitochondria by formation of pyruvate through the malate-aspartate shuttle. *Biochem J,* 443**,** 747-55.

GEMES, G., BANGARU, M. L., WU, H. E., TANG, Q., WEIHRAUCH, D., KOOPMEINERS, A. S., CRUIKSHANK, J. M., KWOK, W. M. & HOGAN, Q. H. 2011. Store-operated Ca2+ entry in sensory neurons: functional role and the effect of painful nerve injury. *J Neurosci,* 31**,** 3536-49.

GIACOMELLO, M., DRAGO, I., BORTOLOZZI, M., SCORZETO, M., GIANELLE, A., PIZZO, P. & POZZAN, T. 2010. Ca2+ hot spots on the mitochondrial surface are generated by Ca2+ mobilization from stores, but not by activation of store-operated Ca2+ channels. *Mol Cell,* 38**,** 280-90.

GIESSEL, A. J. & SABATINI, B. L. 2010. M1 muscarinic receptors boost synaptic potentials and calcium influx in dendritic spines by inhibiting postsynaptic SK channels. *Neuron,* 68**,** 936-47.

GILABERT, J. A. & PAREKH, A. B. 2000. Respiring mitochondria determine the pattern of activation and inactivation of the store-operated Ca(2+) current I(CRAC). *EMBO J,* 19**,** 6401-7.

GLADDING, C. M., FITZJOHN, S. M. & MOLNAR, E. 2009. Metabotropic glutamate receptor-mediated long-term depression: molecular mechanisms. *Pharmacol Rev,* 61**,** 395-412.

GLANCY, B. & BALABAN, R. S. 2012. Role of mitochondrial Ca2+ in the regulation of cellular energetics. *Biochemistry,* 51**,** 2959-73.

GONZALEZ-SANCHEZ, P., PLA-MARTIN, D., MARTINEZ-VALERO, P., RUEDA, C. B., CALPENA, E., DEL ARCO, A., PALAU, F. & SATRUSTEGUI, J. 2017. CMT-linked loss-of-function mutations in GDAP1 impair store-operated Ca2+ entry-stimulated respiration. *Sci Rep,* 7**,** 42993.

GREEN, A., ELLIS, K. A., ELLIS, J., BARTHOLOMEUSZ, C. F., ILIC, S., CROFT, R. J., PHAN, K. L. & NATHAN, P. J. 2005. Muscarinic and nicotinic receptor modulation of object and spatial n-back working memory in humans. *Pharmacol Biochem Behav,* 81**,** 575-84.

GRIENBERGER, C. & KONNERTH, A. 2012. Imaging calcium in neurons. *Neuron,* 73**,** 862-85.

GROSS, S. A., GUZMAN, G. A., WISSENBACH, U., PHILIPP, S. E., ZHU, M. X., BRUNS, D. & CAVALIE, A. 2009. TRPC5 is a Ca2+-activated channel functionally coupled to Ca2+-selective ion channels. *J Biol Chem,* 284**,** 34423-32.

GRUSZCZYNSKA-BIEGALA, J., POMORSKI, P., WISNIEWSKA, M. B. & KUZNICKI, J. 2011. Differential roles for STIM1 and STIM2 in store-operated calcium entry in rat neurons. *PLoS One,* 6**,** e19285.

GRUSZCZYNSKA-BIEGALA, J., SLADOWSKA, M. & KUZNICKI, J. 2016. AMPA Receptors Are Involved in Store-Operated Calcium Entry and Interact with STIM Proteins in Rat Primary Cortical Neurons. *Front Cell Neurosci,* 10**,** 251.

HAJ-DAHMANE, S. & ANDRADE, R. 1996. Muscarinic activation of a voltage-dependent cation nonselective current in rat association cortex. *J Neurosci,* 16**,** 3848-61.

HARTMANN, J., KARL, R. M., ALEXANDER, R. P., ADELSBERGER, H., BRILL, M. S., RUHLMANN, C., ANSEL, A., SAKIMURA, K., BABA, Y., KUROSAKI, T., MISGELD, T. & KONNERTH, A. 2014.

STIM1 controls neuronal Ca(2)(+) signaling, mGluR1-dependent synaptic transmission, and cerebellar motor behavior. *Neuron,* 82**,** 635-44.

HARVEY, J. & COLLINGRIDGE, G. L. 1992. Thapsigargin blocks the induction of long-term potentiation in rat hippocampal slices. *Neurosci Lett,* 139**,** 197-200.

HASSELMO, M. E. 2006. The role of acetylcholine in learning and memory. *Curr Opin Neurobiol,* 16**,** 710-5.

HASSELMO, M. E. & SARTER, M. 2011. Modes and models of forebrain cholinergic neuromodulation of cognition. *Neuropsychopharmacology,* 36**,** 52-73.

HAYAKAWA, Y., NEMOTO, T., IINO, M. & KASAI, H. 2005. Rapid Ca2+-dependent increase in oxygen consumption by mitochondria in single mammalian central neurons. *Cell Calcium,* 37**,** 359-70.

HE, L. P., HEWAVITHARANA, T., SOBOLOFF, J., SPASSOVA, M. A. & GILL, D. L. 2005. A functional link between store-operated and TRPC channels revealed by the 3,5-bis(trifluoromethyl)pyrazole derivative, BTP2. *J Biol Chem,* 280**,** 10997-1006.

HIGLEY, M. J. & SABATINI, B. L. 2012. Calcium signaling in dendritic spines. *Cold Spring Harb Perspect Biol,* 4**,** a005686.

HOLBRO, N., GRUNDITZ, A. & OERTNER, T. G. 2009. Differential distribution of endoplasmic reticulum controls metabotropic signaling and plasticity at hippocampal synapses. *Proc Natl Acad Sci U S A,* 106**,** 15055-60.

HOLLENBECK, P. J. & SAXTON, W. M. 2005. The axonal transport of mitochondria. *J Cell Sci,* 118**,** 5411-9.

HOTH, M., BUTTON, D. C. & LEWIS, R. S. 2000. Mitochondrial control of calcium-channel gating: a mechanism for sustained signaling and transcriptional activation in T lymphocytes. *Proc Natl Acad Sci U S A,* 97**,** 10607-12.

HOTH, M., FANGER, C. M. & LEWIS, R. S. 1997. Mitochondrial regulation of store-operated calcium signaling in T lymphocytes. *J Cell Biol,* 137**,** 633-48.

HOTH, M. & PENNER, R. 1992. Depletion of intracellular calcium stores activates a calcium current in mast cells. *Nature,* 355**,** 353-6.

HOU, P. F., LIU, Z. H., LI, N., CHENG, W. J. & GUO, S. W. 2015. Knockdown of STIM1 improves neuronal survival after traumatic neuronal injury through regulating mGluR1-dependent Ca(2+) signaling in mouse cortical neurons. *Cell Mol Neurobiol,* 35**,** 283-92.

HUANG, G. N., ZENG, W., KIM, J. Y., YUAN, J. P., HAN, L., MUALLEM, S. & WORLEY, P. F. 2006. STIM1 carboxyl-terminus activates native SOC, I(crac) and TRPC1 channels. *Nat Cell Biol,* 8**,** 1003-10.

HUANG, H. M., CHEN, H. L. & GIBSON, G. E. 2014. Interactions of endoplasmic reticulum and mitochondria Ca(2+) stores with capacitative calcium entry. *Metab Brain Dis,* 29**,** 1083-93.

HUBER, N., GUIMARAES, S., SCHRADER, M., SUTER, U. & NIEMANN, A. 2013. Charcot-Marie-Tooth disease-associated mutants of GDAP1 dissociate its roles in peroxisomal and mitochondrial fission. *EMBO Rep,* 14**,** 545-52.

ISHII, M. & KURACHI, Y. 2006. Muscarinic acetylcholine receptors. *Curr Pharm Des,* 12**,** 3573-81.

JALIL, M. A., BEGUM, L., CONTRERAS, L., PARDO, B., IIJIMA, M., LI, M. X., RAMOS, M., MARMOL, P., HORIUCHI, M., SHIMOTSU, K., NAKAGAWA, S., OKUBO, A., SAMESHIMA, M., ISASHIKI, Y., DEL ARCO, A., KOBAYASHI, K., SATRUSTEGUI, J. & SAHEKI, T. 2005. Reduced N-acetylaspartate levels in mice lacking aralar, a brain- and muscle-type mitochondrial aspartate-glutamate carrier. *J Biol Chem,* 280**,** 31333-9.

JIANG, M. & CHEN, G. 2006. High Ca2+-phosphate transfection efficiency in low-density neuronal cultures. *Nat Protoc,* 1**,** 695-700.

JO, J., HEON, S., KIM, M. J., SON, G. H., PARK, Y., HENLEY, J. M., WEISS, J. L., SHENG, M., COLLINGRIDGE, G. L. & CHO, K. 2008. Metabotropic glutamate receptor-mediated LTD involves two interacting Ca(2+) sensors, NCS-1 and PICK1. *Neuron,* 60**,** 1095-111.

JORNTELL, H. & HANSEL, C. 2006. Synaptic memories upside down: bidirectional plasticity at cerebellar parallel fiber-Purkinje cell synapses. *Neuron,* 52**,** 227-38.

JOUAVILLE, L. S., PINTON, P., BASTIANUTTO, C., RUTTER, G. A. & RIZZUTO, R. 1999. Regulation of mitochondrial ATP synthesis by calcium: evidence for a long-term metabolic priming. *Proc Natl Acad Sci U S A,* 96**,** 13807-12.

JOUSSET, H., FRIEDEN, M. & DEMAUREX, N. 2007. STIM1 knockdown reveals that store-operated Ca2+ channels located close to sarco/endoplasmic Ca2+ ATPases (SERCA) pumps silently refill the endoplasmic reticulum. *J Biol Chem,* 282**,** 11456-64.

JOYAL, J. L. & APRILLE, J. R. 1992. The ATP-Mg/Pi carrier of rat liver mitochondria catalyzes a divalent electroneutral exchange. *J Biol Chem,* 267**,** 19198-203.

JUAREZ, P. & PALAU, F. 2012. Neural and molecular features on Charcot-Marie-Tooth disease plasticity and therapy. *Neural Plast,* 2012**,** 171636.

KANN, O. & KOVACS, R. 2007. Mitochondria and neuronal activity. *Am J Physiol Cell Physiol,* 292**,** C641-57.

KANN, O., TAUBENBERGER, N., HUCHZERMEYER, C., PAPAGEORGIOU, I. E., BENNINGER, F., HEINEMANN, U. & KOVACS, R. 2012. Muscarinic receptor activation determines the effects of store-operated Ca(2+)-entry on excitability and energy metabolism in pyramidal neurons. *Cell Calcium,* 51**,** 40-50.

KANO, M., HASHIMOTO, K. & TABATA, T. 2008. Type-1 metabotropic glutamate receptor in cerebellar Purkinje cells: a key molecule responsible for long-term depression, endocannabinoid signalling and synapse elimination. *Philos Trans R Soc Lond B Biol Sci,* 363**,** 2173-86.

KARLSTAD, J., SUN, Y. & SINGH, B. B. 2012. Ca(2+) signaling: an outlook on the characterization of Ca(2+) channels and their importance in cellular functions. *Adv Exp Med Biol,* 740**,** 143-57.

KERR, J. N., GREENBERG, D. & HELMCHEN, F. 2005. Imaging input and output of neocortical networks in vivo. *Proc Natl Acad Sci U S A,* 102**,** 14063-8.

KIM, H. H., LEE, K. H., LEE, D., HAN, Y. E., LEE, S. H., SOHN, J. W. & HO, W. K. 2015. Costimulation of AMPA and metabotropic glutamate receptors underlies phospholipase C activation by glutamate in hippocampus. *J Neurosci,* 35**,** 6401-12.

KIM, M. S., ZENG, W., YUAN, J. P., SHIN, D. M., WORLEY, P. F. & MUALLEM, S. 2009. Native Store-operated Ca2+ Influx Requires the Channel Function of Orai1 and TRPC1. *J Biol Chem,* 284**,** 9733-41.

KLEJMAN, M. E., GRUSZCZYNSKA-BIEGALA, J., SKIBINSKA-KIJEK, A., WISNIEWSKA, M. B., MISZTAL, K., BLAZEJCZYK, M., BOJARSKI, L. & KUZNICKI, J. 2009. Expression of STIM1 in brain and puncta-like co-localization of STIM1 and ORAI1 upon depletion of Ca(2+) store in neurons. *Neurochem Int,* 54**,** 49-55.

KLINGENBERG, M. 2008. The ADP and ATP transport in mitochondria and its carrier. *Biochim Biophys Acta,* 1778**,** 1978-2021.

KOPACH, O., KRUGLIKOV, I., PIVNEVA, T., VOITENKO, N., VERKHRATSKY, A. & FEDIRKO, N. 2011. Mitochondria adjust Ca(2+) signaling regime to a pattern of stimulation in salivary acinar cells. *Biochim Biophys Acta,* 1813**,** 1740-8.

KORKOTIAN, E., ONI-BITON, E. & SEGAL, M. 2017. The role of the store-operated calcium entry channel Orai1 in cultured rat hippocampal synapse formation and plasticity. *J Physiol,* 595**,** 125-140.

KORKOTIAN, E. & SEGAL, M. 2017. Orai1 regulates calcium entry into dendritic spines. *Channels (Austin),* 11**,** 99-100.

KRAJEWSKI, K. M., LEWIS, R. A., FUERST, D. R., TURANSKY, C., HINDERER, S. R., GARBERN, J., KAMHOLZ, J. & SHY, M. E. 2000. Neurological dysfunction and axonal degeneration in Charcot-Marie-Tooth disease type 1A. *Brain,* 123 (Pt 7)**,** 1516-27.

KREBS, J., AGELLON, L. B. & MICHALAK, M. 2015. Ca(2+) homeostasis and endoplasmic reticulum (ER) stress: An integrated view of calcium signaling. *Biochem Biophys Res Commun,* 460**,** 114-21.

KRNJEVIC, K. 1993. Central cholinergic mechanisms and function. *Prog Brain Res,* 98**,** 285-92.

KWONG, J. Q., LU, X., CORRELL, R. N., SCHWANEKAMP, J. A., VAGNOZZI, R. J., SARGENT, M. A., YORK, A. J., ZHANG, J., BERS, D. M. & MOLKENTIN, J. D. 2015. The Mitochondrial Calcium Uniporter Selectively Matches Metabolic Output to Acute Contractile Stress in the Heart. *Cell Rep,* 12**,** 15-22.

LALONDE, J., SAIA, G. & GILL, G. 2014. Store-operated calcium entry promotes the degradation of the transcription factor Sp4 in resting neurons. *Sci Signal,* 7**,** ra51.

LEE, K. P., YUAN, J. P., ZENG, W., SO, I., WORLEY, P. F. & MUALLEM, S. 2009. Molecular determinants of fast Ca2+-dependent inactivation and gating of the Orai channels. *Proc Natl Acad Sci U S A,* 106**,** 14687-92.

LEFKIMMIATIS, K., SRIKANTHAN, M., MAIELLARO, I., MOYER, M. P., CURCI, S. & HOFER, A. M. 2009. Store-operated cyclic AMP signalling mediated by STIM1. *Nat Cell Biol,* 11**,** 433-42.

LEVEY, A. I., KITT, C. A., SIMONDS, W. F., PRICE, D. L. & BRANN, M. R. 1991. Identification and localization of muscarinic acetylcholine receptor proteins in brain with subtype-specific antibodies. *J Neurosci,* 11**,** 3218-26.

LEWIS, R. S. 2007. The molecular choreography of a store-operated calcium channel. *Nature,* 446**,** 284-7.

LIOU, J., KIM, M. L., HEO, W. D., JONES, J. T., MYERS, J. W., FERRELL, J. E., JR. & MEYER, T. 2005. STIM is a Ca2+ sensor essential for Ca2+-store-depletion-triggered Ca2+ influx. *Curr Biol,* 15**,** 1235-41.

LU, B. & FIVAZ, M. 2016. Neuronal SOCE: Myth or Reality? *Trends Cell Biol,* 26**,** 890-893.

LUJAN, R., NUSSER, Z., ROBERTS, J. D., SHIGEMOTO, R. & SOMOGYI, P. 1996. Perisynaptic location of metabotropic glutamate receptors mGluR1 and mGluR5 on dendrites and dendritic spines in the rat hippocampus. *Eur J Neurosci,* 8**,** 1488-500.

LUONGO, T. S., LAMBERT, J. P., YUAN, A., ZHANG, X., GROSS, P., SONG, J., SHANMUGHAPRIYA, S., GAO, E., JAIN, M., HOUSER, S. R., KOCH, W. J., CHEUNG, J. Y., MADESH, M. & ELROD, J. W. 2015. The Mitochondrial Calcium Uniporter Matches Energetic Supply with Cardiac Workload during Stress and Modulates Permeability Transition. *Cell Rep,* 12**,** 23-34.

LUSCHER, C. & HUBER, K. M. 2010. Group 1 mGluR-dependent synaptic long-term depression: mechanisms and implications for circuitry and disease. *Neuron,* 65**,** 445-59.

LLORENTE-FOLCH, I., RUEDA, C. B., AMIGO, I., DEL ARCO, A., SAHEKI, T., PARDO, B. & SATRUSTEGUI, J. 2013. Calcium-regulation of mitochondrial respiration maintains ATP homeostasis and requires ARALAR/AGC1-malate aspartate shuttle in intact cortical neurons. *J Neurosci,* 33**,** 13957-71, 13971a.

LLORENTE-FOLCH, I., RUEDA, C. B., PARDO, B., SZABADKAI, G., DUCHEN, M. R. & SATRUSTEGUI, J. 2015a. The regulation of neuronal mitochondrial metabolism by calcium. *J Physiol,* 593**,** 3447-62.

LLORENTE-FOLCH, I., RUEDA, C. B., PARDO, B., SZABADKAI, G., DUCHEN, M. R. & SATRUSTEGUI, J. 2015b. The regulation of neuronal mitochondrial metabolism by calcium. *J Physiol*.

MA, H. T., PENG, Z., HIRAGUN, T., IWAKI, S., GILFILLAN, A. M. & BEAVEN, M. A. 2008. Canonical transient receptor potential 5 channel in conjunction with Orai1 and STIM1 allows Sr2+ entry, optimal influx of Ca2+, and degranulation in a rat mast cell line. *J Immunol,* 180**,** 2233-9.

MAGGIO, N. & VLACHOS, A. 2014. Synaptic plasticity at the interface of health and disease: New insights on the role of endoplasmic reticulum intracellular calcium stores. *Neuroscience,* 281**,** 135-46.

MAJEWSKI, L. & KUZNICKI, J. 2015. SOCE in neurons: Signaling or just refilling? *Biochim Biophys Acta,* 1853**,** 1940-52.

MAJEWSKI, L., MACIAG, F., BOGUSZEWSKI, P. M., WASILEWSKA, I., WIERA, G., WOJTOWICZ, T., MOZRZYMAS, J. & KUZNICKI, J. 2017. Overexpression of STIM1 in neurons in mouse brain improves contextual learning and impairs long-term depression. *Biochim Biophys Acta,* 1864**,** 1071-1087.

MALLI, R., FRIEDEN, M., OSIBOW, K., ZORATTI, C., MAYER, M., DEMAUREX, N. & GRAIER, W. F. 2003. Sustained Ca2+ transfer across mitochondria is Essential for mitochondrial Ca2+ buffering, sore-operated Ca2+ entry, and Ca2+ store refilling. *J Biol Chem,* 278**,** 44769-79.

MALLILANKARAMAN, K., CARDENAS, C., DOONAN, P. J., CHANDRAMOORTHY, H. C., IRRINKI, K. M., GOLENAR, T., CSORDAS, G., MADIREDDI, P., YANG, J., MULLER, M., MILLER, R., KOLESAR, J. E., MOLGO, J., KAUFMAN, B., HAJNOCZKY, G., FOSKETT, J. K. & MADESH, M. 2012a. MCUR1 is an essential component of mitochondrial Ca2+ uptake that regulates cellular metabolism. *Nat Cell Biol,* 14**,** 1336-43.

MALLILANKARAMAN, K., DOONAN, P., CARDENAS, C., CHANDRAMOORTHY, H. C., MULLER, M., MILLER, R., HOFFMAN, N. E., GANDHIRAJAN, R. K., MOLGO, J., BIRNBAUM, M. J., ROTHBERG, B. S., MAK, D. O., FOSKETT, J. K. & MADESH, M. 2012b. MICU1 is an essential gatekeeper for MCU-mediated mitochondrial Ca(2+) uptake that regulates cell survival. *Cell,* 151**,** 630-44.

MARCO, A., CUESTA, A., PEDROLA, L., PALAU, F. & MARIN, I. 2004. Evolutionary and structural analyses of GDAP1, involved in Charcot-Marie-Tooth disease, characterize a novel class of glutathione transferase-related genes. *Mol Biol Evol,* 21**,** 176-87.

MARTINEZ-VALERO, P. 2017. *Enfermedad de Charcot-Marie-Tooth asociada a GDAP1: alteraciones en nocicepción y señalización por calcio.* Universidad Autónoma de Madrid.

MATANIS, T., AKHMANOVA, A., WULF, P., DEL NERY, E., WEIDE, T., STEPANOVA, T., GALJART, N., GROSVELD, F., GOUD, B., DE ZEEUW, C. I., BARNEKOW, A. & HOOGENRAAD, C. C. 2002. Bicaudal-D regulates COPI-independent Golgi-ER transport by recruiting the dynein-dynactin motor complex. *Nat Cell Biol,* 4**,** 986-92.

MCCLURE, C., COLE, K. L., WULFF, P., KLUGMANN, M. & MURRAY, A. J. 2011. Production and titering of recombinant adeno-associated viral vectors. *J Vis Exp***,** e3348.

MCGAUGHY, J., KOENE, R. A., EICHENBAUM, H. & HASSELMO, M. E. 2005. Cholinergic deafferentation of the entorhinal cortex in rats impairs encoding of novel but not familiar stimuli in a delayed nonmatch-to-sample task. *J Neurosci,* 25**,** 10273-81.

MIRONOV, S. L. 2006. Spontaneous and evoked neuronal activities regulate movements of single neuronal mitochondria. *Synapse,* 59**,** 403-11.

MITCHELL, P. & MOYLE, J. 1967. Chemiosmotic hypothesis of oxidative phosphorylation. *Nature,* 213**,** 137-9.

MIYATA, M., FINCH, E. A., KHIROUG, L., HASHIMOTO, K., HAYASAKA, S., ODA, S. I., INOUYE, M., TAKAGISHI, Y., AUGUSTINE, G. J. & KANO, M. 2000. Local calcium release in dendritic spines required for long-term synaptic depression. *Neuron,* 28**,** 233-44.

MOCCIA, F., ZUCCOLO, E., SODA, T., TANZI, F., GUERRA, G., MAPELLI, L., LODOLA, F. & D'ANGELO, E. 2015. Stim and Orai proteins in neuronal Ca(2+) signaling and excitability. *Front Cell Neurosci,* 9**,** 153.

MOCKETT, B. G., GUEVREMONT, D., WUTTE, M., HULME, S. R., WILLIAMS, J. M. & ABRAHAM, W. C. 2011. Calcium/calmodulin-dependent protein kinase II mediates group I metabotropic glutamate receptor-dependent protein synthesis and long-term depression in rat hippocampus. *J Neurosci,* 31**,** 7380-91.

MONTALVO, G. B., ARTALEJO, A. R. & GILABERT, J. A. 2006. ATP from subplasmalemmal mitochondria controls Ca2+-dependent inactivation of CRAC channels. *J Biol Chem,* 281**,** 35616-23.

MORENO-SANCHEZ, R. 1983. Inhibition of oxidative phosphorylation by a Ca2+-induced diminution of the adenine nucleotide translocator. *Biochim Biophys Acta,* 724**,** 278-85.

MURPHY, T. H., BLATTER, L. A., WIER, W. G. & BARABAN, J. M. 1992. Spontaneous synchronous synaptic calcium transients in cultured cortical neurons. *J Neurosci,* 12**,** 4834-45.

NAGHDI, S., WALDECK-WEIERMAIR, M., FERTSCHAI, I., POTESER, M., GRAIER, W. F. & MALLI, R. 2010. Mitochondrial Ca2+ uptake and not mitochondrial motility is required for STIM1-Orai1-dependent store-operated Ca2+ entry. *J Cell Sci,* 123**,** 2553-64.

NASH, M. S., WILLETS, J. M., BILLUPS, B., JOHN CHALLISS, R. A. & NAHORSKI, S. R. 2004. Synaptic activity augments muscarinic acetylcholine receptor-stimulated inositol 1,4,5-trisphosphate production to facilitate Ca2+ release in hippocampal neurons. *J Biol Chem,* 279**,** 49036-44.

NG, A. N., KROGH, M. & TORESSON, H. 2011. Dendritic EGFP-STIM1 activation after type I metabotropic glutamate and muscarinic acetylcholine receptor stimulation in hippocampal neuron. *J Neurosci Res,* 89**,** 1235-44.

NIEMANN, A., HUBER, N., WAGNER, K. M., SOMANDIN, C., HORN, M., LEBRUN-JULIEN, F., ANGST, B., PEREIRA, J. A., HALFTER, H., WELZL, H., FELTRI, M. L., WRABETZ, L., YOUNG, P., WESSIG, C., TOYKA, K. V. & SUTER, U. 2014. The Gdap1 knockout mouse mechanistically links redox control to Charcot-Marie-Tooth disease. *Brain,* 137**,** 668-82.

NIEMANN, A., RUEGG, M., LA PADULA, V., SCHENONE, A. & SUTER, U. 2005. Ganglioside-induced differentiation associated protein 1 is a regulator of the mitochondrial network: new implications for Charcot-Marie-Tooth disease. *J Cell Biol,* 170**,** 1067-78.

NIEMANN, A., WAGNER, K. M., RUEGG, M. & SUTER, U. 2009. GDAP1 mutations differ in their effects on mitochondrial dynamics and apoptosis depending on the mode of inheritance. *Neurobiol Dis,* 36**,** 509-20.

NISWENDER, C. M. & CONN, P. J. 2010. Metabotropic glutamate receptors: physiology, pharmacology, and disease. *Annu Rev Pharmacol Toxicol,* 50**,** 295-322.

NOACK, R., FREDE, S., ALBRECHT, P., HENKE, N., PFEIFFER, A., KNOLL, K., DEHMEL, T., MEYER ZU HORSTE, G., STETTNER, M., KIESEIER, B. C., SUMMER, H., GOLZ, S., KOCHANSKI, A., WIEDAU-PAZOS, M., ARNOLD, S., LEWERENZ, J. & METHNER, A. 2012. Charcot-Marie-Tooth disease CMT4A: GDAP1 increases cellular glutathione and the mitochondrial membrane potential. *Hum Mol Genet,* 21**,** 150-62.

NOSYREVA, E. D. & HUBER, K. M. 2005. Developmental switch in synaptic mechanisms of hippocampal metabotropic glutamate receptor-dependent long-term depression. *J Neurosci,* 25**,** 2992-3001.

NUMAKAWA, T., YAMAGISHI, S., ADACHI, N., MATSUMOTO, T., YOKOMAKU, D., YAMADA, M. & HATANAKA, H. 2002. Brain-derived neurotrophic factor-induced potentiation of Ca(2+) oscillations in developing cortical neurons. *J Biol Chem,* 277**,** 6520-9.

NUNEZ, L., VALERO, R. A., SENOVILLA, L., SANZ-BLASCO, S., GARCIA-SANCHO, J. & VILLALOBOS, C. 2006. Cell proliferation depends on mitochondrial Ca2+ uptake: inhibition by salicylate. *J Physiol,* 571**,** 57-73.

NUNNARI, J. & SUOMALAINEN, A. 2012. Mitochondria: in sickness and in health. *Cell,* 148**,** 1145-59.

OGURA, A., IIJIMA, T., AMANO, T. & KUDO, Y. 1987. Optical monitoring of excitatory synaptic activity between cultured hippocampal neurons by a multi-site Ca2+ fluorometry. *Neurosci Lett,* 78**,** 69-74.

OLIANAS, M. C., DEDONI, S. & ONALI, P. 2014. Involvement of store-operated Ca(2+) entry in activation of AMP-activated protein kinase and stimulation of glucose uptake by M3 muscarinic acetylcholine receptors in human neuroblastoma cells. *Biochim Biophys Acta,* 1843**,** 3004-17.

OLIET, S. H., MALENKA, R. C. & NICOLL, R. A. 1997. Two distinct forms of long-term depression coexist in CA1 hippocampal pyramidal cells. *Neuron,* 18**,** 969-82.

OPITZ, T., DE LIMA, A. D. & VOIGT, T. 2002. Spontaneous development of synchronous oscillatory activity during maturation of cortical networks in vitro. *J Neurophysiol,* 88**,** 2196-206.

OTANI, S. & CONNOR, J. A. 1998. Requirement of rapid Ca2+ entry and synaptic activation of metabotropic glutamate receptors for the induction of long-term depression in adult rat hippocampus. *J Physiol,* 511 (Pt 3)**,** 761-70.

PALMER, A. E., GIACOMELLO, M., KORTEMME, T., HIRES, S. A., LEV-RAM, V., BAKER, D. & TSIEN, R. Y. 2006. Ca2+ indicators based on computationally redesigned calmodulin-peptide pairs. *Chem Biol,* 13**,** 521-30.

PALMIERI, L., PARDO, B., LASORSA, F. M., DEL ARCO, A., KOBAYASHI, K., IIJIMA, M., RUNSWICK, M. J., WALKER, J. E., SAHEKI, T., SATRUSTEGUI, J. & PALMIERI, F. 2001. Citrin and aralar1 are Ca(2+)-stimulated aspartate/glutamate transporters in mitochondria. *EMBO J,* 20**,** 5060-9.

PALTY, R., SILVERMAN, W. F., HERSHFINKEL, M., CAPORALE, T., SENSI, S. L., PARNIS, J., NOLTE, C., FISHMAN, D., SHOSHAN-BARMATZ, V., HERRMANN, S., KHANANSHVILI, D. & SEKLER, I. 2010. NCLX is an essential component of mitochondrial Na+/Ca2+ exchange. *Proc Natl Acad Sci U S A,* 107**,** 436-41.

PAN, X., LIU, J., NGUYEN, T., LIU, C., SUN, J., TENG, Y., FERGUSSON, M. M., ROVIRA, II, ALLEN, M., SPRINGER, D. A., APONTE, A. M., GUCEK, M., BALABAN, R. S., MURPHY, E. & FINKEL, T. 2013. The physiological role of mitochondrial calcium revealed by mice lacking the mitochondrial calcium uniporter. *Nat Cell Biol,* 15**,** 1464-72.

PARDO, B., CONTRERAS, L., SERRANO, A., RAMOS, M., KOBAYASHI, K., IIJIMA, M., SAHEKI, T. & SATRUSTEGUI, J. 2006. Essential role of aralar in the transduction of small Ca2+ signals to neuronal mitochondria. *J Biol Chem,* 281**,** 1039-47.

PAREKH, A. B. 2003. Store-operated Ca2+ entry: dynamic interplay between endoplasmic reticulum, mitochondria and plasma membrane. *J Physiol,* 547**,** 333-48.

PAREKH, A. B. 2008. Mitochondrial regulation of store-operated CRAC channels. *Cell Calcium,* 44**,** 6-13.

PAREKH, A. B. & PENNER, R. 1997. Store depletion and calcium influx. *Physiol Rev,* 77**,** 901-30.

PAREKH, A. B. & PUTNEY, J. W., JR. 2005. Store-operated calcium channels. *Physiol Rev,* 85**,** 757-810.

PARK, C. Y., SHCHEGLOVITOV, A. & DOLMETSCH, R. 2010. The CRAC channel activator STIM1 binds and inhibits L-type voltage-gated calcium channels. *Science,* 330**,** 101-5.

PATRON, M., CHECCHETTO, V., RAFFAELLO, A., TEARDO, E., VECELLIO REANE, D., MANTOAN, M., GRANATIERO, V., SZABO, I., DE STEFANI, D. & RIZZUTO, R. 2014. MICU1 and MICU2 finely tune the mitochondrial Ca2+ uniporter by exerting opposite effects on MCU activity. *Mol Cell,* 53**,** 726-37.

PEDROLA, L., ESPERT, A., VALDES-SANCHEZ, T., SANCHEZ-PIRIS, M., SIRKOWSKI, E. E., SCHERER, S. S., FARINAS, I. & PALAU, F. 2008. Cell expression of GDAP1 in the nervous system and pathogenesis of Charcot-Marie-Tooth type 4A disease. *J Cell Mol Med,* 12**,** 679-89.

PEROCCHI, F., GOHIL, V. M., GIRGIS, H. S., BAO, X. R., MCCOMBS, J. E., PALMER, A. E. & MOOTHA, V. K. 2010. MICU1 encodes a mitochondrial EF hand protein required for Ca(2+) uptake. *Nature,* 467**,** 291-6.

PICCIOTTO, M. R., CALDARONE, B. J., KING, S. L. & ZACHARIOU, V. 2000. Nicotinic receptors in the brain. Links between molecular biology and behavior. *Neuropsychopharmacology,* 22**,** 451-65.

PICCIOTTO, M. R., HIGLEY, M. J. & MINEUR, Y. S. 2012. Acetylcholine as a neuromodulator: cholinergic signaling shapes nervous system function and behavior. *Neuron,* 76**,** 116-29.

PIVOVAROVA, N. B. & ANDREWS, S. B. 2010. Calcium-dependent mitochondrial function and dysfunction in neurons. *FEBS J,* 277**,** 3622-36.

PLA-MARTIN, D., CALPENA, E., LUPO, V., MARQUEZ, C., RIVAS, E., SIVERA, R., SEVILLA, T., PALAU, F. & ESPINOS, C. 2015. Junctophilin-1 is a modifier gene of GDAP1-related Charcot-Marie-Tooth disease. *Hum Mol Genet,* 24**,** 213-29.

PLA-MARTIN, D., RUEDA, C. B., ESTELA, A., SANCHEZ-PIRIS, M., GONZALEZ-SANCHEZ, P., TRABA, J., DE LA FUENTE, S., SCORRANO, L., RENAU-PIQUERAS, J., ALVAREZ, J., SATRUSTEGUI, J. & PALAU, F. 2013. Silencing of the Charcot-Marie-Tooth disease-associated gene GDAP1 induces abnormal mitochondrial distribution and affects Ca2+ homeostasis by reducing store-operated Ca2+ entry. *Neurobiol Dis,* 55**,** 140-51.

POPUGAEVA, E., PCHITSKAYA, E., SPESHILOVA, A., ALEXANDROV, S., ZHANG, H., VLASOVA, O. & BEZPROZVANNY, I. 2015. STIM2 protects hippocampal mushroom spines from amyloid synaptotoxicity. *Mol Neurodegener,* 10**,** 37.

PRADO, V. F., JANICKOVA, H., AL-ONAIZI, M. A. & PRADO, M. A. 2017. Cholinergic circuits in cognitive flexibility. *Neuroscience,* 345**,** 130-141.

PRAKRIYA, M., FESKE, S., GWACK, Y., SRIKANTH, S., RAO, A. & HOGAN, P. G. 2006. Orai1 is an essential pore subunit of the CRAC channel. *Nature,* 443**,** 230-3.

PUTNEY, J. W., JR. 1986. A model for receptor-regulated calcium entry. *Cell Calcium,* 7**,** 1-12.

PUTNEY, J. W., JR. 2003. Capacitative calcium entry in the nervous system. *Cell Calcium,* 34**,** 339-44.

QIAN, W. & VAN HOUTEN, B. 2010. Alterations in bioenergetics due to changes in mitochondrial DNA copy number. *Methods,* 51**,** 452-7.

QIU, J., TAN, Y. W., HAGENSTON, A. M., MARTEL, M. A., KNEISEL, N., SKEHEL, P. A., WYLLIE, D. J., BADING, H. & HARDINGHAM, G. E. 2013. Mitochondrial calcium uniporter Mcu controls excitotoxicity and is transcriptionally repressed by neuroprotective nuclear calcium signals. *Nat Commun,* 4**,** 2034.

QUINTANA, A. & HOTH, M. 2012. Mitochondrial dynamics and their impact on T cell function. *Cell Calcium,* 52**,** 57-63.

QUINTANA, A., SCHWARZ, E. C., SCHWINDLING, C., LIPP, P., KAESTNER, L. & HOTH, M. 2006. Sustained activity of calcium release-activated calcium channels requires translocation of mitochondria to the plasma membrane. *J Biol Chem,* 281**,** 40302-9.

QUINTANA, A., SCHWINDLING, C., WENNING, A. S., BECHERER, U., RETTIG, J., SCHWARZ, E. C. & HOTH, M. 2007. T cell activation requires mitochondrial translocation to the immunological synapse. *Proc Natl Acad Sci U S A,* 104**,** 14418-23.

RAFFAELLO, A., DE STEFANI, D., SABBADIN, D., TEARDO, E., MERLI, G., PICARD, A., CHECCHETTO, V., MORO, S., SZABO, I. & RIZZUTO, R. 2013. The mitochondrial calcium uniporter is a multimer that can include a dominant-negative pore-forming subunit. *EMBO J,* 32**,** 2362-76.

RAFFAELLO, A., MAMMUCARI, C., GHERARDI, G. & RIZZUTO, R. 2016. Calcium at the Center of Cell Signaling: Interplay between Endoplasmic Reticulum, Mitochondria, and Lysosomes. *Trends Biochem Sci,* 41**,** 1035-1049.

RAMOS, M., DEL ARCO, A., PARDO, B., MARTINEZ-SERRANO, A., MARTINEZ-MORALES, J. R., KOBAYASHI, K., YASUDA, T., BOGONEZ, E., BOVOLENTA, P., SAHEKI, T. & SATRUSTEGUI, J. 2003. Developmental changes in the Ca2+-regulated mitochondrial aspartate-glutamate carrier aralar1 in brain and prominent expression in the spinal cord. *Brain Res Dev Brain Res,* 143**,** 33-46.

RANGARAJU, V., CALLOWAY, N. & RYAN, T. A. 2014. Activity-driven local ATP synthesis is required for synaptic function. *Cell,* 156**,** 825-35.

REILLY, M. M., MURPHY, S. M. & LAURA, M. 2011. Charcot-Marie-Tooth disease. *J Peripher Nerv Syst,* 16**,** 1-14.

RINTOUL, G. L., FILIANO, A. J., BROCARD, J. B., KRESS, G. J. & REYNOLDS, I. J. 2003. Glutamate decreases mitochondrial size and movement in primary forebrain neurons. *J Neurosci,* 23**,** 7881-8.

RIZZUTO, R., DE STEFANI, D., RAFFAELLO, A. & MAMMUCARI, C. 2012. Mitochondria as sensors and regulators of calcium signalling. *Nat Rev Mol Cell Biol,* 13**,** 566-78.

ROOS, J., DIGREGORIO, P. J., YEROMIN, A. V., OHLSEN, K., LIOUDYNO, M., ZHANG, S., SAFRINA, O., KOZAK, J. A., WAGNER, S. L., CAHALAN, M. D., VELICELEBI, G. & STAUDERMAN, K. A. 2005. STIM1, an essential and conserved component of store-operated Ca2+ channel function. *J Cell Biol,* 169**,** 435-45.

ROSADO, J. A., DIEZ, R., SMANI, T. & JARDIN, I. 2015. STIM and Orai1 Variants in Store-Operated Calcium Entry. *Front Pharmacol,* 6**,** 325.

ROSS, R. S., MCGAUGHY, J. & EICHENBAUM, H. 2005. Acetylcholine in the orbitofrontal cortex is necessary for the acquisition of a socially transmitted food preference. *Learn Mem,* 12**,** 302-6.

ROSSOR, A. M., POLKE, J. M., HOULDEN, H. & REILLY, M. M. 2013. Clinical implications of genetic advances in Charcot-Marie-Tooth disease. *Nat Rev Neurol,* 9**,** 562-71.

RUEDA, C. B., LLORENTE-FOLCH, I., AMIGO, I., CONTRERAS, L., GONZALEZ-SANCHEZ, P., MARTINEZ-VALERO, P., JUARISTI, I., PARDO, B., DEL ARCO, A. & SATRUSTEGUI, J. 2014. Ca(2+) regulation of mitochondrial function in neurons. *Biochim Biophys Acta,* 1837**,** 1617-24.

RUIZ, F., ALVAREZ, G., PEREIRA, R., HERNANDEZ, M., VILLALBA, M., CRUZ, F., CERDAN, S., BOGONEZ, E. & SATRUSTEGUI, J. 1998. Protection by pyruvate and malate against glutamate-mediated neurotoxicity. *Neuroreport,* 9**,** 1277-82.

SAMANTA, K., DOUGLAS, S. & PAREKH, A. B. 2014. Mitochondrial calcium uniporter MCU supports cytoplasmic Ca2+ oscillations, store-operated Ca2+ entry and Ca2+-dependent gene expression in response to receptor stimulation. *PLoS One,* 9**,** e101188.

SAMTLEBEN, S., WACHTER, B. & BLUM, R. 2015. Store-operated calcium entry compensates fast ER calcium loss in resting hippocampal neurons. *Cell Calcium,* 58**,** 147-59.

SANCAK, Y., MARKHARD, A. L., KITAMI, T., KOVACS-BOGDAN, E., KAMER, K. J., UDESHI, N. D., CARR, S. A., CHAUDHURI, D., CLAPHAM, D. E., LI, A. A., CALVO, S. E., GOLDBERGER, O. & MOOTHA, V. K. 2013. EMRE is an essential component of the mitochondrial calcium uniporter complex. *Science,* 342**,** 1379-82.

SATRUSTEGUI, J., PARDO, B. & DEL ARCO, A. 2007. Mitochondrial transporters as novel targets for intracellular calcium signaling. *Physiol Rev,* 87**,** 29-67.

SCHERER, S. S. & WRABETZ, L. 2008. Molecular mechanisms of inherited demyelinating neuropathies. *Glia,* 56**,** 1578-89.

SCHNABEL, R., KILPATRICK, I. C. & COLLINGRIDGE, G. L. 1999. An investigation into signal transduction mechanisms involved in DHPG-induced LTD in the CA1 region of the hippocampus. *Neuropharmacology,* 38**,** 1585-96.

SCHWINDLING, C., QUINTANA, A., KRAUSE, E. & HOTH, M. 2010. Mitochondria positioning controls local calcium influx in T cells. *J Immunol,* 184**,** 184-90.

SENDEREK, J., BERGMANN, C., STENDEL, C., KIRFEL, J., VERPOORTEN, N., DE JONGHE, P., TIMMERMAN, V., CHRAST, R., VERHEIJEN, M. H., LEMKE, G., BATTALOGLU, E., PARMAN, Y., ERDEM, S., TAN, E., TOPALOGLU, H., HAHN, A., MULLER-FELBER, W., RIZZUTO, N., FABRIZI, G. M., STUHRMANN, M., RUDNIK-SCHONEBORN, S., ZUCHNER, S., MICHAEL SCHRODER, J., BUCHHEIM, E., STRAUB, V., KLEPPER, J., HUEHNE, K., RAUTENSTRAUSS, B., BUTTNER, R., NELIS, E. & ZERRES, K. 2003. Mutations in a gene encoding a novel SH3/TPR domain protein cause autosomal recessive Charcot-Marie-Tooth type 4C neuropathy. *Am J Hum Genet,* 73**,** 1106-19.

SETHNA, F., ZHANG, M., KAPHZAN, H., KLANN, E., AUTIO, D., COX, C. L. & WANG, H. 2016. Calmodulin activity regulates group I metabotropic glutamate receptor-mediated signal transduction and synaptic depression. *J Neurosci Res,* 94**,** 401-8.

SHINDE, A. V., MOTIANI, R. K., ZHANG, X., ABDULLAEV, I. F., ADAM, A. P., GONZALEZ-COBOS, J. C., ZHANG, W., MATROUGUI, K., VINCENT, P. A. & TREBAK, M. 2013. STIM1 controls endothelial barrier function independently of Orai1 and Ca2+ entry. *Sci Signal,* 6**,** ra18.

SINGARAVELU, K., NELSON, C., BAKOWSKI, D., DE BRITO, O. M., NG, S. W., DI CAPITE, J., POWELL, T., SCORRANO, L. & PAREKH, A. B. 2011. Mitofusin 2 regulates STIM1 migration from the

Ca2+ store to the plasma membrane in cells with depolarized mitochondria. *J Biol Chem,* 286**,** 12189-201.

SIVERA, R., ESPINOS, C., VILCHEZ, J. J., MAS, F., MARTINEZ-RUBIO, D., CHUMILLAS, M. J., MAYORDOMO, F., MUELAS, N., BATALLER, L., PALAU, F. & SEVILLA, T. 2010. Phenotypical features of the p.R120W mutation in the GDAP1 gene causing autosomal dominant Charcot-Marie-Tooth disease. *J Peripher Nerv Syst,* 15**,** 334-44.

SOHN, J. W., YU, W. J., LEE, D., SHIN, H. S., LEE, S. H. & HO, W. K. 2011. Cyclic ADP ribose-dependent Ca2+ release by group I metabotropic glutamate receptors in acutely dissociated rat hippocampal neurons. *PLoS One,* 6**,** e26625.

SPACEK, J. & HARRIS, K. M. 1997. Three-dimensional organization of smooth endoplasmic reticulum in hippocampal CA1 dendrites and dendritic spines of the immature and mature rat. *J Neurosci,* 17**,** 190-203.

SPITZER, N. C., LAUTERMILCH, N. J., SMITH, R. D. & GOMEZ, T. M. 2000. Coding of neuronal differentiation by calcium transients. *Bioessays,* 22**,** 811-7.

SPITZER, N. C., OLSON, E. & GU, X. 1995. Spontaneous calcium transients regulate neuronal plasticity in developing neurons. *J Neurobiol,* 26**,** 316-24.

SUN, S., ZHANG, H., LIU, J., POPUGAEVA, E., XU, N. J., FESKE, S., WHITE, C. L., 3RD & BEZPROZVANNY, I. 2014. Reduced synaptic STIM2 expression and impaired store-operated calcium entry cause destabilization of mature spines in mutant presenilin mice. *Neuron,* 82**,** 79-93.

TAI, C., HINES, D. J., CHOI, H. B. & MACVICAR, B. A. 2011. Plasma membrane insertion of TRPC5 channels contributes to the cholinergic plateau potential in hippocampal CA1 pyramidal neurons. *Hippocampus,* 21**,** 958-67.

TAKEUCHI, A., KIM, B. & MATSUOKA, S. 2015. The destiny of Ca(2+) released by mitochondria. *J Physiol Sci,* 65**,** 11-24.

TANG, S., WANG, X., SHEN, Q., YANG, X., YU, C., CAI, C., CAI, G., MENG, X. & ZOU, F. 2015. Mitochondrial Ca(2)(+) uniporter is critical for store-operated Ca(2)(+) entry-dependent breast cancer cell migration. *Biochem Biophys Res Commun,* 458**,** 186-93.

TERRY, A. V., JR. & BUCCAFUSCO, J. J. 2003. The cholinergic hypothesis of age and Alzheimer's disease-related cognitive deficits: recent challenges and their implications for novel drug development. *J Pharmacol Exp Ther,* 306**,** 821-7.

TIAN, G., TEPIKIN, A. V., TENGHOLM, A. & GYLFE, E. 2012. cAMP induces stromal interaction molecule 1 (STIM1) puncta but neither Orai1 protein clustering nor store-operated Ca2+ entry (SOCE) in islet cells. *J Biol Chem,* 287**,** 9862-72.

TSIEN, R. W. & TSIEN, R. Y. 1990. Calcium channels, stores, and oscillations. *Annu Rev Cell Biol,* 6**,** 715-60.

VALERO, R. A., SENOVILLA, L., NUNEZ, L. & VILLALOBOS, C. 2008. The role of mitochondrial potential in control of calcium signals involved in cell proliferation. *Cell Calcium,* 44**,** 259-69.

VARADI, A., CIRULLI, V. & RUTTER, G. A. 2004. Mitochondrial localization as a determinant of capacitative Ca2+ entry in HeLa cells. *Cell Calcium,* 36**,** 499-508.

VERKHRATSKY, A. 2005. Physiology and pathophysiology of the calcium store in the endoplasmic reticulum of neurons. *Physiol Rev,* 85**,** 201-79.

WALDECK-WEIERMAIR, M., JEAN-QUARTIER, C., ROST, R., KHAN, M. J., VISHNU, N., BONDARENKO, A. I., IMAMURA, H., MALLI, R. & GRAIER, W. F. 2011. Leucine zipper EF hand-containing transmembrane protein 1 (Letm1) and uncoupling proteins 2 and 3 (UCP2/3) contribute to two distinct mitochondrial Ca2+ uptake pathways. *J Biol Chem,* 286**,** 28444-55.

WANG, G. J. & THAYER, S. A. 1996. Sequestration of glutamate-induced Ca2+ loads by mitochondria in cultured rat hippocampal neurons. *J Neurophysiol,* 76**,** 1611-21.

WANG, G. J. & THAYER, S. A. 2002. NMDA-induced calcium loads recycle across the mitochondrial inner membrane of hippocampal neurons in culture. *J Neurophysiol,* 87**,** 740-9.

WANG, Y., DENG, X., MANCARELLA, S., HENDRON, E., EGUCHI, S., SOBOLOFF, J., TANG, X. D. & GILL, D. L. 2010. The calcium store sensor, STIM1, reciprocally controls Orai and CaV1.2 channels. *Science,* 330**,** 105-9.

WATSON, R. & PAREKH, A. B. 2012. Mitochondrial regulation of CRAC channel-driven cellular responses. *Cell Calcium,* 52**,** 52-6.

WHITE, R. J. & REYNOLDS, I. J. 1995. Mitochondria and Na+/Ca2+ exchange buffer glutamate-induced calcium loads in cultured cortical neurons. *J Neurosci,* 15**,** 1318-28.

WILLIAMS, R. T., MANJI, S. S., PARKER, N. J., HANCOCK, M. S., VAN STEKELENBURG, L., EID, J. P., SENIOR, P. V., KAZENWADEL, J. S., SHANDALA, T., SAINT, R., SMITH, P. J. & DZIADEK, M. A. 2001. Identification and characterization of the STIM (stromal interaction molecule) gene family: coding for a novel class of transmembrane proteins. *Biochem J,* 357**,** 673-85.

WOOLF, N. J. 1991. Cholinergic systems in mammalian brain and spinal cord. *Prog Neurobiol,* 37**,** 475-524.

WORLEY, P. F., ZENG, W., HUANG, G. N., YUAN, J. P., KIM, J. Y., LEE, M. G. & MUALLEM, S. 2007. TRPC channels as STIM1-regulated store-operated channels. *Cell Calcium,* 42**,** 205-11.

WU, J., RYSKAMP, D. A., LIANG, X., EGOROVA, P., ZAKHAROVA, O., HUNG, G. & BEZPROZVANNY, I. 2016. Enhanced Store-Operated Calcium Entry Leads to Striatal Synaptic Loss in a Huntington's Disease Mouse Model. *J Neurosci,* 36**,** 125-41.

XIA, J., PAN, R., GAO, X., MEUCCI, O. & HU, H. 2014. Native store-operated calcium channels are functionally expressed in mouse spinal cord dorsal horn neurons and regulate resting calcium homeostasis. *J Physiol,* 592**,** 3443-61.

YAMADA-HANFF, J. & BEAN, B. P. 2013. Persistent sodium current drives conditional pacemaking in CA1 pyramidal neurons under muscarinic stimulation. *J Neurosci,* 33**,** 15011-21.

YAP, K. A., SHETTY, M. S., GARCIA-ALVAREZ, G., LU, B., ALAGAPPAN, D., OH-HORA, M., SAJIKUMAR, S. & FIVAZ, M. 2017. STIM2 regulates AMPA receptor trafficking and plasticity at hippocampal synapses. *Neurobiol Learn Mem,* 138**,** 54-61.

YEROMIN, A. V., ZHANG, S. L., JIANG, W., YU, Y., SAFRINA, O. & CAHALAN, M. D. 2006. Molecular identification of the CRAC channel by altered ion selectivity in a mutant of Orai. *Nature,* 443**,** 226-9.

YI, M., WEAVER, D. & HAJNOCZKY, G. 2004. Control of mitochondrial motility and distribution by the calcium signal: a homeostatic circuit. *J Cell Biol,* 167**,** 661-72.

YIN, S. & NISWENDER, C. M. 2014. Progress toward advanced understanding of metabotropic glutamate receptors: structure, signaling and therapeutic indications. *Cell Signal,* 26**,** 2284-97.

YOSHIDA, M., KNAUER, B. & JOCHEMS, A. 2012. Cholinergic modulation of the CAN current may adjust neural dynamics for active memory maintenance, spatial navigation and time-compressed replay. *Front Neural Circuits,* 6**,** 10.

YOUNG, K. W., BILLUPS, D., NELSON, C. P., JOHNSTON, N., WILLETS, J. M., SCHELL, M. J., CHALLISS, R. A. & NAHORSKI, S. R. 2005. Muscarinic acetylcholine receptor activation enhances hippocampal neuron excitability and potentiates synaptically evoked Ca(2+) signals via phosphatidylinositol 4,5-bisphosphate depletion. *Mol Cell Neurosci,* 30**,** 48-57.

ZHANG, H., WU, L., PCHITSKAYA, E., ZAKHAROVA, O., SAITO, T., SAIDO, T. & BEZPROZVANNY, I. 2015. Neuronal Store-Operated Calcium Entry and Mushroom Spine Loss in Amyloid Precursor Protein Knock-In Mouse Model of Alzheimer's Disease. *J Neurosci,* 35**,** 13275-86.

ZHANG, L. I. & POO, M. M. 2001. Electrical activity and development of neural circuits. *Nat Neurosci,* 4 Suppl**,** 1207-14.

ZHANG, Z., REBOREDA, A., ALONSO, A., BARKER, P. A. & SEGUELA, P. 2011. TRPC channels underlie cholinergic plateau potentials and persistent activity in entorhinal cortex. *Hippocampus,* 21**,** 386-97.

ZHAO, Y., ARAKI, S., WU, J., TERAMOTO, T., CHANG, Y. F., NAKANO, M., ABDELFATTAH, A. S., FUJIWARA, M., ISHIHARA, T., NAGAI, T. & CAMPBELL, R. E. 2011. An expanded palette of genetically encoded Ca(2)(+) indicators. *Science,* 333**,** 1888-91.

ZUCKER, R. S. 1999. Calcium- and activity-dependent synaptic plasticity. *Curr Opin Neurobiol,* 9**,** 305-13.